

Evaluation of hydrogen recycling from a long duration plasma-exposed tungsten specimen using Fast Ejecting System of Targeted sAmple (FESTA) on QUEST

岳, 其霖

<https://hdl.handle.net/2324/7157375>

出版情報 : Kyushu University, 2023, 博士 (工学), 課程博士
バージョン :
権利関係 :

Kyushu University

Interdisciplinary Graduate School of Engineering Sciences

Advanced Energy Engineering Science

Doctor Thesis

Evaluation of hydrogen recycling from a long
duration plasma-exposed tungsten specimen using
Fast Ejecting System of Targeted sAmple (FESTA)
on QUEST

Name Yue Qilin

Supervisor Professor Hanada Kazuaki

Index

Chapter 1 Introduction	1
Section 1 Significance and Overview of Nuclear Fusion Reactor Development.	1
Section 2 Issues in the Development of Plasma Facing Materials in Nuclear Fusion Reactors.....	7
Section 3 Materials Choice of Plasma Facing Walls	9
Section 4 Research Objective and Overview	12
Chapter 2 Development of Hydrogen Behavior Model inside Metals	13
Section 1 Pick & Sonnenberg model	13
Section 2 Full calculation using Pick & Sonnenberg model proposed by K. Schmid	19
Chapter 3 Experiments	30
Section 1 Fast Ejecting System of Targeted sAmple - FESTA	30
Section 2 Quadrupole Mass Analysis - QMA.....	36
3.2.1 QMA Calibration	38
Section 3 Experiment Overview	42
Section 4 FESTA Experiments.....	45
Section 5 Evaluation of Hydrogen Retention in QUEST and FESTA.....	50
3.5.1 Evaluation of Hydrogen Retention in QUEST	50
3.5.2 Verification of Measurements from FESTA	55
Section 6 Calculation of Plasma-induced Background Model	58
Section 7 Practical Application of Plasma-induced Background Model in FESTA Experiments	61
Chapter 4 Measurement of Hydrogen Recycling	67
Section 1 Plasma-exposed Sample.....	67
Section 2 Measurement of Hydrogen Recycling Using FESTA	68
Section 3 Verification and Analysis of Experimental Data	73
Chapter 5 Future Work	84
Chapter 6 Discussion	86

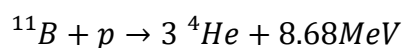
Impact of QUEST plasma exposure.....	86
Chapter 7 Conclusion.....	91
Reference.....	92
Acknowledgement.....	97
Appendix	99

Chapter 1 Introduction

Section 1 Significance and Overview of Nuclear Fusion Reactor Development.

Due to the increase in population and improvement in living standards, the energy consumption per capita is increasing, and humanity's overall energy consumption is steadily increasing. In any case, it is expected to reach several times the current population within the next 100 years, and obviously the world's energy consumption will continue to increase. The current primary source of energy is fossil fuels, but even optimistically estimating, they are predicted to be depleted by the middle of the 21st century. Therefore, various alternative energy sources are being developed. Nuclear fusion energy is also one of them, and various research is being conducted in Japan and overseas. In addition, since these studies require large amounts of funds and many human resources over a long period of time, international joint research is actively conducted. Developing a fusion reactor requires various cutting-edge technologies and involves many technical challenges as well.

The deuterium-tritium (D-T) reaction in fusion do have the potential to ultimately solve the energy problem since it utilizes the abundant deuterium in the sea. Currently, the following reactions are considered to be effective for fusion power generation:



where the cross-section of the D-T reaction is larger than that of the D-D, D-He and other reactions, making it easier to initiate the fusion reaction and resulting in a larger energy output as shown in Fig. 1.1.1. Here D and T are deuterium and tritium, p and n are proton and neutron, He , Li and B are helium, lithium and boron, respectively.

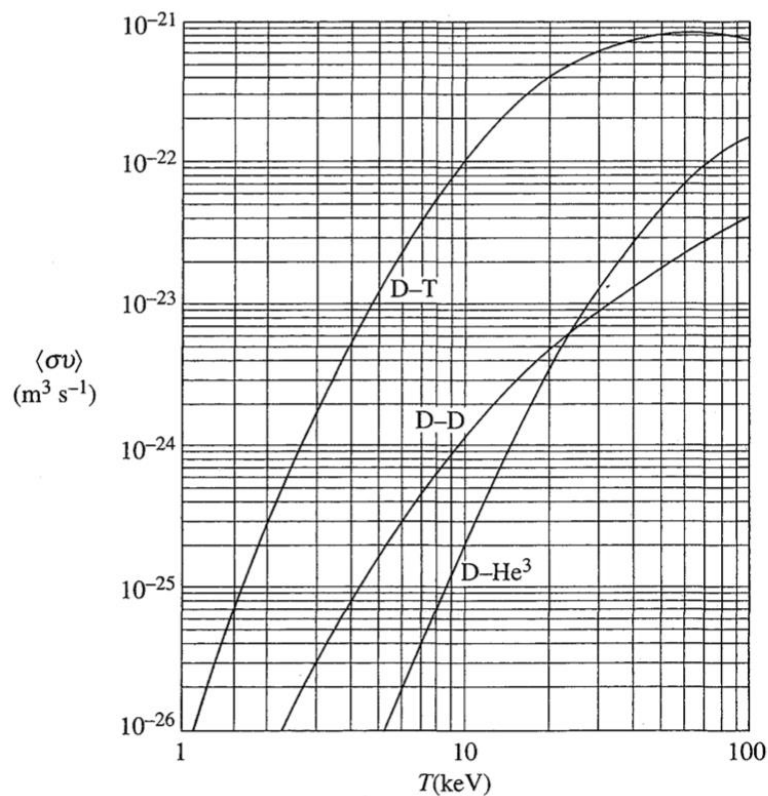


Fig. 1.1.1 Cross-section of typical fusion reactions [1]

The D-³He reaction has the potential for high-efficiency direct power generation. Additionally, there are fewer issues with material degradation and radioactivity caused by neutron irradiation. While ³He is known to exist in large quantities on the Moon and Jupiter, for example, it is almost nonexistent on Earth. Therefore, currently as the technology for nuclear fusion reactions is not yet established, the achievement of nuclear fusion through the D-T reaction, which is considered the most feasible, is being

pursued.

In order to cause a nuclear fusion reaction, it is necessary to bring the nuclei of particles closer together, but atomic nuclei are positive charges so that they will repel each other and will be prevented due to Coulomb barrier at low collision energies as shown in Fig. 1.1.2.

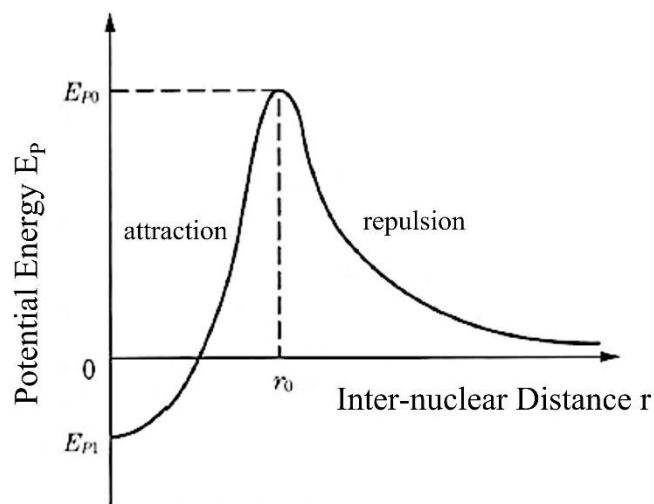


Fig. 1.1.2 Relation between inter-nuclear distance r and potential energy E_P [2]

In the region where the nuclear distance $r \geq r_0$, the repulsive force due to the Coulomb force becomes dominant, while in the region where $r \leq r_0$, the attractive force due to the nuclear force becomes dominant. It can be seen that when the energy potential E_P exceeds the Coulomb barrier E_{P0} , E_P approaches E_{P1} as r approaches 0, meaning that the two particles are more stable to be bounded other than separated. Therefore, it is necessary to input enough energy to overcome the Coulomb barrier to trigger nuclear fusion reaction, and to maintain a high-density and high-temperature plasma for a period of time. The minimum condition required to sustain such a nuclear fusion reaction is calculated from the energy balance of a fusion reactor which is called the

Lawson criterion as shown in Eq. (1.1.1) [3].

$$n\tau = \frac{3T}{\frac{\eta}{1-\eta} \frac{Q_T}{4} \langle \sigma v \rangle - \alpha T^{\frac{1}{2}}} \quad (1.1.1)$$

Here, n represents plasma density; τ represents confinement time; T represents plasma temperature; Q_T represents the output of nuclear fusion; $\langle \sigma v \rangle$ represents the cross-section of collision; and η represents the product power generation and heating efficiency. According to Eq. (1.1.1), to obtain the Lawson criterion for the D-T reaction, it is necessary to obtain that $n\tau > 10^{20} \text{ s/m}^3$ when the plasma temperature in the core is 10 keV, which is the current target parameter for fusion research.

To make a nuclear fusion reactor economically viable, it is necessary not only to confine the plasma for a long time and sustain the nuclear reaction, but also to ensure that the fusion output from the plasma is greater than the input power. Here, the fusion output is the sum of the energy of neutrons and α particles. Therefore, the ratio of the fusion output to the plasma heating input power (energy multiplication factor Q) becomes an important parameter that represents the performance of nuclear fusion. The condition that $Q = 1$ is called the critical plasma condition, and $Q = \infty$ is called the self-ignition plasma condition. When $Q = \infty$, the plasma is heated only by the energy of alpha particles. However, in actual plasma devices, heating input power is still required, so Q cannot reach infinity for now.

There are two main methods for confining high-temperature and high-density plasma: magnetic confinement and inertial confinement. Several confinement types are divided, and research is being conducted on them. Nowadays, the Tokamak magnetic

confinement approach is considered the most promising among them, which is chosen by JT-60U [4] and JT-60SA [5] in Japan, JET (Joint European Torus) [6] in Europe, TFTR (Tokamak Fusion Test Reactor) [7] in America, EAST (Experimental Advanced Superconducting Tokamak) [8] in China and ITER (International Thermonuclear Experimental Reactor) , etc. “TOKAMAK” comes from Russian: TOroidalnaya KAMERA and MAgnitnaya KATUSHKA, which means “toroidal chamber” and “magnetic coil”. Like its name, in a tokamak device, there is a toroidal vacuum vessel at the center, composed of toroidal magnetic field (TF) coils that can create toroidal magnetic field in the toroidal direction, and poloidal magnetic field (PF) coils that create poloidal magnetic field that perpendicular to the toroidal magnetic field. Since a collection of charged particles gathers in the plasma state, they can be confined in the vacuum vessel by winding around the main magnetic field, toroidal magnetic field. However, it is not sufficient to confine the plasma particles in a tokamak device relying on the toroidal magnetic field alone. The toroidal magnetic field strongly decreases along the radius direction, and due to ∇B drift, electrons and ions are separated vertically, which causes an electric field E . Combined with that, $E \times B$ drift is then created by the toroidal magnetic field, leading to those charged particles to collide with the vacuum vessel walls. Therefore, to prevent the separation of charged plasma particles, a poloidal magnetic field created by PF coils and a magnetic field created by the plasma current in the toroidal direction are needed, where the plasma particles can be confined by wrapping around these magnetic field lines [9]. As shown in Fig. 1.1.3, is the schematic of Tokamak device.

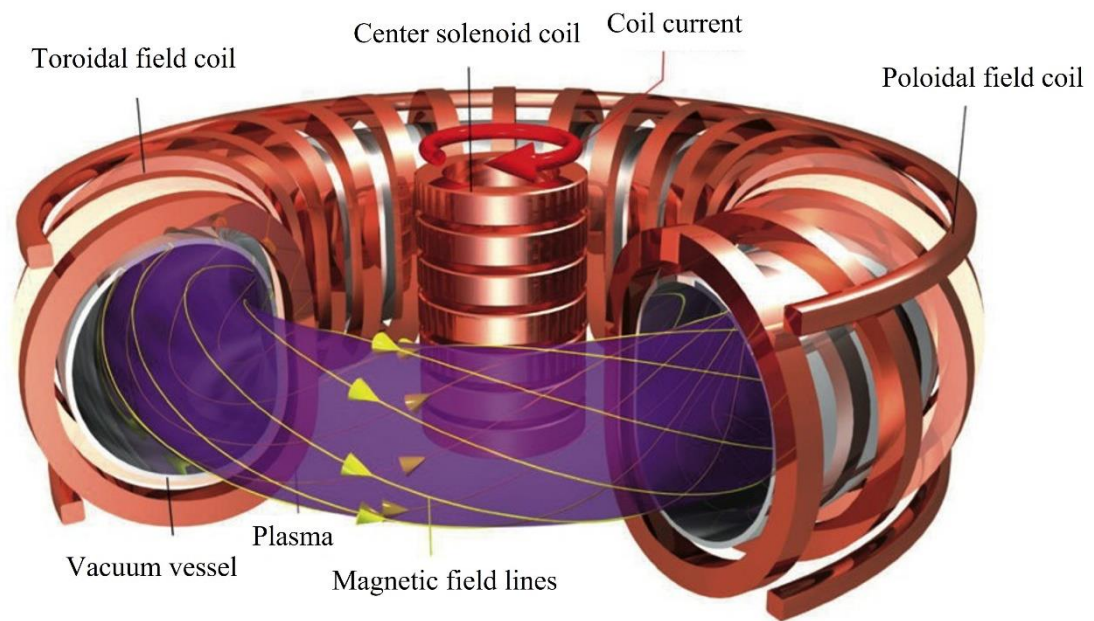


Fig. 1.1.3 Schematic of Tokamak device [10]

So far, in the research on large Tokamak devices, the major goal is to generate high-temperature plasma equivalent to that in a nuclear fusion reactor. However, the challenges in this task include issues related to the confinement, transport, and plasma heating in the plasma core, as well as issues related to the plasma facing walls (PFWs) and divertor plates, which are subject to internal damages and changes in surface properties due to the plasma surface interaction (PSI).

PFWs are always exposed to harsh environments that are irradiation of plasma particles, charged particles such as ions and neutral particles, and even neutrons with energy of 14.1 MeV produced due to D-T reactions. They are expected to suffer serious material damages from particle loads and heat loads. Table 1.2.1 is showing the operating conditions of PFWs and divertors predicted in ITER [11].

Table 1.2.1 Operating conditions of the divertor plates on the technology phase

Average neutron load (MW/m ²)	0.6
Average neutron fluence (MW/y/m ²)	0.1-0.4
Maximum particle flux (m ⁻² s ⁻¹)	(1-5) × 10 ²³
Maximum number of displacements (dpa)	2
Maximum heat load (MW/m ²)	11-15
Number of pulses	(4-10) × 10 ²
Tile temperature (for tungsten, thickness 5 mm) (°C)	1000-1200
Total allowable erosion (for edge temperature < 50 eV) (mm/yr)	1
Erosion due to disruption (energy < 10 MJ/m ²) (mm)	0.07
Total number of disruptions	20-100

Disruption time (ms)	0.1-3
Heat deposition under disruption (MJ/m ²)	10-20
Runaway electron load (MJ/m ²)	30-100
Plasma edge temperature (eV)	<50

When plasma particles such as hydrogen and its isotopes, are injected into PFWs, they not only create atomic-level defects in the materials but also cause erosion, sputtering, disruption etc. As a result, some of the impurity atoms from the surface of PFWs are transported to the core plasma, significantly affecting the performance of the plasma through radiation loss or other processes, while others form a redeposition layer on the surface. On the other hand, those injected plasma particles are absorbed in the PFWs in the materials, except those who are reflected under injection. Among them, a part of the particles is stored in the PFWs due to the existence of trapping sites in the materials, which is called static retention. The remaining ones with mobility diffuse to the surface of PFWs and then will be released due to surface recombination effect, which is called dynamic retention [12]. Hydrogen particles due to dynamic retention are released from PFWs and back into the vacuum vessel and then become plasma again during plasma discharges. This circulation between plasma and PFWs is called fuel particle recycling [12], which affects the plasma performance to a large extent either [13].

Section 3 Materials Choice of Plasma Facing Walls

Several criteria must be considered when selecting PFWs' material, such as the rates at which impurities are produced, the lifetime, the amount of plasma fuel particles, hydrogen isotopes stored in the vacuum vessel, neutron activation, and safety factors. The lifetime of these components is influenced by various factors, including erosion rates resulting from chemical and physical sputtering, structural strength, thermal conductivity, and thermal shock resistance. Meanwhile, the amount of hydrogen particles stored in the vessel depends on the trapping of ions and neutrals in the solid, the redeposition layer and structural material in areas with net deposition, and the generation of dust.

To reduce the radiation emitted by an impurity atom from PFWs, it is preferable to minimize both its nuclear charge (Z) and the sputter yield. A merit named M_m , based on solely on the impurity level in the plasma, is given as

$$M_m = f_i \frac{1 - Y_m}{Y_p} \quad (1.3.1)$$

and is shown as a function of edge plasma temperature for various material in Fig. 1.3.1. Here, f_i , Y_m , Y_p represents the maximum allowed impurity concentration in the plasma, sputtering coefficients of impurity and plasma particles, respectively [14].

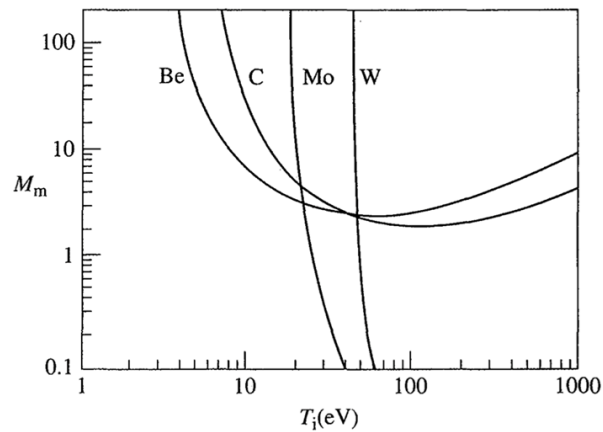


Fig. 1.3.1 An estimate of the degree of contamination of the plasma by limiter or divertor target materials M_m is calculated as a function of plasma ion temperature for beryllium (Be), carbon (C), molybdenum (Mo), and tungsten (W). An ion charge of 3 is assumed.

It could be observed that high-Z refractory materials are more effective at low plasma edge temperatures, while at high edge temperatures, only low-Z materials are feasible. Low-Z materials such as C and Be are widely used in PFWs, but during long-duration plasma discharges in future D-T fusion reactors, it has become clear that even low-Z materials have many disadvantages. For example:

In C case:

- Because of porous, the hydrogen static retention becomes significant at low temperatures (~ 800 K), and the T inventory in PFWs becomes large. Additionally, hydrogen recycling is significantly affected by surface conditions, leading to difficult plasma control during long-duration plasma discharges.
- Around 800~900 K chemical sputtering occurs, above 1300 K radiation-enhanced sublimation occurs, and above 2000 K self-sputtering yield becomes to exceed 1, which causes the sublimation rate increases significantly and results in a severe

material erosion [15]. Furthermore, a rapid increase in carbon concentration in the plasma will be caused, and the plasma operation cannot be controlled either [16].

- PFWs are often exposed to high heat loads so high thermal conductivity is required, but it is said that the thermal conductivity will be significantly reduced by neutron irradiation using C as PFWs [17], which shall be avoid in the future fusion reactors due to the 14 MeV produced from D-T reaction.

In Be case:

- Weak for heat loads, meaning that its sublimation temperature is low, and it sublimates >1300 K. In addition, there is a concern for melting because the melting point is low at 1550K and even for toxicity.
- Influence on the issues related to neutron-induced displacement damage and the generation of He. According to D.S. Gelles [18], significant irradiation embrittlement is induced by neutron irradiation, and it has been reported that helium gas embrittlement becomes prominent at irradiation temperatures above 900K.

Therefore, compared to the low-Z materials, high-Z materials such as W etc. are being focused on. As a refractory metal and owing to its good thermal properties, including sputtering erosion resistance and low radiated activation, W is one of the most promising plasma facing materials for future fusion devices, such as ITER.

During ITER-like wall experiments in the JET, the wall-stored fuel particles dramatically decreased after the adoption of W instead of C[19][20]. This indicates an elevation in the recycling of fuel particles during plasma discharge, which may be linked to the deterioration of the pedestal property with the ITER-like wall [21].

Section 4 Research Objective and Overview

The problem of dynamic retention of hydrogen isotopes from PFWs often leads to density runaway, plasma termination etc. when the fuel particle recycling ratio R exceeds 1. This issue significantly affects the steady state operation (SSO) of fusion experimental devices. Especially, although the use of metallic materials like tungsten in PFWs has been promoted to reduce the wall-stored hydrogen isotopes amount, it is likely to induce the subsequent excessive desorption during plasma discharges. Therefore, further investigation of fuel particle release during plasma discharge is necessary.

Unfortunately, the measurement in fusion experimental devices is limited. In this research, to evaluate the hydrogen recycling from PFWs in an actual machine during long-duration plasma discharges, we developed a new machine – Fast Ejecting System of Targeted sAmple (FESTA) which can expose a prepared sample to QUEST (Q-shu University Experiment with Steady-State Spherical Tokamak) hydrogen plasma. By extracting the plasma-exposed sample into FESTA test chamber within several seconds, the hydrogen desorption is able to be measured according to the hydrogen gas released from the sample with the help of background model. Furthermore, by creating a two-layer model, not only the experimental data has been reproduced, but also the sample surface conditions have been managed to be evaluated during the plasma discharges, which is closely related to the hydrogen release behavior.

Pick and Sonnenberg [22] developed a model for the release of hydrogen isotopes from metal surfaces and the movement of hydrogen isotopes from the surface to the bulk. In this model, the sample is divided into two regions: the surface region which irradiated by hydrogen plasma and the bulk region. The diagram of potential energy and hydrogen flow in each region are shown in Fig 2.1.1, symbols in which are explained as shown in Table 2.1.1.

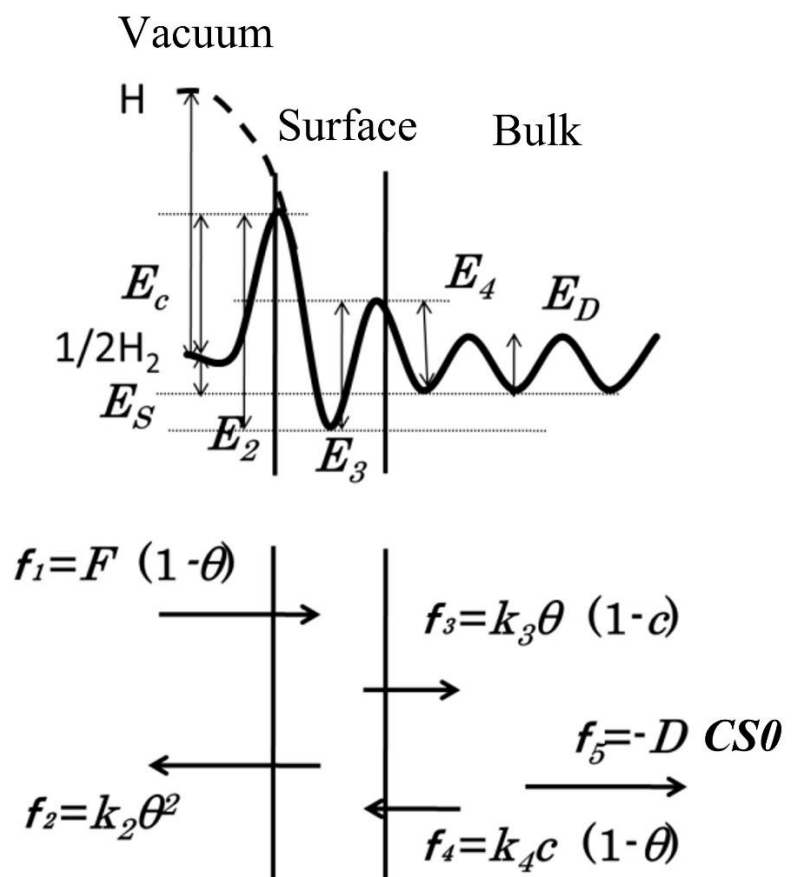


Fig. 2.1.1 Hydrogen behavior model on and inside metal surface [22].

Table 2.1.1 Symbols explanation in Fig. 2.1.1

$c [-]$	relative hydrogen concentration ratio in the subsurface
$CSO [-]$	hydrogen concentration in the subsurface
$D(T) [m^2s^{-1}]$	diffusion coefficient
$E_c [eV]$	surface barrier
$E_b [eV]$	activation energy of diffusion
$E_s [eV]$	heat for dissolution
$E_2 [eV]$	desorption energy for per hydrogen atom for the release from surface
$E_3 [eV]$	activation energy for transition from surface to bulk
$E_4 [eV]$	activation energy for transition from bulk to surface
$F [m^{-2}s^{-1}]$	hydrogen flux coming to the surface
$f_1 [m^{-2}s^{-1}]$	hydrogen transmission flux from vacuum to the surface
$f_2 [m^{-2}s^{-1}]$	hydrogen flux released from the surface to vacuum
$f_3 [m^{-2}s^{-1}]$	hydrogen transmission flux from the surface to the bulk
$f_4 [m^{-2}s^{-1}]$	hydrogen transmission flux from the bulk to the surface
$f_5 [m^{-2}s^{-1}]$	hydrogen diffusion flux in the bulk
$k_2 [m^{-2}s^{-1}]$	reaction rate constant for transmission from the surface to vacuum
$k_3 [m^{-2}s^{-1}]$	reaction rate constant for transmission from the surface to the bulk
$k_4 [m^{-2}s^{-1}]$	reaction rate constant for transmission from the bulk to the surface
$\theta [-]$	surface coverage of hydrogen

The flux of hydrogen that is recombined on the surface and released as hydrogen molecules can be expressed by the following equation.

$$f_2 = k_2\theta^2 \quad (2.1.1)$$

During equilibrium, it is believed that there is a relationship of $f_3 = f_4$, so

$$k_3\theta(1 - c) = k_4c(1 - \theta) \quad (2.1.2)$$

Here, θ can be calculated as

$$\theta = \frac{k_4}{k_3 + k_4c} \quad (2.1.3)$$

The relative concentration of hydrogen in the subsurface can be expressed as follows.

$$c = \frac{CS0}{C_0} \quad (2.1.4)$$

Here, $CS0$ is the hydrogen concentration in the subsurface and C_0 is the number density of solute sites in the subsurface for hydrogen. By substituting Eqs. (2.1.3) and (2.1.4) into Eq. (2.1.1), the hydrogen flux released from the surface can be expressed using the hydrogen in the subsurface as

$$f_2 = k_2 \left(\frac{k_4}{k_3 + k_4c} \right)^2 \left(\frac{CS0}{C_0} \right)^2 \quad (2.1.5)$$

θ is defined as the atomic fraction of hydrogen atoms to surface atoms. Therefore, if θ is much smaller than 1, c then can be ignored and Eq. (2.1.5) can be rewritten as

$$f_2 = k_2 \left(\frac{k_4}{k_3} \right)^2 \left(\frac{CS0}{C_0} \right)^2 \quad (2.1.6)$$

Combining the constant terms in Eq. (2.1.6) into one term and denoting as k_r , the Eq. (2.1.6) can be rewritten further as follows.

$$f_2 = k_r CS_0^2 \quad (2.1.7)$$

$$k_r = \frac{k_4^2 k_2}{k_3^2 C_0^2} \quad (2.1.8)$$

Here,

$$k_2 = k_{20} \exp\left(-\frac{2E_2}{k_B T}\right) \quad (2.1.9)$$

$$k_3 = k_{30} \exp\left(-\frac{E_3}{k_B T}\right) \quad (2.1.10)$$

$$k_4 = k_{40} \exp\left(-\frac{E_4}{k_B T}\right) \quad (2.1.11)$$

where k_B is the Boltzmann constant. Substituting Eqs. (2.1.8) – (2.1.11) into Eq. (2.1.7), k_r can be obtained as

$$k_r = \frac{k_{40}^2 k_{20}}{k_{30}^2 C_0^2} \exp\left(-\frac{2E_2 + 2E_4 - 2E_3}{k_B T}\right) \quad (2.1.12)$$

From Fig. 2.1.1, $E_4 - E_3 + E_2 - E_C = E_S$ can be obtained. Therefore, surface recombination coefficient K_r can be obtained as Eq. (2.1.13).

$$K_r(T) = K_{r0} \exp\left(-\frac{2(E_C - E_S)}{k_B T}\right) \quad (2.1.13)$$

where $K_r(T)$ is further summarized [22]-[26] as

$$K_r(T) = \frac{s(T)\mu}{K_s^2(T)} = \frac{s_0\mu}{K_{s0}^2} \exp\left(-\frac{2(E_c - E_s)}{k_B T}\right) \quad (2.1.14)$$

using Sieverts' law, sticking rate $s(T) = s_0 e^{\frac{-2E_c}{k_B T}}$ [22][27] in it. Here μ and $K_s(T)$ are gas kinetic coefficient and solubility in metal. E_c is defined as “surface barrier” in Fig. 2.1.1. Due to contamination on the metal surface, the surface barrier potential E_c will be changed, and it has been pointed out that the recombination coefficient $K_r(T)$ strongly depends on the conditions of the metal surface [22][25][27][28]. If the metal surface is absolutely clean corresponding to the case of non-activated hydrogen chemisorption, $E_c = 0$ eV and $K_r(T) = \frac{s_0\mu}{K_{s0}^2} e^{\frac{2E_s}{k_B T}}$ [22][28] are obtained.

Fig. 2.1.2 below shows the temperature dependence of $K_r(T)$ according to the Pick & Sonnenberg model, Eq. (2.1.14) described in previous studies [22][27]-[33].

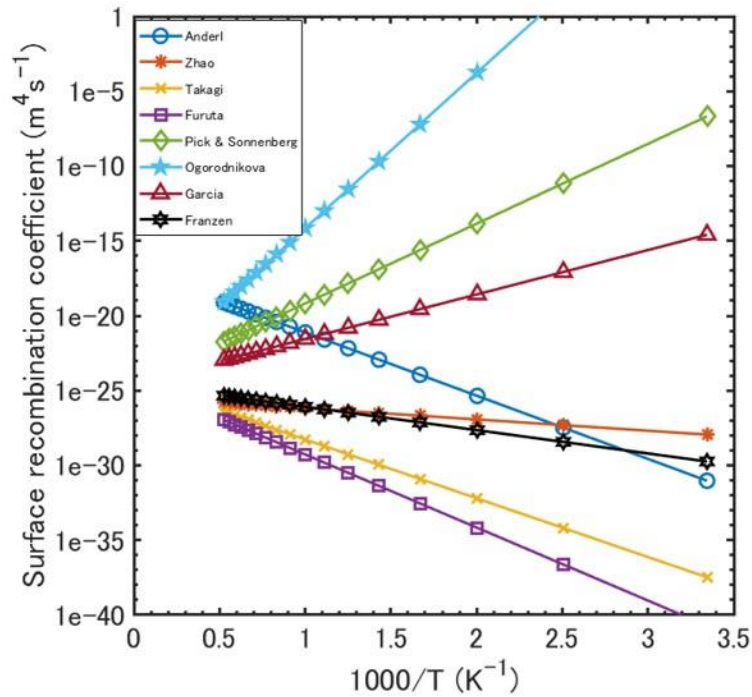


Fig. 2.1.2 The temperature dependence of each K_r in previous studies

Here, the light blue solid line (with stars) represents $E_C = 0 \text{ eV}$, showing the case that the surface of metal is clean.

However, although there are always two different hydrogen concentrations: hydrogen atomic concentration CA on the metal surface, and hydrogen atomic concentration in the subsurface solute sites CS_0 , due to its complexity, the hydrogen release was often assumed to be proportional to CS_0^2 , which alleviates the need to treat chemisorbed hydrogen [37][38].

In that case, K. Schmid [40] gave a full calculation using Pick & Sonnenberg model, which is introduced in next section.

Section 2 Full calculation using Pick & Sonnenberg model proposed by K. Schmid

The uptake of hydrogen isotopes into metals has been widely studied in the literature, and various models have been proposed and compared [22][34]-[39]. Among them, the model proposed by Pick and Sonnenberg in 1985 [22] for the hydrogen behaviors in metals is currently widely accepted, where the incorporation of hydrogen isotopes from the gas phase into the metal is explained as a two-stage process accompanying an endothermic heat of dissolution for the hydrogen isotopes, where hydrogen molecules (H_2) first dissociate and are chemically adsorbed on the metal surface and then the adsorbed hydrogen atoms (H) pass over the surface barrier (the activation energy being for dissolution, ΔE_{Sol}) and enter the metal bulk by an Arrhenius process. Those H atoms dissolve into the metal. There are also two-stage processes when H leaves the metal bulk. Firstly, the dissolved H atoms overcome a barrier by the Arrhenius process (the activation energy for diffusion is ΔE_{Diff}) and transit back to the initial surface state as chemical adsorption. Then, they recombine through the Langmuir-Hinshelwood process to become a diatomic molecule and desorb from the metal surface into the gas phase. Those recombination flux of hydrogen isotopes is proportional to the square of the concentration of chemisorbed atoms, and the recombination coefficient K_r [m^4s^{-1}] is derived. In the model proposed by Pick & Sonnenberg, the metal is divided into two parts: surface and bulk. Therefore, the model clearly distinguishes between two H concentrations: the concentration of chemisorbed atoms on the metal surface, CA , and the concentration of H in subsurface dissolution sites, CS_0 . Generally, $\Delta E_{Sol} > \Delta E_{Diff}$, so above processes are asymmetric, and the transition from the metal surface to the metal bulk becomes much smaller than the transition from the metal bulk to the metal surface. The potential energy diagram for H and H_2 on the metal surface proposed by K.

Schmid is shown below, and symbols are shown in Table 2.2.1.

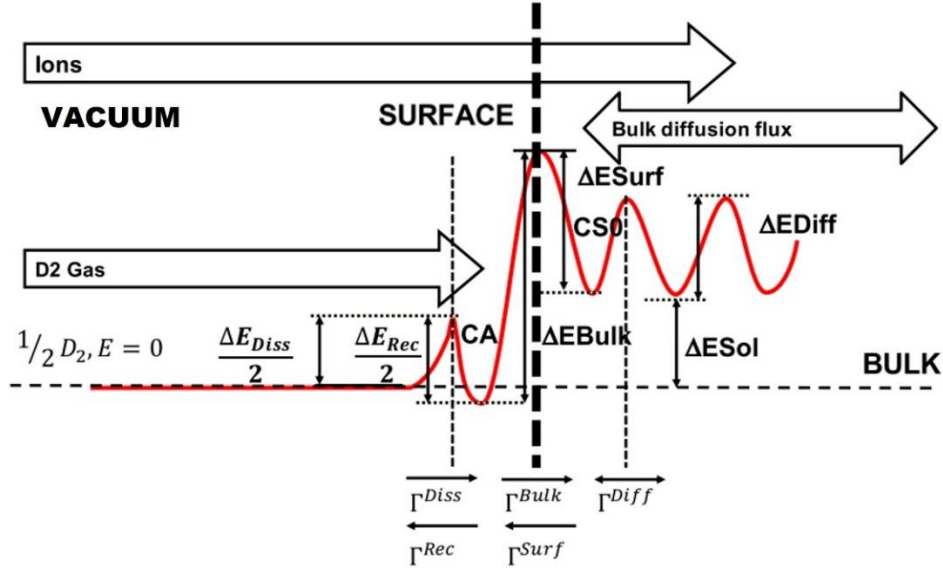


Fig. 2.2.1 Potential energy diagram of hydrogen atoms (H) and molecules (H₂) on the metal surface. The flux of hydrogen isotopes to/from the chemical adsorption state and to/from subsurface dissolution sites is also shown. [40]

Table 2.2.1 Symbols explanation in Fig. 2.2.1

$\Delta E_{Diss} [eV]$	activation energy for dissociation from H ₂ into H
$\Delta E_{Rec} [eV]$	activation energy for recombination from H into H ₂
$\Delta E_{Bulk} [eV]$	activation energy for transition from surface to bulk
$\Delta E_{Surf} [eV]$	activation energy for transition from bulk to surface
$\Delta E_{Sol} [eV]$	heat for dissolution
$\Delta E_{Diff} [eV]$	activation energy for diffusion
$\Gamma_{Diss} [m^{-2}s^{-1}]$	flux of hydrogen molecules dissociating on the surface
$\Gamma_{Rec} [m^{-2}s^{-1}]$	flux of hydrogen atoms recombining on the surfaces
$\Gamma_{Bulk} [m^{-2}s^{-1}]$	transition flux from surface to bulk
$\Gamma_{Surf} [m^{-2}s^{-1}]$	transition flux from bulk to surface
$\Gamma_{Diff} [m^{-2}s^{-1}]$	diffusion flux

As shown in Fig. 2.2.1, in the case of hydrogen gas infiltration, the concentration of chemisorbed H in the chemisorbed surface state is denoted by CA [-], and the following fluxes [$\text{m}^{-2}\text{s}^{-1}$] are in balance in the steady state:

Flux of hydrogen molecules dissociating on the surface Γ_{Diss} :

$$\Gamma_{Diss} = 2\mu P_{H_2} s(T) \left(1 - \frac{CA}{\eta}\right)^2 \quad (2.2.1)$$

$$\mu = \frac{1}{\sqrt{2\pi m_{H_2} k_B e_0 T}} \quad (2.2.2)$$

$$s(T) = s_0 \exp(-\Delta E_{Diss}/k_B T) \quad (2.2.3)$$

Here, μ is the gas kinetic coefficient, and $s(T)$ [-] is the sticking rate, which is the probability (0-1) of H_2 colliding with the surface and dissociating, resulting in H being adsorbed on the surface of the chemisorption site. η , m_{H_2} , k_B , e_0 and T are the maximum chemisorption concentration [dimensionless quantity -], the mass [kg] of the hydrogen isotope molecule/atom incident on the metal, the Boltzmann constant [JK^{-1}], the electron charge [C], and the absolute temperature [K], respectively.

Flux released from the metal surface due to recombination through Langmuir–Hinshelwood process Γ_{Rec} :

$$\Gamma_{Rec} = 2\chi(T)(\delta_0 CA)^2 \quad (2.2.4)$$

$$\chi(T) = \chi_0 \exp(-\Delta E_{Rec}/k_B T) \quad (2.2.5)$$

Here, δ_0 [m^{-2}] is the areal density of surface metal atom, $\chi(T)$ [m^2s^{-1}] is the

recombination rate.

Flux of H from the surface chemical adsorption sites to the subsurface dissolution sites

Γ_{Bulk} :

$$\Gamma_{Bulk} = \delta_0 v^{SB}(T) CA \quad (2.2.6)$$

$$v^{SB}(T) = v_0^{SB} \exp(-\Delta E_{Bulk}/k_B T) \quad (2.2.7)$$

Here, $v^{SB}(T)$ [s^{-1}] is the transition rate to the metal bulk.

Flux of H from the subsurface dissolution sites to the surface Γ_{Surf} :

$$\Gamma_{Surf} = \delta_0 v^{BS}(T) CS_0 \left(1 - \frac{CA}{\eta}\right)^2 \quad (2.2.8)$$

$$v_0^{BS}(T) = v_0^{BS} \exp(-\Delta E_{Diff}/k_B T) \quad (2.2.9)$$

Here, $v_0^{BS}(T)$ [s^{-1}] is the transition rate the metal surface, and CS_0 [dimensionless quantity -] is the concentration of dissolved H in the metal subsurface.

Diffusion flux Γ_{Diff} from or to the bulk can be expressed

$$\Gamma_{Diff} = D(T) \rho \frac{\partial CS(x_{Surf}, t)}{\partial x} \quad (2.2.10)$$

$$D(T) = D_0 \exp(-\Delta E_{Diff}/k_B T) \quad (2.2.11)$$

Here, $D(T)$ [$m^2 s^{-1}$] is the diffusion coefficient, $CS(x_{Surf}, t)$ is the depth profile of dissolved H at x_{Surf} which represents the metal surface position, and ρ [m^{-3}] is the number density of the metal. If the temperature gradient in the metal is not considered,

the distribution of dissolved H becomes linear in it as shown:

$$\Gamma_{Diff} = D(T)\rho \frac{\Delta CS}{\Delta X_{Grad}} \quad (2.2.12)$$

where ΔCS is the difference of dissolved H through the gradient length ΔX_{Grad} . For calculation convenience, a pre-factor Ω_x is introduced as follows.

$$\Gamma_{Diss} = \Omega_{Diss} P_{HI} \quad (2.2.13)$$

$$\Gamma_{Rec} = \Omega_{Rec} CA^2 \quad (2.2.14)$$

$$\Gamma_{Bulk} = \Omega_{Bulk} CA \quad (2.2.15)$$

$$\Gamma_{Surf} = \Omega_{Surf} CS_0 \quad (2.2.16)$$

, in which

$$\Omega_{Diss} = 2\mu S(T) \quad (2.2.17)$$

$$\Omega_{Rec} = 2\delta_0^2 \chi(T) \quad (2.2.18)$$

$$\Omega_{Bulk} = \delta_0 v^{SB}(T) \quad (2.2.19)$$

$$\Omega_{Surf} = \delta_0 v^{BS}(T) \quad (2.2.20)$$

In the steady state at the surface, fluxes shown in Fig. 2.2.1 are balanced as follows.

$$\Gamma_{Bulk} - \Gamma_{Surf} - \Gamma_{Diff}^{Bulk} \equiv 0 \quad (2.2.21)$$

$$\Gamma_{Surf} - \Gamma_{Bulk} - \Gamma_{Rec} + \Gamma_{Diss} \equiv 0 \quad (2.2.22)$$

CS_0 and CA can be obtained by solving Eq. (2.2.21) and Eq. (2.2.22) with Sieverts' law ($K_S(T) = K_{S0} \exp(-\Delta E_{Sol}/k_B T)$) introduced as:

$$CS0 = \frac{-\Gamma_{Diff}^{Bulk}}{\Omega_{Surf}} + K_s(T) \sqrt{\frac{-\Gamma_{Diff}^{Bulk}}{\Omega_{Diss}} + P_{HI}} \quad (2.2.23)$$

$$CA = \sqrt{\frac{-\Gamma_{Diff}^{Bulk} + \Omega_{Diss}P_{HI}}{\Omega_{Rec}}} \quad (2.2.24)$$

In the case of H ions or H atoms with energy injection, which is important in this study, as shown in Fig. 2.2.2, the balance of those above-mentioned fluxes is expressed by the following equation since the dissociation of gas phase is not considered ($\Gamma_{Diss} = 0$).

$$\Gamma_{ion} + \Gamma_{Diff}^{SURF} \equiv 0 \quad (2.2.25)$$

$$\Gamma_{ion} + \Gamma_{Bulk} - \Gamma_{Surf} \equiv 0 \quad (2.2.26)$$

$$\Gamma_{Surf} - \Gamma_{Bulk} - \Gamma_{Rec} \equiv 0 \quad (2.2.27)$$

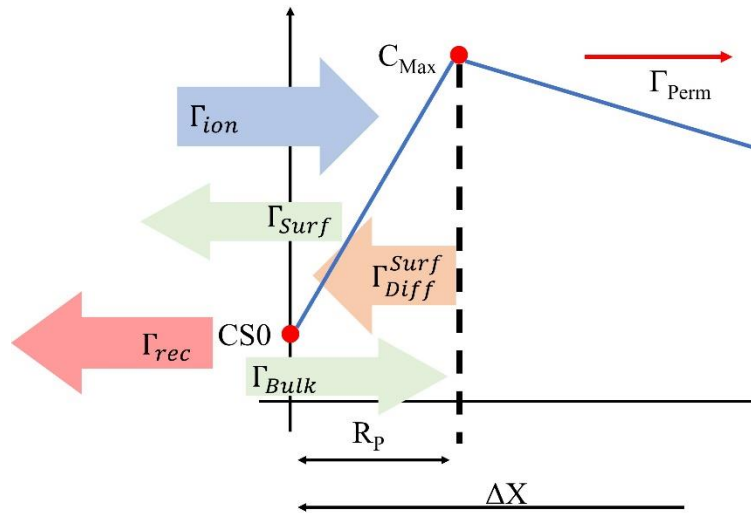


Fig. 2.2.2 The depth distribution of dissolved hydrogen under ion bombardment at steady state, where R_p is the mean penetration depth of hydrogen ions into the metal.

Here, Γ_{Diff}^{SURF} is the diffusion flux from depth R_p to the metal surface, and the permeation flux Γ_{Peam} can be calculated by solving Eqs. (2.2.12), (2.2.25) - (2.2.27) as follows:

$$\Gamma_{Peam} = \frac{R_p}{\Delta X - R_p} \Gamma_{ion} \left(1 + \frac{\Omega_{Diff}^{SURF}}{\Omega_{SURF}} + \frac{K_s(T) \Omega_{Diff}^{SURF}}{\sqrt{\Omega_{Diss} \Gamma_{ion}}} \right) \quad (2.2.28)$$

By assuming that the transition for hydrogen atoms from the subsurface to the chemisorbed surface is one monolayer $a_0 = \rho^{-1/3}$, and following Eq. (2.2.12), Eq. (2.2.28) can be rewritten as:

$$\Gamma_{Peam} = \frac{R_p}{\Delta X - R_p} \Gamma_{ion} \left(1 + \frac{a_0}{6R_p} \exp\left(-\frac{\Delta E_{Diff} - \Delta E_{Surf}}{k_B T}\right) + \frac{K_s(T) \Omega_{Diff}^{SURF}}{\sqrt{\Omega_{Diss} \Gamma_{ion}}} \right) \quad (2.2.29)$$

In K. Schmid's full calculation, sticking rate $S(T)$ is assumed as 1, referring to $\Omega_{Diss} = 2\mu$ [22], and Eq. (2.2.29) becomes

$$\Gamma_{Peam} = \frac{R_p}{\Delta X - R_p} \Gamma_{ion} \quad (2.2.30)$$

$$\times \left(1 + \frac{a_0}{6R_p} \exp\left(-\frac{\Delta E_{Diff} - \Delta E_{Surf}}{k_B T}\right) + \frac{\rho D_0 K_{s0}}{R_p \sqrt{2\mu}} \exp\left(-\frac{\Delta E_{Diff} + \Delta E_{Sol}}{k_B T}\right) \right)$$

The surface recombination coefficient K_r can be calculated from the balance between fluxes: Γ_{Peam} , Γ_{ion} , and Γ_{rec} as follows:

$$K_r = \frac{D(T)^2}{2\Delta X^2} \frac{\Gamma_{ion}}{\Gamma_{Perm}^2} \left(1 - \frac{\Gamma_{ion} R_P}{\Gamma_{Perm} \Delta X}\right)^2 \quad (2.2.31)$$

Substituting Eq. (2.2.28) into Eq. (2.2.29), The K_r value can be obtained as

$$K_r = \frac{D(T)^2}{2R_P^2 \left(\frac{\rho D_0 K_{s0}}{R_P \sqrt{2\mu}} \exp\left(-\frac{\Delta E_{Diff} + \Delta E_{Sol}}{k_B T}\right) + \sqrt{\Gamma_{ion}} \frac{a_0}{6R_P} \exp\left(-\frac{\Delta E_{Diff} - \Delta E_{Surf}}{k_B T}\right) \right)^2} \quad (2.2.32)$$

ΔE_{Surf} represents the metal subsurface barrier potential as mentioned in Fig. 2.2.1. Fig. 2.2.3 below shows the dependence of K_r on the subsurface barrier energy (ΔE_{Surf}) and temperature (T) when the constant hydrogen flux is injected into tungsten (W). In the calculation, $\Gamma_{ion} = 10^{22} [m^2 s^{-1}]$, $D(T) = 2.06 \times 10^{-7} e^{\frac{-0.28}{k_B T}} [m^2 s^{-1}]$ [41], $K_s(T) = 3.3 \times 10^3 e^{\frac{-1.0}{k_B T}} [mol \cdot m^{-3} Pa^{-1/2}]$ [23][42] are applied. When $\Delta E_{Surf} = \Delta E_{Diff}$, the metal surface barrier is absent, which could be implied that the metal surface is clean [40]. According to Eq. (2.2.32), it is evident that the recombination coefficient K_r is strongly dependent on the injected hydrogen flux to the surface and the surface state of the metal, besides the metal surface temperature in K. Schmid's calculation.

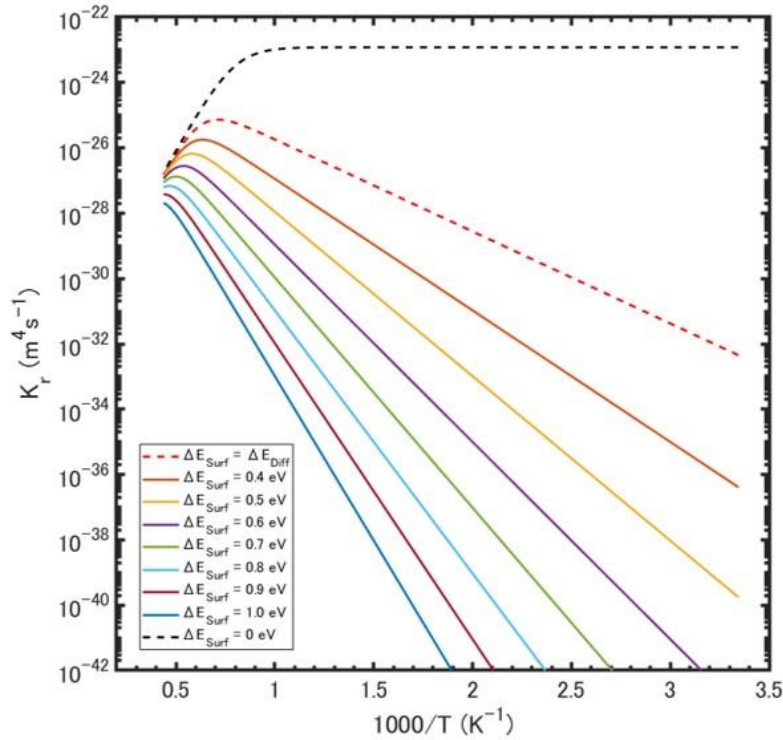


Fig. 2.2.3 The temperature dependence of K_r under different ΔE_{surf} when the incident hydrogen flux is constant

However, it should be noted that it is difficult to measure the solubility of hydrogen in W due to its low solubility. Generally, the solubility of hydrogen in metals is a material constant, but even if the variation in data is quite small, the scarcity of W database, W is a still challenge. T. Tanabe [24] has pointed out that the $K_s(T)$ proposed by R. Frauenfelder [42], A.P. Zakharov [43], and T. Otsuka [44], which have been widely used in the past, have the same order but vastly different in K_{s0} . Furthermore, the commonly used value of $\Delta E_{sol} = 1.0 \text{ eV}$ is also too large. The following Fig. 2.2.4 shows the dependence of K_r on metal temperature for different ΔE_{surf} values using the hydrogen solubility constant in W obtained by T. Tanabe.

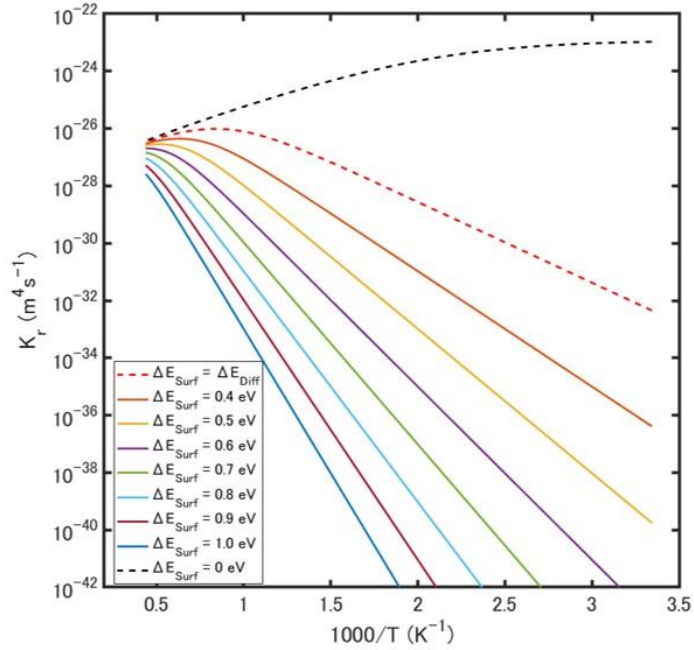


Fig. 2.2.4 The temperature dependence of K_r under different ΔE_{surf} when the incident hydrogen flux is constant, where the hydrogen solubility constant in tungsten is proposed by T. Tanabe

Comparing Fig. 2.2.3 and 2.2.4, it can be seen that the difference in solubility constant affect significantly the recombination coefficient, especially over 600 K.

Furthermore, as mentioned before, the sticking coefficient $s(T)$ is assumed as 1 in this model calculation. The K_r value can be calculated if the sticking coefficient (Eq. (2.2.3)) is considered,

$$K_r = \frac{D(T)^2}{2R_p^2 \left(\frac{\rho D_0 K_{s0}}{R_p \sqrt{2\mu s_0}} \exp\left(-\frac{\Delta E_{Diff} + \Delta E_{Sol} - \frac{1}{2} \Delta E_{Diss}}{k_B T}\right) + \sqrt{\Gamma_{ion}} \frac{a_0}{6R_p} \exp\left(-\frac{\Delta E_{Diff} - \Delta E_{surf}}{k_B T}\right) \right)^2} \quad (2.2.33)$$

In brief, except the sample temperature dependence, comparing two different kinds of model, it is hard to tell which barrier potential (surface barrier potential E_C or subsurface barrier potential ΔE_{surf}) is more significant to surface recombination coefficient K_r , but both are related to K_r and are strongly dependent on the metal surface conditions, and small change of them would cause significant change on K_r as Fig. 2.1.2 and Fig. 2.2.3.

A comparison between them shall be conducted, which is a future work discussed in Chapter 6.

Chapter 3 Experiments

Section 1 Fast Ejecting System of Targeted sAmple - FESTA

After a long duration plasma discharge in QUEST, global hydrogen recycling is demanded from the hydrogen flux released when wall saturation is reached, and experimental verification was conducted with a uniform wall model [45]. On the other hand, local fuel particle recycling from target samples can only be measured by Nuclear Reaction Analysis (NRA) [46][47]. When using NRA, the sample needs to be irradiated with an ion beam by an accelerator.

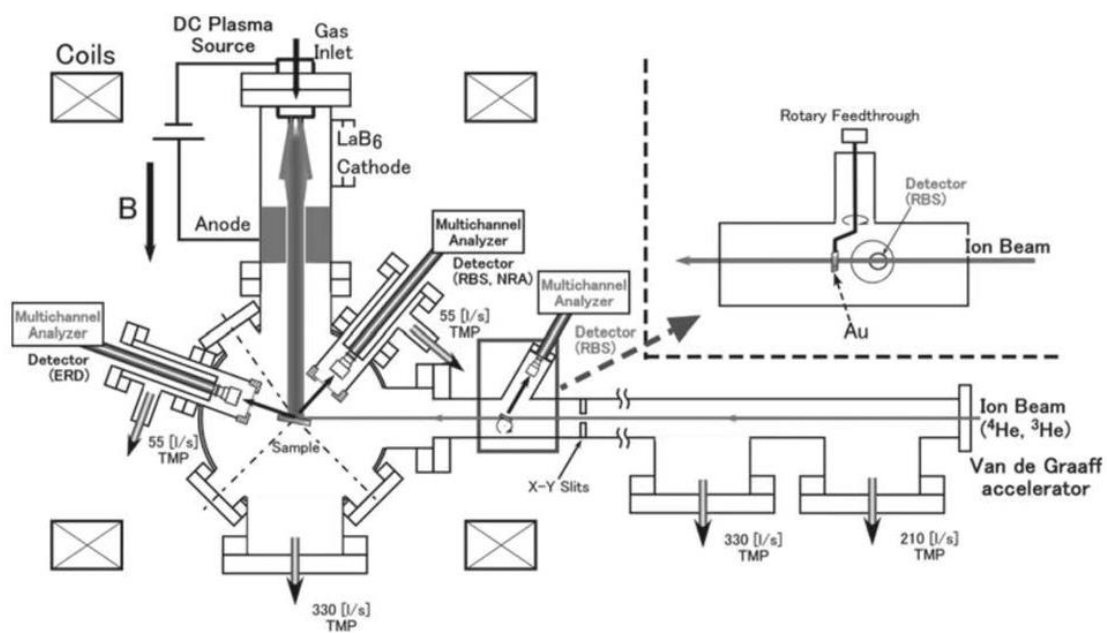


Fig. 3.1.1 PS-DIBA (Plasma Surface Dynamics with Ion Beam Analysis) [48][49]

As shown in Fig. 3.1.1, this is the experimental apparatus in Nagoya University [48][49]. The device consists of a small DC plasma source using a LaB₆ thermionic cathode and water-cooling copper anode, a sample chamber, a semiconductor detector for NRA, and vacuum pumps for exhaust, among others. The size, excluding the ion

beam line, is 1 m×0.8 m×1.5 m, and it goes without saying that a large device such as an accelerator is required. The exposed plasma is not relevant to fusion experimental plasmas, but also when measuring particle recycling using NRA, the sample must be exposed to air after plasma-exposure, which would lead to changes in surface conditions of the sample due to impurities and have a significant impact on the measurement. From this background, it is required to measure the local hydrogen desorption and hydrogen recycling in-situ with more convenience using a compact device. To enable the measurement of the local dynamic retention of fuel particles during long duration tokamak operation in QUEST, a high-speed sample transport system called the Fast Ejecting System of Targeted sAmple (FESTA) has been developed [50].

Fig. 3.1.2 (a) shows the schematic of FESTA, which consists of two gate valves (1 and 2), a test chamber, an exhausting system whose gate valve will be closed during FESTA experiment, and a telescopic device. Inside FESTA, a movable arm (yellow line) that can lift the sample (blue) in the test chamber set horizontally on the sample stage (Fig. 3.1.3) and is connected to the telescopic device, allowing the sample to be lifted (Fig. 3.1.4) and set vertically during exposure (Fig. 3.1.5) to the QUEST plasma at any time. The sample can be withdrawn within 11 seconds during plasma discharge using FESTA. The opening and closing of gate valve 1 and gate valve 2 are controlled by signals from optical sensors that monitor the tip position of movable arm. When movable arm pulls out the sample from plasma exposure, once the sample passes through the position of gate valve 2, gate valve 2 closes. Afterwards, movable arm places the sample horizontally on the sample stage and then leaves it in the test chamber. When movable arm passes through gate valve 1, gate valve 1 closes, so that the test chamber becomes completely isolated. The hydrogen desorption released from the plasma-exposed sample

can be measured using a quadruple mass analysis (QMA). It should be noted that the sample is still exposed to the plasma before the gate valve 2 is closed, and this should be taken into consideration during data analysis, which will be mentioned later. Fig. 3.1.2 (b) is a cross-sectional view of the test chamber from the plasma side. With two thermocouples on each side of the sample stage (four in total), it is possible to measure the temperature of the sample after it is withdrawn from the plasma exposure and placed on the sample stage horizontally. However, since the thermocouples are only present on the sample stage, the temperature of the sample during plasma exposure cannot be measured.

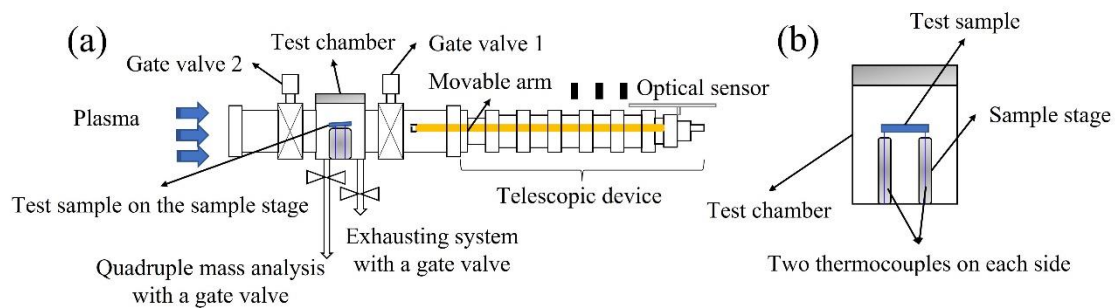


Fig. 3.1.2 FESTA Schematic

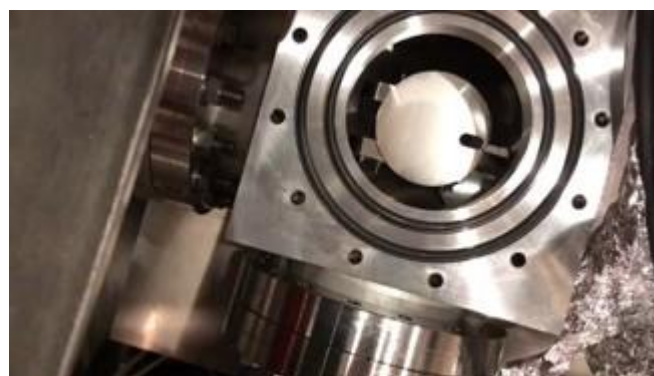


Fig. 3.1.3 Top view from FESTA test chamber. The test sample is set horizontally on the sample stage.

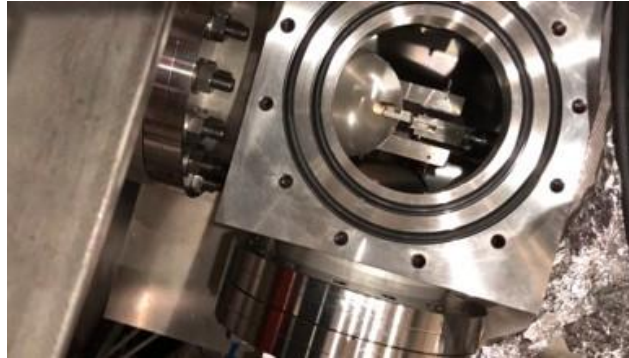


Fig. 3.1.4 Top view from FESTA test chamber. The test sample is lifted by movable arm.



Fig. 3.1.5 Side view from QUEST vacuum vessel. The test sample is exposed vertically to QUEST plasma using movable arm.

Such a series of FESTA operation is programmed in LabVIEW (detailed program information is described in the APPENDIX), and the required operation time is shown in the following table.

Table 3.1.1 Time scale of operating FESTA

FESTA operations	Required Time (s)
End of specimen exposure	0
Closing time of gate valve 2	8
Closing time of gate valve 1	2.8
Partial pressure measurement	~1000

To verify whether the operations are feasible, we conducted multiple tests in both atmospheric and vacuum environments to ensure that FESTA operations are reliable even during the plasma discharges. Fig. 3.1.6 shows the FESTA control panel, which is used to remotely control the operation of FESTA during experiments.

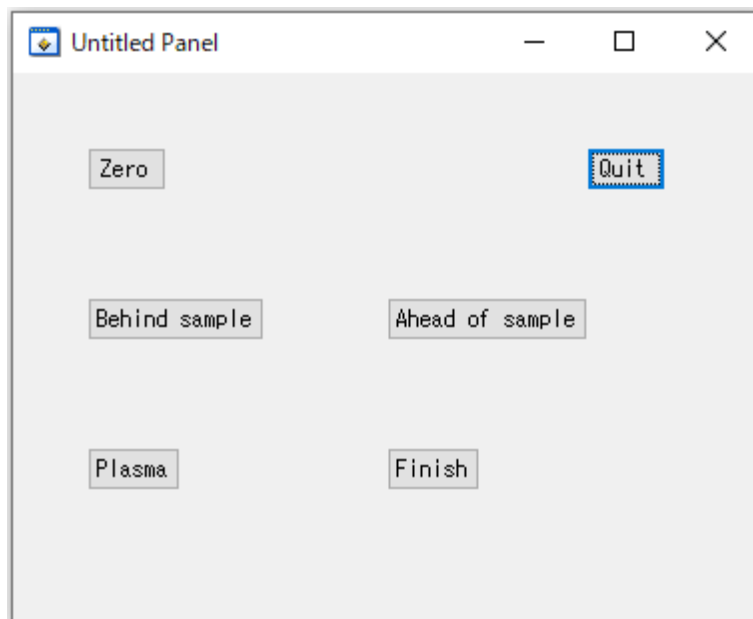


Fig. 3.1.6 Control panel

The “Behind sample” and “Ahead of sample” button allow to lift the sample placed in the test chamber (Fig. 3.1.3 and 3.1.4), and the “Plasma” button and “Finish” button enable to expose the sample to QUEST plasma (Fig. 3.1.5) and extract it from the QUEST plasma exposure.

By measuring the hydrogen partial pressure inside the isolated test chamber using the QMA, it is possible to directly evaluate the so-called hydrogen desorption, which is the hydrogen molecules released from the plasma-exposed sample via a surface recombination process.

Section 2 Quadrupole Mass Analysis - QMA

QMA mainly consists of an ion source section, a filter section, and a detection section. In the ion source section, neutral particles collide with electrons via thermionic emission from the filament and are ionized. The generated ions are sent to the quadrupole in the filter section by an electric field. Applying a voltage to the quadrupole, ions with a specific mass-to-charge ratio are allowed to pass through due to the difference in particle trajectory, and neutral particles can be measured as an ion current value by detecting ions in the detection section. The ion current must be converted to partial pressure of each neutral through calibration experiment as described in the next section [51].

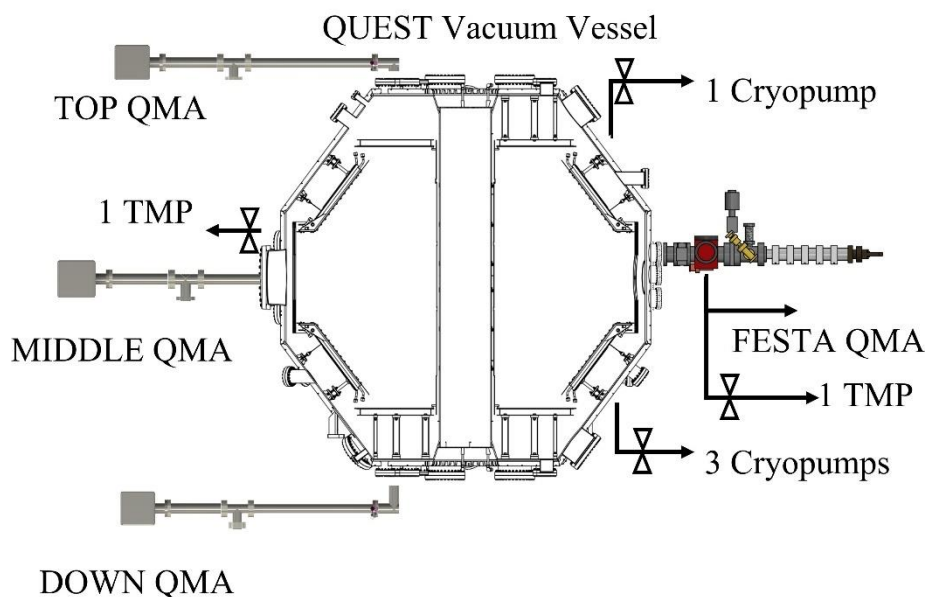


Fig. 3.2.1 Several QMAs are set on QUEST and FESTA in different position. There are four cryopumps and one TMP installed on QUEST, and one TMP installed on FESTA with individual gate valves between them and QUEST vacuum vessel, which are closed during QMA calibration.

As shown in Fig. 3.2.1, the QMAs (BGM102 Qulee series made by ULVAC) are installed in three different positions, top, middle, and bottom, on QUEST vacuum vessel. FESTA is installed at the port on the mid plane of QUEST. There are three ports at the same poloidal section and FESTA is connected to the upper port by 25 cm from the equatorial plane of QUEST vacuum vessel. External pumping system is shown in the figure above, in which there is one cryopump set at the top, 3 cryopumps set at the bottom and one turbo molecule pump (TMP) set in the middle of QUEST vacuum vessel. There is one TMP on FESTA. All of those external pumps have their own gate valves between them and vacuum vessels, which are closed during QMA calibration.

3.2.1 QMA Calibration

The sensitivity coefficient of the ion source in the QMA measurement changes due to contamination on the ion source, so calibration is necessary to convert the obtained ion current value to hydrogen partial pressure. Before QUEST experiments, the QMA sensitivity calibration will be performed by injecting a certain amount of hydrogen molecules using the mass flow controller on QUEST and calibrating the QMA measurement values based on the hydrogen ion current value at that time. The calibration method is shown below.

Firstly, open gate valve 2 on FESTA to keep the QUEST vacuum vessel being connected to FESTA test chamber, and then close the gate valves of the external exhaust pumps to measure the outgassing using the QMAs. During evacuation, gas trapped in the vacuum vessel wall and any other parts is released, which is called outgassing. To measure such a constant amount, the ion current value is measured by QMA during isolation, gate valves for the pumping closed, which proportionally increase within time. Fig. 3.2.2 shows the changes for hydrogen ion current measured by QMAs on QUEST and FESTA when they are connected. The equation for partial pressure is expressed by

$$V_Q \frac{dp}{dt} = -S \cdot p + q_{wall} \quad (3.2.1)$$

p [Pa] is hydrogen partial pressure, V_Q [m³] is the volume of QUEST vacuum vessel which is about 14 m³, S [m³/s] is the effective pumping speed of the external exhaust pumps, and q_{wall} [Pa · m³/s] is the outgas flow rate from the walls. During the isolation, all gate valves of the exhaust pumps are closed, $S = 0$. The exhaust equation is shown as follows:

$$V_Q \frac{dp}{dt} = q_{wall} \quad (3.2.2)$$

The ion current value I measured by QMA is related to the pressure p , as $p = a \cdot I$, where a [Pa/A] is a proportionality constant that relates the pressure and ion current value measured by QMA and is called the sensitivity coefficient. The equation above can be expressed as follows:

$$V_Q a \frac{dI_{BG}}{dt} = q_{wall} \quad (3.2.3)$$

Here, I_{BG} [A] represents the change of ion current value during outgas measurement by QMA.

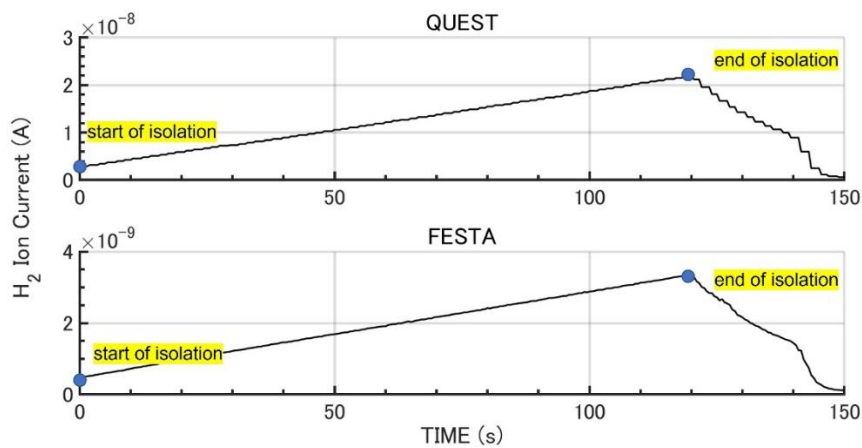


Fig. 3.2.2 The measurement value of the background during the isolation

The isolation is performed from 0 s to 120 s. After that, the measured hydrogen ion current values decreased due to the vacuum pumping by opening the gate valves of the exhaust pumps.

Secondly, after the hydrogen ion current values stabilized due to the vacuum pumping, close the gate valves again to isolate QUEST and FESTA vacuum vessel, and then inject a fixed amount of neutral hydrogen gas at a flow rate of 0.5 ml/min for 10 seconds using the mass flow controller. Fig. 3.2.3 shows the changes in the hydrogen ion current value measured by QMA in QUEST and FESTA during the isolation period. The exhaust equation at this time is as follows:

$$V_Q \frac{dp}{dt} = q_{MF} + q_{wall} \quad (3.2.4)$$

q_{MF} [Pa · m³/s] is the flow rate applied by mass flow. Since the mass flow of hydrogen gas was calibrated using the mass flow controller installed in QUEST [45][51][52], we have the following relationship:

$$1 \text{ Mass flow } \left[\frac{ml}{min} \right] \text{ at room temp.} = 3.4 \times 10^{17} \left[\frac{molecule}{s} \right] \quad (3.2.5)$$

Assuming hydrogen gas as an ideal gas and injecting it at a flow rate of 0.5 ml/min for 10 s, the hydrogen partial pressure at that time can be calculated with the equation, $pV = nkT$ for ideal gas as:

$$\begin{aligned} \Delta p &= \frac{nk_B T}{V_Q} \quad (3.2.6) \\ &= \frac{0.5 \times 3.4 \times 10^{17} \left[\frac{molecule}{s} \right] \times 10[s] \times 1.38 \times 10^{-23} [m^2 kg s^{-2} K^{-1}] \times 373[K]}{14[m^3]} \end{aligned}$$

$$\approx 6.25 \times 10^{-4} [\text{Pa}]$$

To determine the pressure change Δp [Pa] caused only by the injected hydrogen gas, it is necessary to subtract the outgassing from the walls. As a result, the sensitivity coefficient a of the QMA is shown below in Fig. 3.2.3:

$$a = \frac{\Delta p}{I_{QMA} - I_{BG}} \quad (3.2.7)$$

Here, I_{QMA} [A] is the change of ion current value measured by QMA when hydrogen gas was injected using the mass flow controller. Therefore, the measured ion current value obtained from QMA was converted to hydrogen partial pressure by multiplying the sensitivity coefficient a .

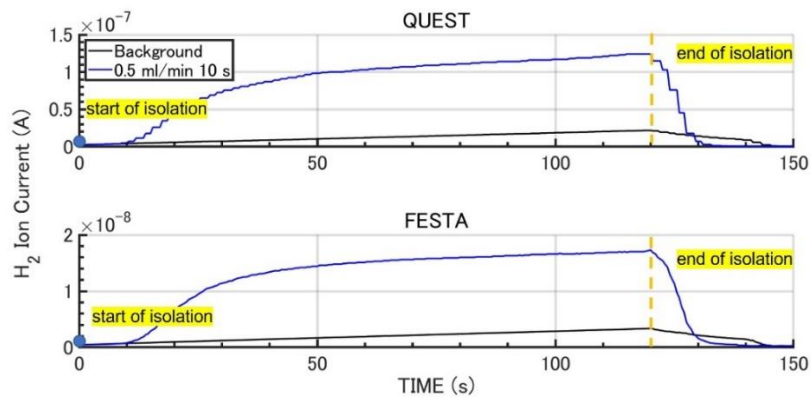


Fig. 3.2.3 Time evolution of measurement values of ion current during isolation when a fixed amount of hydrogen (1.7×10^{17} H₂/s for 10 s) (blue solid line) was injected and background measurement values of ion current (black solid line).

The isolation is performed from 0 s to 120 s. After that, the measured hydrogen ion current values decreased due to the pumping by opening the gate valves of the external pumps.

Section 3 Experiment Overview

Q-shu University Experiment with Steady-State Spherical Tokamak – QUEST is a Spherical Tokamak (ST) device installed in Kyushu University, capable of steady-state operation. ST is a Tokamak device that is more stable than traditional Tokamak devices [53], operating at high β , the ratio of plasma pressure to magnetic pressure, due to the high plasma pressure against the magnetic pressure. It is expected to be a compact and cost-effective plasma experimental device. Various studies have been conducted on QUEST on the interaction between plasma and the plasma-facing walls (PFWs) during steady state operation (SSO), as well as research focusing on non-inductive current drive, resulting in numerous achievements [45].

QUEST is a ST device that has been in operation at Advanced Fusion Research Center, Research Institute for Applied Mechanics, Kyushu University, since October 2008. The main experimental research objectives during the construction of QUEST were as the following three[53].

- Conduct academic research towards achieving high- β SSO, specifically on plasma production and steady-state current drive in a spherical tokamak
- Conduct research on diverter configuration that is suitable for the unique magnetic field configuration of the spherical tokamak and establish particle and heat load control methods over a long period of plasma discharges using diverter configuration.
- Promote comprehensive research on fuel particle recycling control over a long period of plasma discharges, advanced wall control, and plasma performance in the spherical tokamak as a scientific foundation for SSO.

Fig. 3.3.1 shows an overview diagram of QUEST. QUEST has 2 turns \times 8 toroidal

field (TF) coils, and a total current of 800 kA inside the torus when 50 kA is applied by the power supply. This allows the generation of a toroidal magnetic field of 0.25 T at the position of $R = 0.64$ m. In addition, 5 pairs of 10 poloidal field (PF) coils are installed symmetrically above and below the vacuum vessel. One of these pairs, HCU and HCL, have currents flowing in opposite directions on the upper and lower coils, creating a horizontal magnetic field inside the vacuum vessel, which is used for vertical positioning control of the plasma. The other 4 pairs are used to create a vertical magnetic field, with the current flowing in the same direction. In the center stack of the hollow central part of the vacuum vessel, there is a center solenoid (CS) coil, which is used for induction heating (ohmic heating) and shape control of the plasma. In addition, cancellation coils (CC) are installed outside of the PF17 coils to cancel the vertical magnetic field created by the CS coil. Furthermore, only QUEST has fully equipped temperature-control PFWs in the world, which are called hot wall.

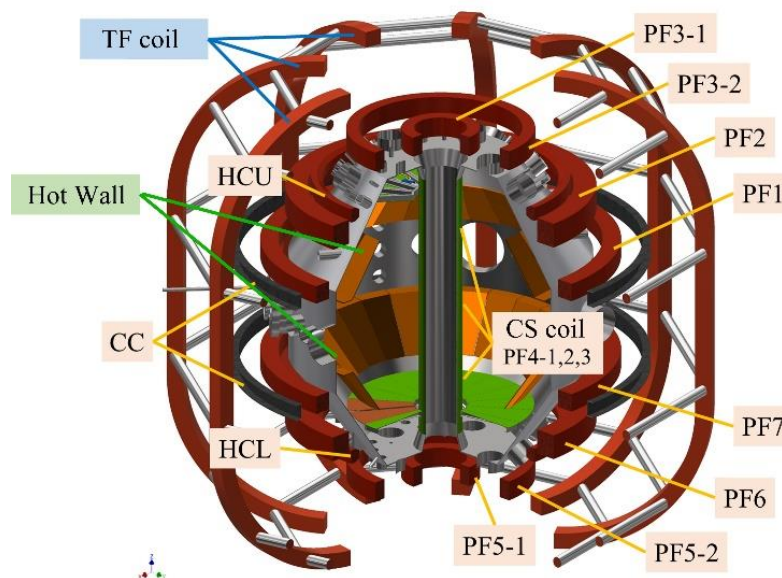


Fig. 3.3.1 The main schematic diagram of QUEST

Table 3.3.1 shows the main parameters of QUEST.

Table 3.3.1 The main parameters of QUEST

	Phase I	Phase II (Steady state)	Phase II (Pulse)	Final Goal
Major Radius R (m)		0.68		0.64
Minor Radius a (m)		0.4		0.36
Aspect Ratio R/a		1.7		1.78
Radius of Vacuum Vessel R_{Vessel} (m)	1.4			
Height of Vacuum Vessel H_{Vessel} (m)	2.8			
Toroidal Magnetic Field B_T (T)	0.25	0.25	0.5	0.25
Plasma Current I_p (Ma)	0.02	0.1	0.3	0.5
Power Injection P_{inj} (MW)	0.45	1	3	3

Section 4 FESTA Experiments

Before plasma discharge starts, the temperature of hot walls was set at 473 K, while the temperature of the QUEST vacuum vessel was set at 373 K. Impurities such as water and oxygen in PFWs were removed by using electron cyclotron resonance (ECR) plasma produced by radio frequency (RF) power at 8.2 GHz and working gas of the wall cleaning is hydrogen. The electron temperature and density of ECR plasma is significantly low, and it is considered that the surface conditions of the wall were not significantly altered except removing water etc.

The magnetic field configuration is an inner limiter configuration where the plasma comes into contact with the limiter located on the center stack side, as shown in Fig. 3.4.1.

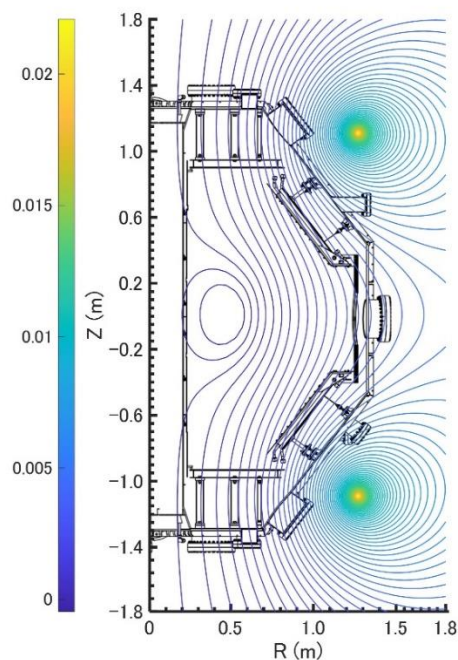


Fig. 3.4.1 The magnetic field configuration of plasma discharge in the FESTA experiments.

In this study, we focused on the release of hydrogen gas from the wall. To minimize the effect of the previous plasma discharge on the measurements, we waited until the hydrogen pressure observed by QMA reached a constant value of 2.5×10^{-5} Pa before each subsequent discharge.

In 2022 Spring/Summer (SS) campaign, plasma discharges were conducted at a hot wall temperature of 473 K, the vacuum vessel temperature of 373 K, electron temperature of 50 eV, and electron density of 10^{17} m^{-3} . Fig. 3.4.2-3.4.7 show the time evolution of plasma current [a.u.], H_α Intensity [a.u.], RF power [kW], radial distribution of electron density [m^{-3}], and electron temperature [eV] and density [m^{-3}] during a typical long-duration plasma discharge in QUEST.

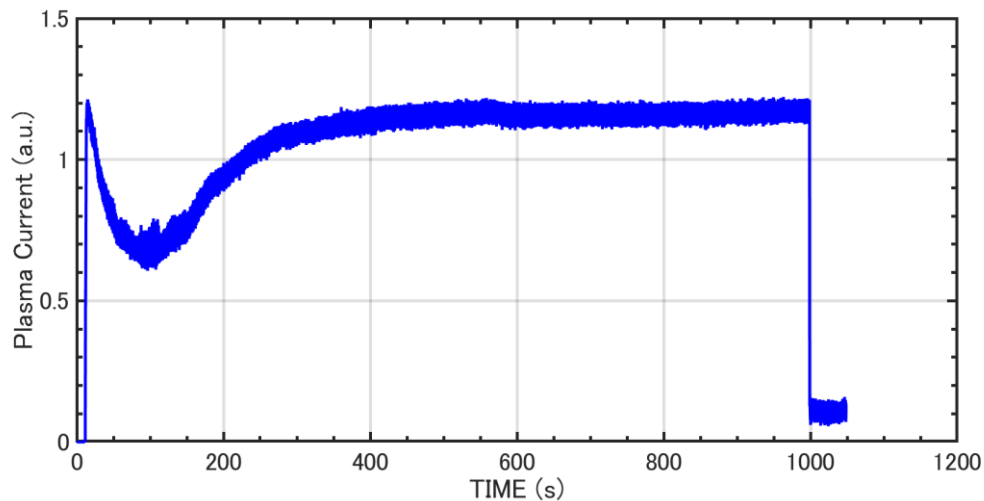


Fig. 3.4.2 Time evolution of plasma current signal

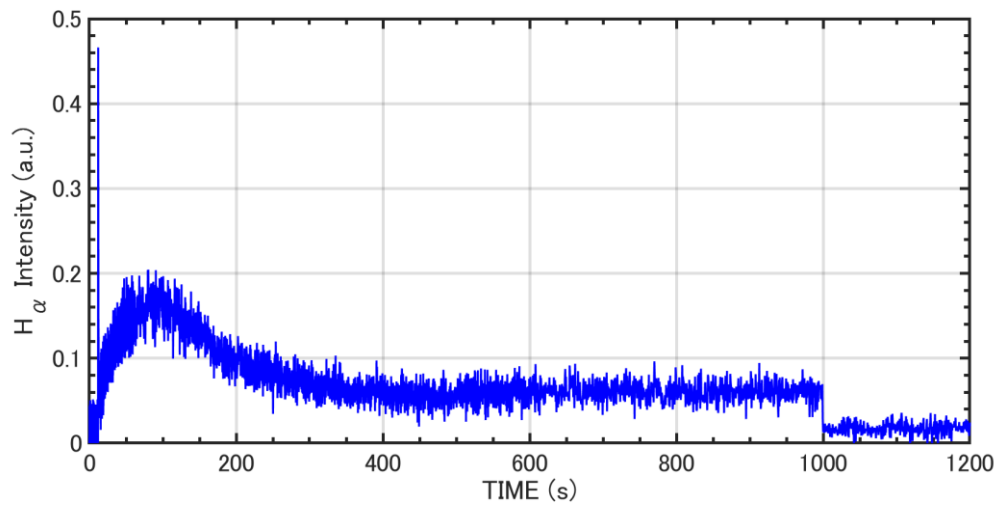


Fig. 3.4.3 Time evolution of H_α Intensity signal

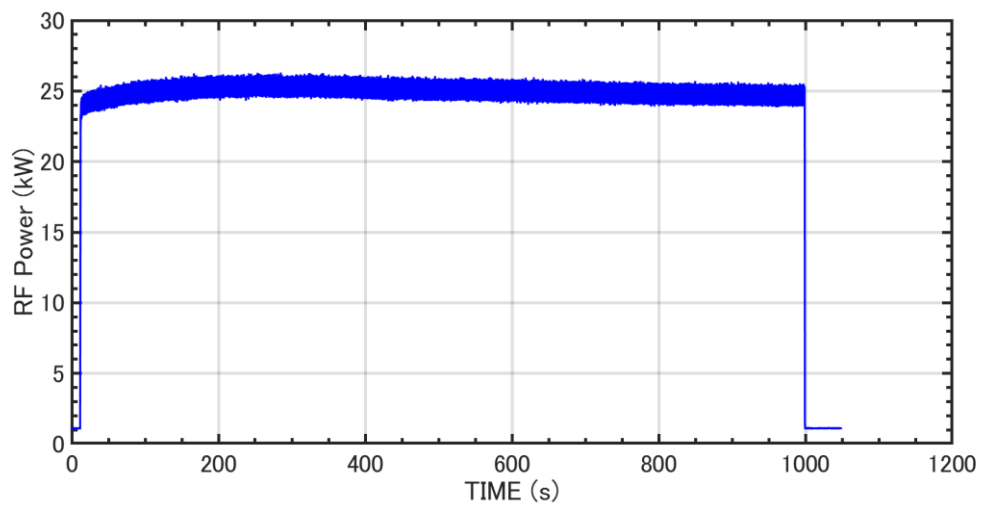


Fig. 3.4.4 Time evolution of RF power

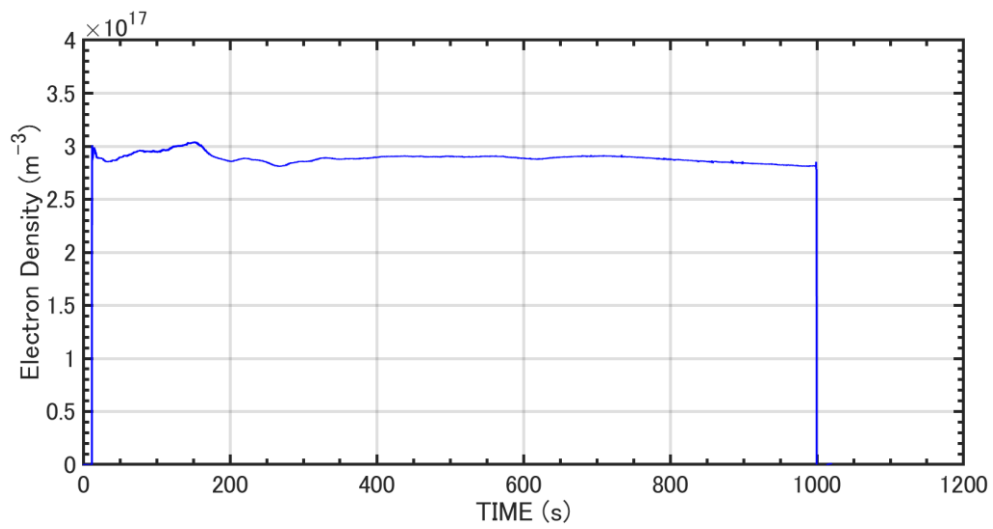


Fig. 3.4.5 Time evolution of electron density

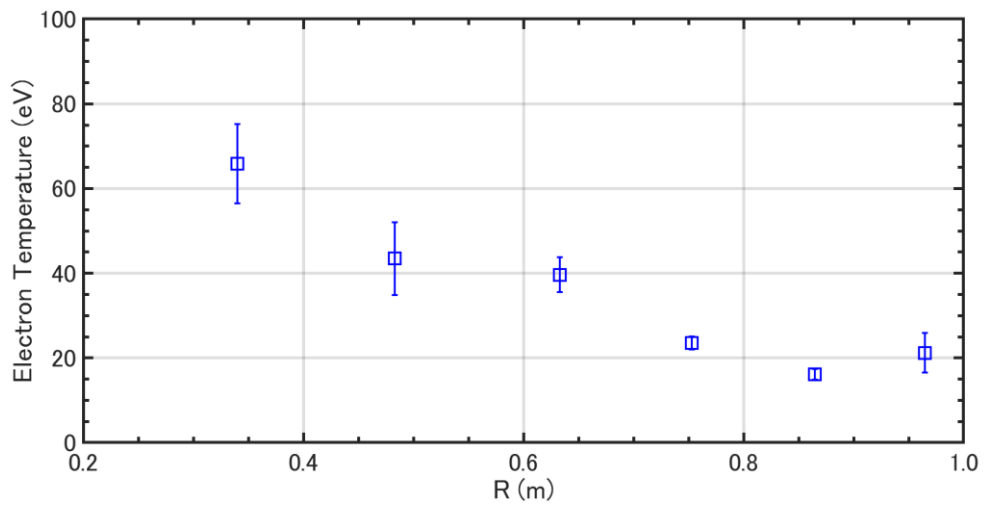


Fig. 3.4.6 Radius distribution of electron temperature

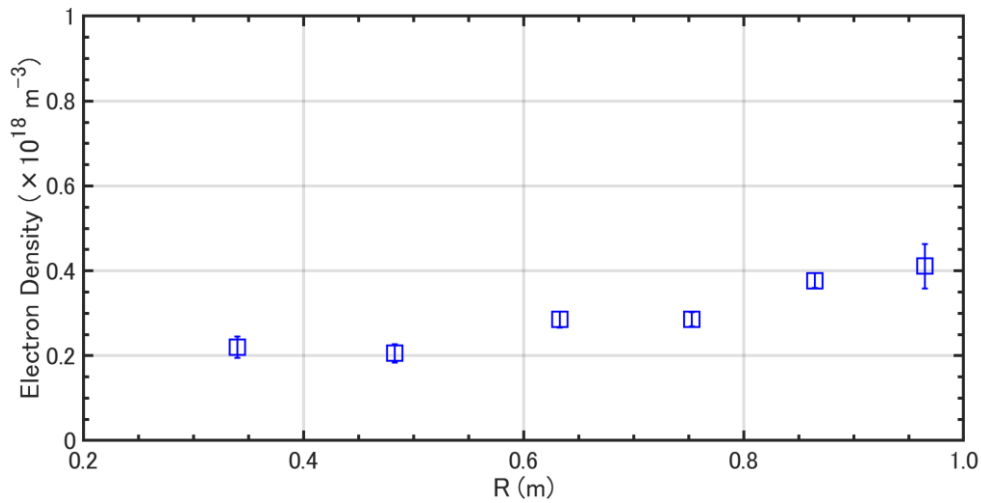


Fig. 3.4.7 Radius distribution of electron density

The plasma current signal and H_{α} Intensity signal are in arbitrary units, and the electron density of the plasma is significantly lower than that of a fusion reactor plasma. Different to hydrogen gas penetration, the penetration of hydrogen ions and atoms with energies of several eVs or higher can penetrate into PFWs. Indeed, phenomena commonly observed in fusion experimental devices such as the formation of plasma-induced redeposition layers[45][52], sputtering [52], and wall saturation [45][52] are also observed in QUEST. As a result, the experimental results obtained in QUEST can be regarded as experimental results of the plasma wall interaction (PWI) predicted in fusion experimental devices.

Section 5 Evaluation of Hydrogen Retention in QUEST and FESTA

3.5.1 Evaluation of Hydrogen Retention in QUEST

Dynamic retention is immediately released after the plasma discharge, so the net particle flux $dH_{wall} [molecule]/dt = \Gamma_{wall} [molecule/s]$ absorbed by the entire QUEST wall can be determined by particle balance, as shown in Eq. 3.5.1, which is the difference between the injected flux ($\Gamma_{in} [molecule/s]$) into the entire wall and the released flux ($\Gamma_{out} [molecule/s]$) from it. When considering the content of Γ_{wall} , the wall absorption flux ($\gamma_{wall} [molecule/m^2/s]$) per unit area is obtained by subtracting the reflected particle flux ($\gamma_{ref} [molecule/m^2/s]$) from the injected particle flux ($\gamma_{in} [molecule/m^2/s]$) per unit area to the wall and subtracting the released flux from the wall ($\gamma_{out} [molecule/m^2/s]$) per unit area.

$$\frac{dH_{wall}}{dt} = \int (1 - R_{ref})\gamma_{in}dS - \int \gamma_{out}dS = \Gamma_{in} - \Gamma_{out} = \Gamma_{wall} \quad (3.5.1)$$

Here, $R_{ref} [-]$ is reflection rate on the wall.

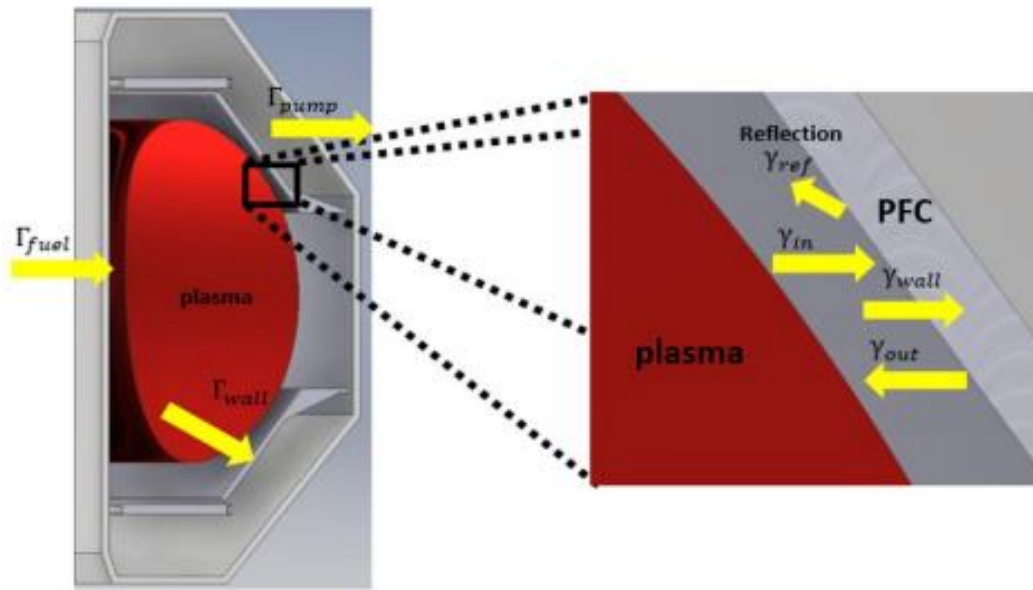


Fig. 3.5.1 Conceptual diagram of local plasma-wall interaction.

Fig. 3.5.2 shows a macroscopic conceptual diagram of particle balance in steady state. Γ_{wall} is balance to the difference between the fuel particle flux supplied externally to the vacuum vessel (Γ_{fuel} [molecule/s]) and the particle flux exhausted by the external pumps (Γ_{pump} [molecule/s]) as shown in Eq. (3.5.2).

$$\Gamma_{fuel} - \Gamma_{pump} - \Gamma_{wall} = 0 \quad (3.5.2)$$

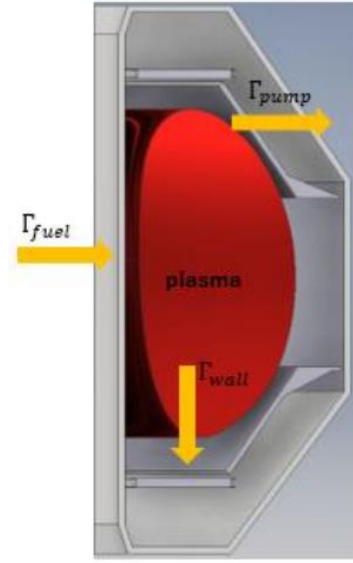


Fig. 3.5.2 Conceptual diagram of macroscopic plasma balance during steady state.

After plasma discharge, there is no further injection of hydrogen particles from the plasma to the wall, so Γ_{in} becomes zero. As shown in Eq. (3.5.1), hydrogen particles are released from the wall to the QUEST vacuum vessel through surface recombination, and a portion of these particles (H_{vv} [molecule]) remains in the QUEST vacuum vessel while the rest (H_{pump} [molecule]) is exhausted by the external pumps. Consequently, Γ_{out} can be expressed as the following Eq. (3.5.3).

$$\Gamma_{out} = \frac{dH_{vv} + dH_{pump}}{dt} \quad (3.5.3)$$

As shown in Fig. 3.5.3, due to wall saturation effect which will be discussed in Chapter 4, when the hydrogen flux released from QUEST PFWs reached peaks, the time variation of the particles in the QUEST vacuum vessel becomes zero ($dH_{vv}/dt = 0$), and Γ_{out} coincides with $dH_{pump}/dt = \Gamma_{pump}$. The ion current measured by QMA is

converted to pressure value as mentioned in previous section, so the Γ_{out} can be evaluated as shown in Fig. 3.5.3.

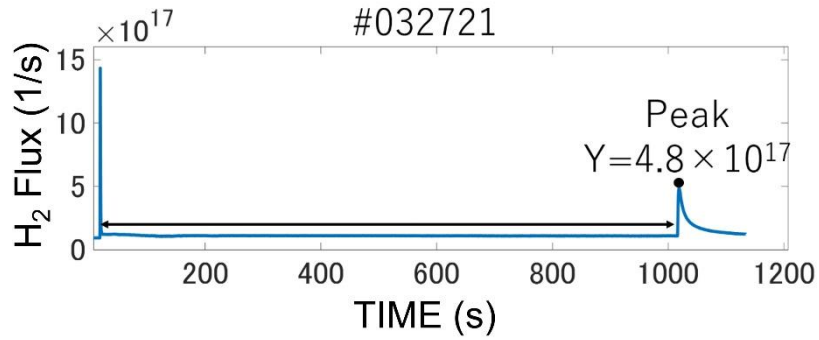


Fig. 3.5.3 Time evolution of the hydrogen flux measured in QUEST vacuum vessel

After the plasma discharge, the hydrogen flux emitted from the wall of the QUEST vacuum vessel was about $\Gamma_{outQ} \approx 4.8 \times 10^{17}$ [molecule/s]. Here the suffix “Q” means the QUEST vacuum vessel.

At the end of the plasma discharge, the number of hydrogen particles released from the QUEST wall is the difference between the incoming and outgoing particle amount, as shown in Fig. 3.5.4, and is approximately $N_{retQ} \approx 2.3 \times 10^{19}$ [molecule].

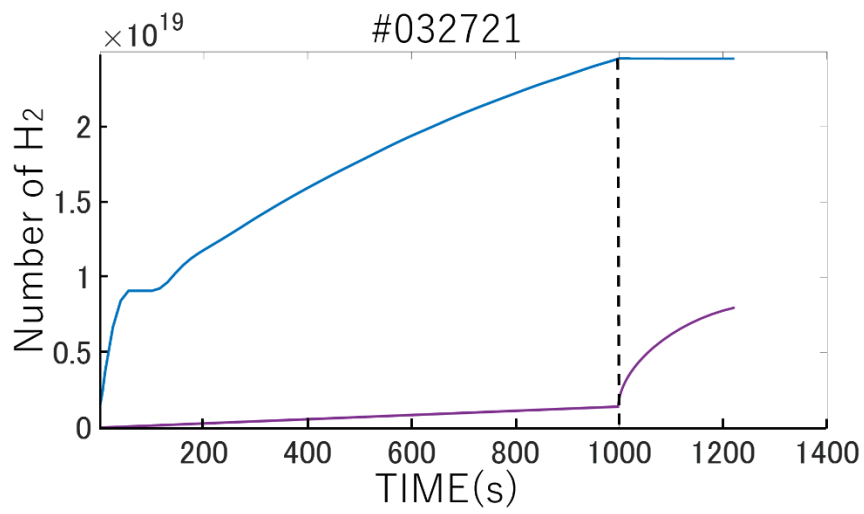


Fig. 3.5.4 Integrated amount of hydrogen particles injected into the QUEST vacuum vessel by mass flow (blue trace), and integrated amount of hydrogen particles pumped out (purple trace). The plasma discharge duration is 1000 s.

3.5.2 Verification of Measurements from FESTA

During FESTA experiment, when the sample is exposed to the plasma, the test chamber is connected to the QUEST vacuum vessel, allowing hydrogen and other gas particles to freely pass-through gate valve 2 as mentioned before. After the sample extracted, when gate valve 1 and gate valve 2 are closed, a certain amount of hydrogen in the test chamber remains as the hydrogen partial pressure background to be measured (N_{backgC}). The background hydrogen amount in the QUEST vessel (N_{backgQ}) is about 6.8×10^{16} [molecule], under the assumption that the gas is assumed to be an ideal gas, their pressures are uniform, and the gas temperature can be regarded as the vacuum vessel temperature, so the hydrogen amount in the test chamber N_{backgC} is

$$N_{backgC} = N_{backgQ} \frac{V_C}{V_Q} \approx 2.4 \times 10^{13} \text{ [molecule]} \quad (3.5.4)$$

where $V_C = 5 \times 10^{-3} [m^3]$ and $V_Q = 14 [m^3]$ are the volume of the FESTA test chamber and the QUEST vacuum vessel, respectively. Here, the suffix “Q” and “C” indicate “QUEST vacuum vessel” and “test chamber”, respectively.

According to Fig. 3.5.3, the number of hydrogen particles released from the plasma-exposed sample after 1000-second plasma exposure can be evaluated by the following Eq. (3.5.5).

$$N_{rets} = N_{retQ} \frac{S_S}{S_Q} \approx 2.2 \times 10^{15} \text{ [molecule]} \quad (3.5.5)$$

Here, $S_S = 2.5 \times 10^{-3} [m^2]$ and $S_Q = 26.6 [m^2]$ are the surface area of the plasma-exposed sample and the PFWs of the QUEST vacuum vessel, respectively. It could be

concluded that the amount of hydrogen particles released from the sample N_{rets} is hundred times more than the background H_2 content in the test chamber N_{backgc} , so N_{backgc} should be negligible. During QUEST hydrogen plasma discharges, hydrogen amount is a main source, as a result, any other elements' amount is not considered in this study.

Moreover, the outgassing flux Γ_{outC} [$molecule \cdot s^{-1}$] from the wall of the test chamber also exists. Before exposing the sample to plasma in FESTA, it is necessary to measure the outflux released from the test chamber. Fig. 3.5.5 shows the calibrated hydrogen gas from the wall of the test chamber, with the FESTA test chamber isolated.

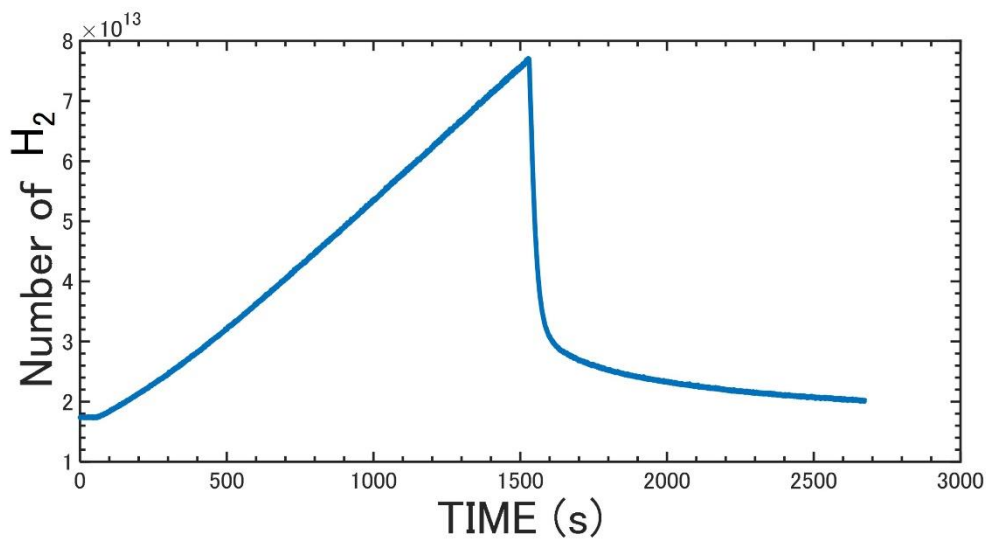


Fig. 3.5.5 Time evolution of hydrogen molecules released from the test chamber was measured by isolating the test chamber. When opening the gate valve of external pumps, followed by evacuation with the external exhaust pumps, the signal dropped.

The released hydrogen flux is indicated by the slope of the curve shown above and is

approximately $\Gamma_{outC} = 4.1 \times 10^{10}[\text{molecule/s}]$. The outflux of hydrogen from the PFWs of QUEST, Γ_{outQ} , can be obtained from the peak in Fig. 3.5.3. Therefore, the hydrogen flux released from the sample can be estimated using the following Eq. (3.5.6):

$$\Gamma_{outs} = \Gamma_{outQ} \frac{S_s}{S_Q} \approx 4.5 \times 10^{13}[\text{molecule/s}] \quad (3.5.6)$$

Γ_{outs} is thousand times larger than Γ_{outC} , so Γ_{outC} could be predicted to be ignored during FESTA experiments.

Section 6 Calculation of Plasma-induced Background Model

However, in actual FESTA measurements, hydrogen gas is not only released from the plasma-exposed sample, but plasma-induced hydrogen also comes into the test chamber and becomes admixed to the measurement. It is believed that there are several processes involved in such a background amount. During FESTA experiment, while exposing the sample to QUEST plasma, gate valve 1 and gate valve 2 are open and the test chamber is connected to the QUEST vacuum vessel. Therefore, hydrogen particles, including charge-exchange hydrogen atoms, pass through the gate valves and moved back and forth. As hydrogen atoms produced by charge-exchange process essentially have high energy, they can pass through gate valve 2 and be more easily absorbed into the inner wall of the test chamber. After extracting the sample and isolating the test chamber, the outgas contains the release of fuel particles absorbed in the wall of the test chamber. The background generated in this process is called plasma-induced background [50]. During plasma exposure, low-energy neutral hydrogen molecules also move back and forth between the FESTA test chamber and the QUEST vacuum vessel and outgassing from the walls of the vacuum vessel also occurs, so the amounts of these also contribute to the background, and Fig. 3.6.1 is showing such background components.

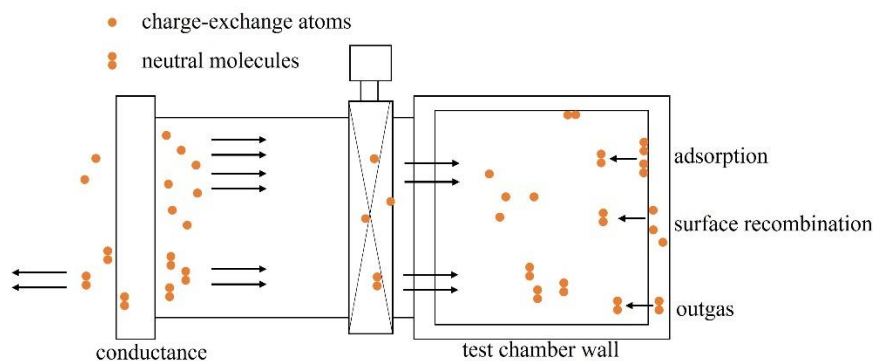


Fig. 3.6.1 Background components in the test chamber released from the test chamber wall

To evaluate the plasma-induced background, a model was created using Eqs. (3.6.1) – (3.6.3).

$$V_c \frac{dy(t)}{dt} = A \cdot Hw(t)^2 + B \cdot gam(t) + outgas + pump(t)(Vv(t) - y(t)) \quad (3.6.1)$$

$$- wallpump(t)y(t) \left(1 - \frac{Sw(t)}{Sw0} \right)$$

$$\frac{dHw(t)}{dt} = (1 - B) \cdot gam(t) - A \cdot Hw(t)^2 \quad (3.6.2)$$

$$\frac{dSw(t)}{dt} = wallpump(t)y(t) \left(1 - \frac{Sw(t)}{Sw0} \right) \quad (3.6.3)$$

V_c [m^3] and $y(t)$ [$molecule/m^3$] on the left side of Eq. (3.6.1) represent the volume of the test chamber and the number of hydrogen molecules per unit volume in it, respectively. The first term on the right side is the released hydrogen flux due to plasma-induced background, where coefficient A [m^4/s] indicates surface recombination effect and $Hw(t)$ [$atom/m^2$] represents the number of hydrogen atoms absorbed in the test chamber wall. The second term indicates the charge-exchange hydrogen flux coming from plasma. Part of them is injected into the test chamber wall and the remains exist in the test chamber, which expressed through a constant B [–]. This phenomenon is denoted using $gam(t)$ [$atom/s$] which represents the charge-exchange hydrogen flux coming from the QUEST vacuum vessel during plasma discharge. The third term is showing the outgassing effect from the test chamber wall, expressed by $outgas$ [$molecule/s$]. The fourth term is the hydrogen flux due to the pressure difference between QUEST and FESTA vacuum vessel, where $pump(t)$ [m^3/s] is the conductance between the QUEST and FESTA vacuum vessels and $Vv(t)$ [$molecule/$

m^3] represents the number of hydrogen molecules per unit volume in the QUEST vacuum vessel. The fifth term is expressed as surface adsorption effect, where $Sw(t)$ [–] and $Sw0$ [–] represents the number of hydrogen particles adsorbed on the surface of the test chamber wall and the adsorption sites on the test chamber wall [54], and $wallpump(t)$ [m^3/s] is the surface adsorption coefficient of the test chamber wall. During plasma discharge, high-speed hydrogen atoms fly into, and the surface is activated, making sticking less likely. Therefore, the surface adsorption coefficient is assumed to be zero when gate valve 2 is open during plasma discharges. When the plasma exposure ends, there are almost no adsorbed particles on the surface, reflecting that adsorption is more likely to occur.

Section 7 Practical Application of Plasma-induced Background Model in FESTA Experiments

As mentioned in the previous section, it is necessary to subtract the plasma-induced background in order to measure the hydrogen released from plasma-exposed sample. A mock operation shown in Fig. 3.7.1 without a sample was performed using the same procedure as the sample exposure.

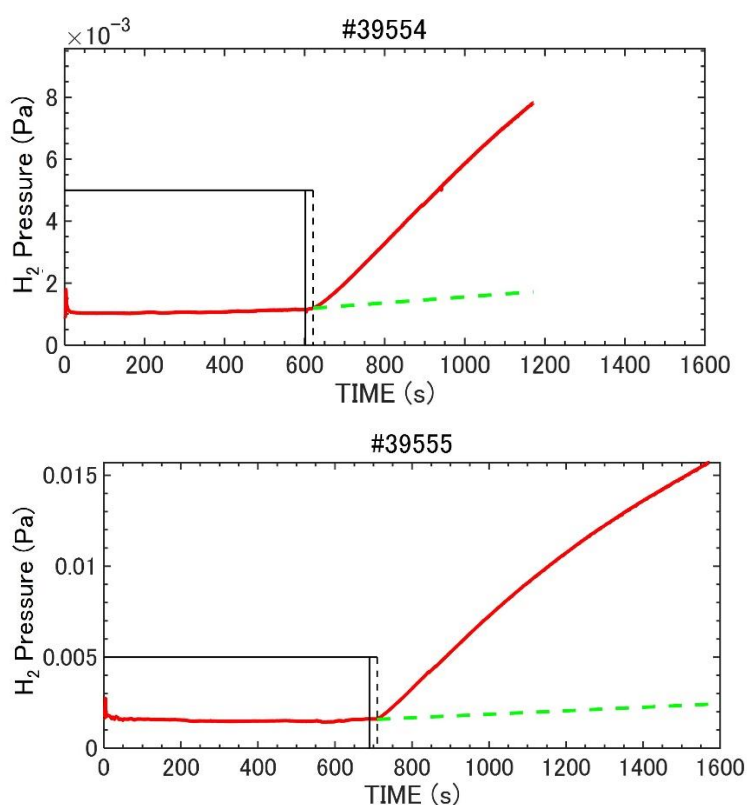


Fig. 3.7.1 Time evolution of the hydrogen partial pressure in FESTA test chamber measured with a mock operation (#39554 (top) and #39555 (bottom)). The black solid square line indicates the plasma discharge, and the black dashed line indicates the timing of closing gate valve 1 and gate valve 2. The dashed green line represents the outgas released from the wall of the isolated test chamber measured before FESTA experiments. The red lines show the pronounced outgassing of the test chamber walls after it is exposed to a plasma discharge.

From the results of the mock operation (#39554 (top) and #39555 (bottom)), it is observed that the plasma discharge started from $t = 0$ s, and the hydrogen partial pressure in the test chamber was almost constant before closing gate valves 1 and 2. When gate valves 1 and 2 were closed, the hydrogen partial pressure increased, but there was a clear difference in the hydrogen partial pressure in the test chamber between #39554 and #39555 measurements as shown in Fig. 3.7.2, which indicates the influence of plasma-induced background.

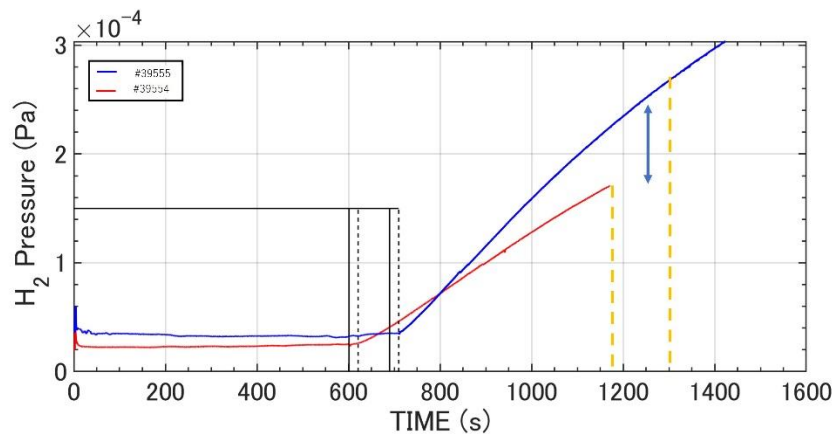


Fig. 3.7.2 Time evolution of the hydrogen partial pressure in FESTA test chamber measured with a mock operation (#39554 (red) and #39555 (blue)). The pressure in the test chamber between two measurements were different after isolating the test chamber for about 600 s as shown the yellow dashed line.

As shown in Fig. 3.7.3, the experiment conditions during the FESTA mock operation (#39554 & #39555) are shown as H_{α} intensity signal, RF power and TF current for #39554 and #39555, respectively.

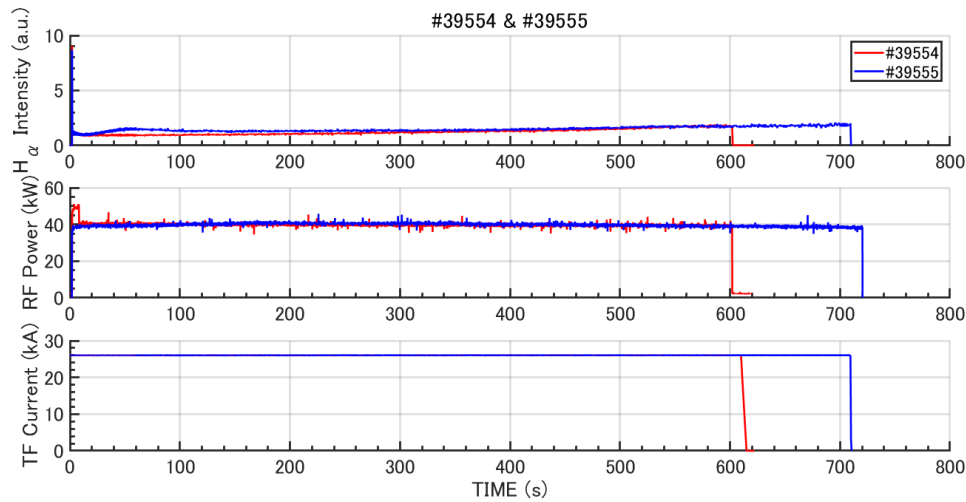


Fig. 3.7.3 Time evolution of H_{α} intensity signal, RF Power and toroidal coil current during mock operation in #39554 (red line) and #39555 (blue line)

When neutral particles collide with electrons, they will be ionized, and then plasma is generated. The ionization rate is proportional to the H_{α} intensity [52][55]. When the electron density is steady, the ionization rate of neutral particles and the particle flux lost from the plasma per unit time are balanced. According to calculations, the charge-exchange particle flux by collisions is also proportional to the H_{α} intensity [52][55]. As a result, the particle flux injected to the PFWs is proportional to the H_{α} intensity. The number of ionized hydrogen particles and charge-exchange hydrogen particles is proportional to the H_{α} intensity [45]. $game(t)$ in the plasma-induced background model could be evaluated from H_{α} intensity. Assuming a constant H_{α} intensity, $game(t)$ is experimentally determined as shown in the figure. After the plasma discharge, it becomes zero. The RF power and TF coil current of #39554 and #39555 have the same waveform during the plasma discharge duration. All plasma discharge conditions were similar for both discharges (#39554 and #39555) except the duration of plasma

discharges, indicating clearly that a plasma-induced background was present. The initial value of the plasma-induced background is determined by the number of hydrogen partial pressure present in the FESTA test chamber before the start of the plasma discharge. Furthermore, as mentioned in the previous section, the $game(t)$ and $outgas(t)$ are determined by H_α intensity and the hydrogen outgassing flux released from the test chamber wall, respectively. To match the simulated measurement data, the coefficients of the plasma-induced background model, were determined one by one according to the following equation.

$$V_c \frac{dy(t)}{dt} = 0.03 \times 10^{-6} Hw(t)^2 + 0.87 gam(t) \quad (3.7.1)$$

$$+ outgas + pump(Vv(t) - y(t)) - wallpump(t)y(t)\left(1 - \frac{Sw(t)}{Sw0}\right)$$

$$\frac{dHw(t)}{dt} = 0.13 gam(t) - 0.03 \times 10^{-6} Hw(t)^2 \quad (3.7.2)$$

$$\frac{dSw(t)}{dt} = wallpump(t)y(t) \left(1 - \frac{Sw(t)}{Sw0}\right) \quad (3.7.3)$$

As shown in Fig. 3.7.4, the background model was used to predict the time evolution of hydrogen partial pressure in the test chamber by substituting the plasma discharge duration.

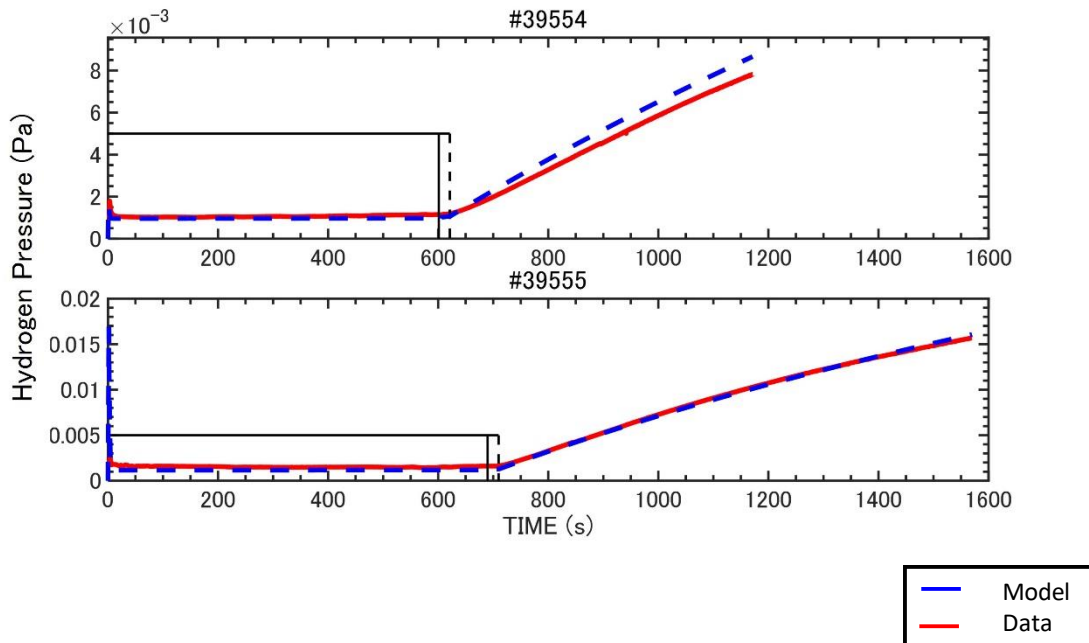


Fig. 3.7.4 Hydrogen pressure data without sample (solid lines) and the model calculation (dashed lines) from the start of plasma discharge to the end of measurement in #39554 (top) and #39555 (bottom). The coefficients of the model calculation were not changed, only the plasma discharge duration was varied in the two discharges.

The accuracy of the background model has been verified by performing mock FESTA operations without sample for several ten times. In Fig. 3.7.5 as shown the red solid line, the background hydrogen flux predicted by the background model matches the measured background hydrogen flux obtained by FESTA as a positive correlation. Moreover, Fig 3.7.5 gives an error-range for the background model as well.

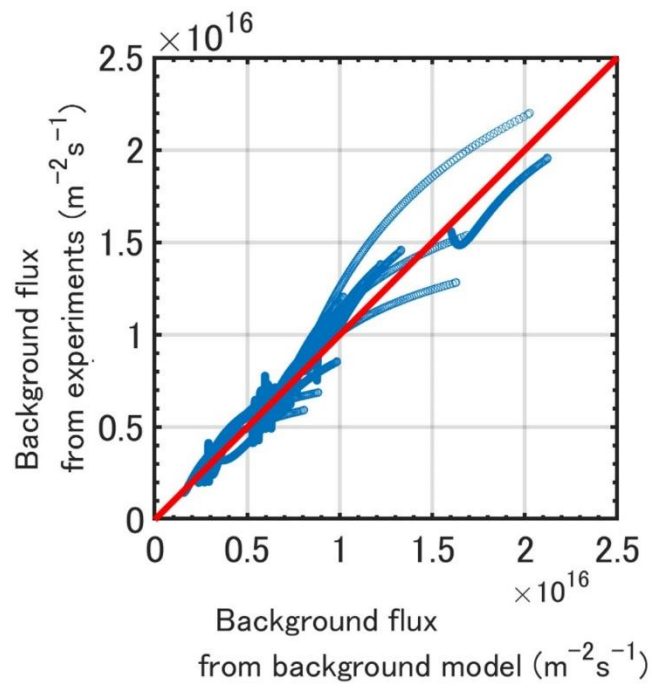


Fig. 3.7.5 The measured background hydrogen flux in FESTA experiment is almost proportional to the predicted hydrogen flux by the background model.

Chapter 4 Measurement of Hydrogen Recycling

Section 1 Plasma-exposed Sample

In this study, hydrogen recycling was evaluated by exposing a sample to the QUEST plasma using FESTA. Fig. 4.1.1 shows the sample used in this experiment. The sample is a circular substrate made of tungsten (W) provided by Nilaco Co. with a diameter of 60 mm and a thickness of 0.5 mm. There is a hole on the sample surface that allows a sample catcher at the tip of movable arm to pass through. Before starting the FESTA experiment, the sample was cleaned using ethanol and ultrasonic cleaning.

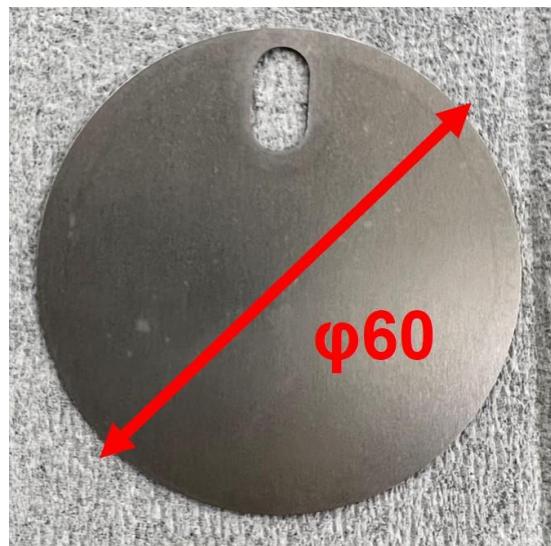


Fig. 4.1.1 Tungsten sample used in FESTA experiments

Section 2 Measurement of Hydrogen Recycling Using FESTA

The following Fig. 4.2.1 shows the position of the sample exposed to the QUEST long-duration hydrogen plasma during FESTA experiments.

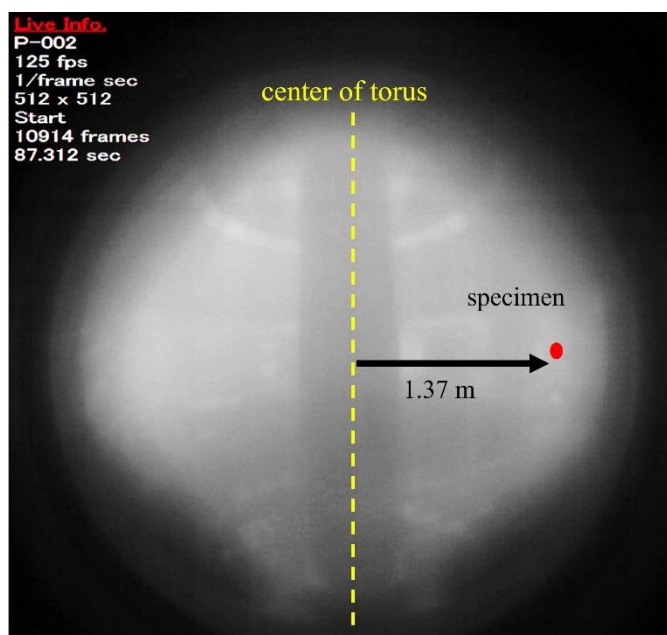


Fig. 4.2.1 A photo of QUEST tokamak plasma and the position of plasma-exposed specimen in shot #48772

The image of plasma is taken by fast camera and the specimen was set at 1.37 m from the center of torus indicated by yellow dotted line. The dark black rectangle at the center of the photo is the center stuck of QUEST.

In the experiment, the sample temperature measured by thermocouples is shown in Fig. 4.2.2. During plasma exposure, the background temperature in the test chamber increased from 303 K to 305 K. When the sample was extracted from exposure by FESTA and left in the test chamber, the temperature rapidly increased to 308 K as soon as it was placed on the sample stage. It should be noted the data from 0 s to 910 s is not

the specimen temperature, because the specimen is not located on the stage during the plasma exposure.

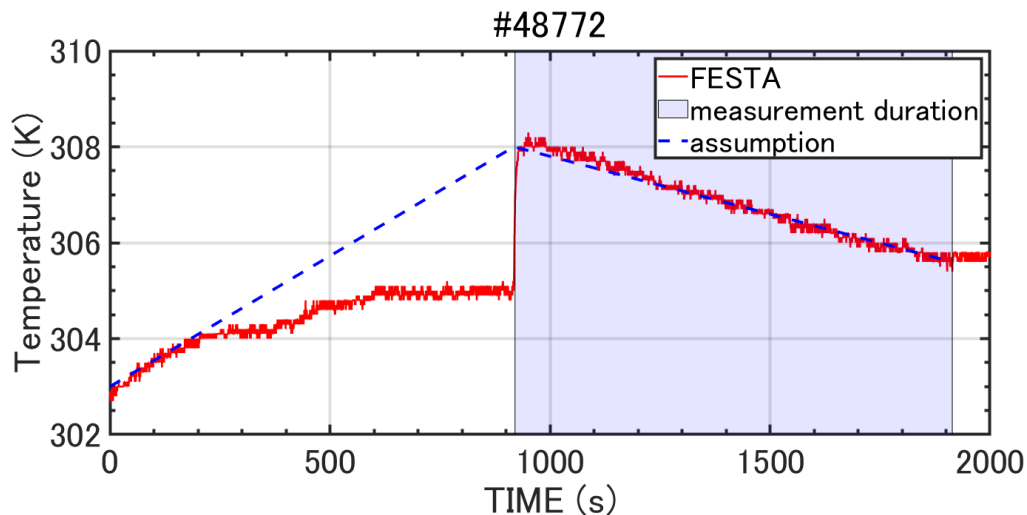


Fig. 4.2.2 Time evolution of temperature of plasma-exposed specimen during and after plasma discharge in #48772. The blue dashed line indicates an assumed temperature of the specimen during the plasma exposure. The hatched area denotes the duration of the hydrogen recycling measurement.

As shown in Fig. 4.2.2, the temperature measured by the thermocouples increased during plasma exposure due to plasma, charge exchange, wall radiation, and RF deposition, but it was still near room temperature. In this experiment, it was assumed that the sample temperature is proportional to the plasma exposure time, as shown by the blue dashed line. Such temperature changes will be considered in the model calculations which will be described later. Additionally, the measured temperature was much lower than the hot wall temperature (~ 473 K), indicating that the surrounding hot wall did not affect the FESTA sample temperature. It was also observed that when the plasma-exposed sample was placed on the sample stage, the temperature gradually

decreased due to thermal radiation and conduction.

In the experiment, the W sample was exposed to the QUEST plasma under the same conditions as previously mentioned for three consecutive discharges with a 70-minute interval between each discharge, which could allow sufficient hydrogen particle release [20]. Fig. 4.2.3 shows the hydrogen partial pressure in the FESTA test chamber after three consecutive plasma exposures.

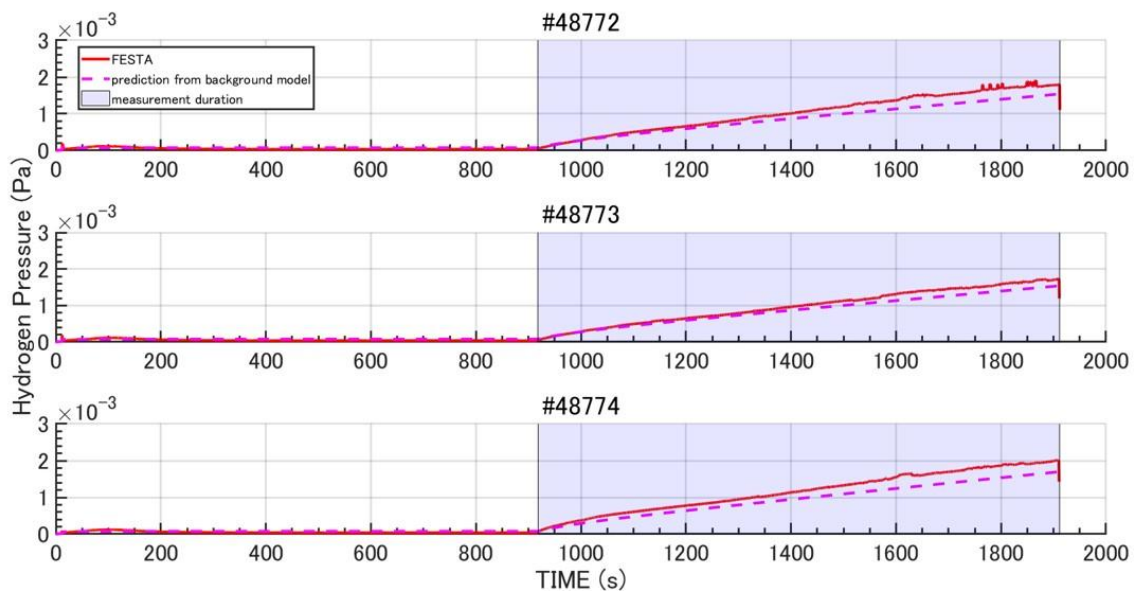


Fig. 4.2.3 Time evolution of hydrogen pressure in #48772 - #48774 from the start of the plasma discharge to the end of the FESTA measurement. The duration when the test chamber is isolated is denoted by the hatched area. The duration of plasma exposure is from the 0 s to 910 s before the hatched area. The experiment data are shown by the red solid line, and the pink dotted line represents the background predicted by the background model.

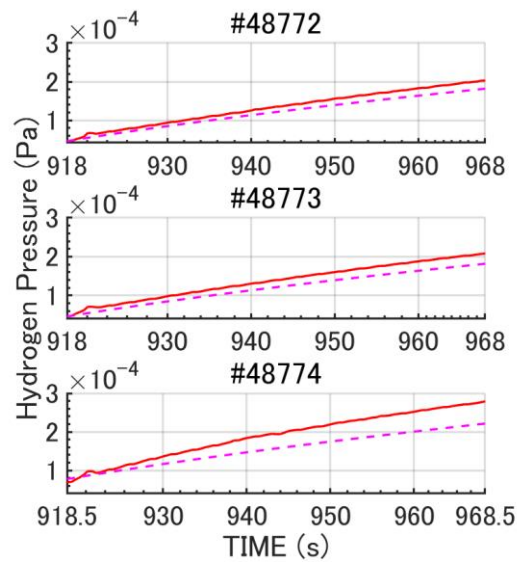


Fig. 4.2.4 Time evolution of hydrogen partial pressure inside the test chamber within 50 seconds after extracting the sample and isolating the test chamber

Fig. 4.2.4 shows the time evolution of the hydrogen partial pressure in the FESTA test chamber during the first 50 seconds of the measurement after isolation. It is observed that the hydrogen gas released from the sample gradually increased due to consecutive plasma exposures. The expected gas release from the FESTA chamber, based on the background model, is shown as the pink dashed line. The observed hydrogen partial pressure is larger than the predicted background release from the model, indicating that hydrogen desorption from the plasma-exposed sample just after the QUEST plasma exposure can be measured with FESTA. The time derivative of the hydrogen flux released from the plasma-exposed sample was also obtained as shown in Fig. 4.2.5.

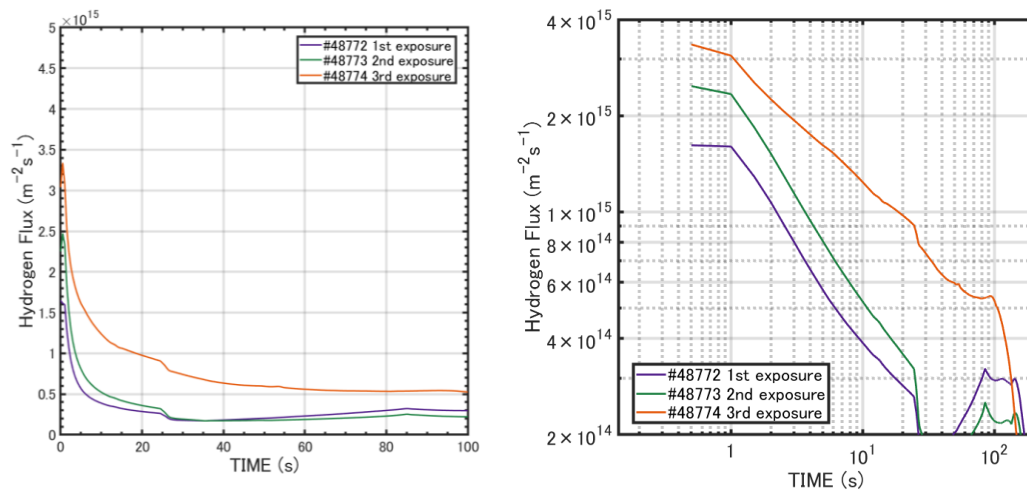


Fig. 4.2.5 (a) Time evolutions of the hydrogen flux released from the exposed specimen from the beginning of the isolation of the test chamber to the end of measurement in #48772 - #48774 are plotted in the linear scale. (b) The same data are plotted in the logarithmic axes.

Section 3 Verification and Analysis of Experimental Data

To verify the experimental data and clarify the physical processes, a two-layer model was constructed and analyzed, as shown in Fig. 4.3.1.

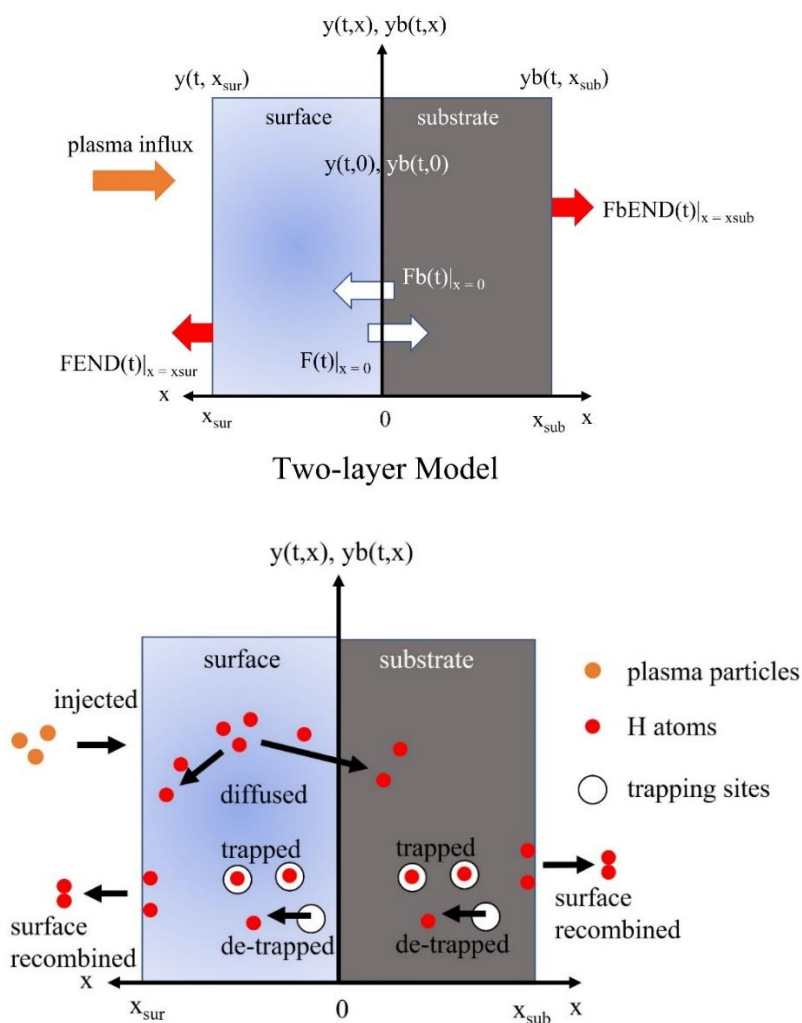


Fig. 4.3.1 Two-layer model schematic figure and main physical process in each layer.

The above figure displays the definition of x-coordinates, y-coordinates, and the hydrogen concentration $y(t, x)$ on the surface and $y_b(t, x)$ in the substrate.

The below figure displays the main physical process: injection, diffusion, trapping, de-trapping, and surface recombination in the two-layer model. The desorption of hydrogen is assumed to be only in the surface layer.

The figure above shows a two-layer model used to distinguish possible physical processes and analyze the experimental data from the previous chapter. In the surface layer, surface recombination, deposition distribution, trap/de-trapping, and diffusion are considered. In the substrate layer, only deposition distribution is not considered. In two-layer model, the boundary is set between the surface layer and the substrate at $x = 0$ for convenience in the calculations. $FEND(t)$ [$m^{-2}s^{-1}$] and $F(t)$ [$m^{-2}s^{-1}$] represent the hydrogen fluxes released on the sample surface $x = x_{sur}$ and on the boundary at $x = 0$, respectively. Here, x_{sur} represents the thickness of the sample surface, and $x_{sur} = 10nm$ in the calculation according to the TRIM code [56]. The deposition length was obtained less than 10 nm at then injection hydrogen particles energy of ~ 0.03 keV during plasma exposure. $FbEND(t)$ [$m^{-2}s^{-1}$] and $Fb(t)$ [$m^{-2}s^{-1}$] represent the hydrogen fluxes released on the sample substrate surface at $x = x_{sub}$ and on the boundary at $x = 0$, respectively. Here, x_{sub} represents the thickness of the substrate, and $x_{sub} = 50000x_{sur}$ in the calculation as the plasma-exposed sample thickness. Since the sample surface is complex, the analysis is performed using the diffusion equation for hydrogen atoms, which includes surface recombination, trapping, and de-trapping effects, in the two-layer model as shown in Eqs. (4.3.1) – (4.3.2)

$$\frac{\partial y(t, x)}{\partial t} = D(T) \frac{\partial^2 y(t, x)}{\partial x^2} + SRC(t, x) - \frac{\partial y_{trap}(t, x)}{\partial t} \quad (4.3.1)$$

$$\frac{\partial y_b(t, x)}{\partial t} = D(T) \frac{\partial^2 y_b(t, x)}{\partial x^2} - \frac{\partial y_{trapb}(t, x)}{\partial t} \quad (4.3.2)$$

$$\frac{\partial y_{trap}(t, x)}{\partial t} = a_{tk} \cdot y(t, x) k_{untrap}(t, x) - a_{dk} \cdot y_{trap}(t, x) \quad (4.3.3)$$

$$\frac{\partial y_{trapb}(t, x)}{\partial t} = a_{tk} \cdot y_b(t, x) k_{untrap}(t, x) - a_{dk} \cdot y_{trapb}(t, x) \quad (4.3.4)$$

$$F(t) = -D(T) \frac{\partial y(t, x)}{\partial x} \Big|_{x=0}, Fb(t) = D(T) \frac{\partial yb(t, x)}{\partial x} \Big|_{x=0} \quad (4.3.5)$$

$$F(t) = -Fb(t), \text{ at } x = 0 \quad (4.3.6)$$

$$FEND(t) = D(T) \frac{\partial y(t, x)}{\partial x} \Big|_{x=x_{sur}} = 2K_r(T)y^2(t, x) \Big|_{x=x_{sur}} \quad (4.3.7)$$

$$FbEND(t) = -D(T) \frac{\partial yb(t, x)}{\partial x} \Big|_{x=x_{sub}} = 2K_r(T)y^2(t, x) \Big|_{x=x_{sub}} \quad (4.3.8)$$

$$y(0, x) = 0; yb(0, x) = 0; ytrap(0, x) = 0; ytrapb(0, x) = 0 \quad (4.3.9)$$

Above the equations, the diffusion coefficient $D(T)$ [m^2s^{-1}], recombination coefficient $K_r(T)$ [m^4s^{-1}], trapping coefficient $a_{tk}(T)$ [s^{-1}], and detrapping coefficient $a_{dk}(T)$ [s^{-1}] depend on sample temperature. It is assumed that the hydrogen fluxes from the sample surface and the substrate side is opposite, as shown in Eqs. (4.3.5) – (4.3.8). The hydrogen concentration $y(t, x)$ [m^{-3}] on the sample surface as a function of time is related to three processes: diffusion of hydrogen atoms, distribution of incident hydrogen atoms, and changes in the concentration of hydrogen atoms captured at trapping sites, as shown in Eq. (4.3.1). The hydrogen concentration $yb(t, x)$ [m^{-3}] in the sample substrate layer with respect to time, as shown in Eq. (4.3.2) is only related to the other two processes the same as that in Eq. (4.3.1) with hydrogen deposition excluded. The first term on the right-hand side of Eqs. (4.3.1) and (4.3.2) represent the diffusion processes in the W sample, and the diffusion coefficient $D(T) = 1.5 \times 10^{-10} \exp(-0.25 [eV]/RT)$ was obtained in previous studies [29]. Here, R [$JK^{-1}mol^{-1}$] is the gas constant and T [K] is the sample temperature. The second term in Eq. 4.3.1 represents the generation of dissolved hydrogen atoms in the surface layer due to the incident hydrogen atoms. The amount of dissolved hydrogen atoms generated $SRC(t, x)$ is expressed in Eq. (4.3.10).

$$SRC(t, x) = \begin{cases} \frac{F_{avg} \cdot \exp\left(-\frac{(x - x_{sur} + x_0)^2}{x_w^2}\right)}{\int_0^{x_{max}} \exp\left(-\frac{(x - x_{max} + x_0)^2}{x_w^2}\right) dx}, & 0 \leq t < tpulse \\ 0, & t > tpulse \end{cases} \quad (4.3.10)$$

The symbols F_{avg} , x_w , x_0 and $tpulse$ in the equation above represent the average injected hydrogen flux during plasma discharge, e-holding length of deposition distribution, peak depth of the deposition distribution in the W sample [27][29][56], and the plasma exposure time, respectively. The third term in Eq. (4.3.1) and the second term in Eq. (4.3.2) represent the trapping and de-trapping processes related to the hydrogen activation energy of the trapping sites, and their details are expressed in Eqs. (4.3.3) and (4.3.4). The trapping coefficient is given as $a_{tk}(T) = D(T)/\lambda^2$, which represents the trapping rate per unit time by the trapping sites, indicating the frequency of passing through the lattice by diffusion. The lattice constant of W, $\lambda = 0.3165 \text{ nm}$, is referred to the database [57]. The de-trapping coefficient is $a_{dk}(T) = \nu_0 \exp(-E_d [eV]/k_B T)$, where $\nu_0 = 10^{13} [\text{s}^{-1}]$ is the Debye frequency and E_d is the activation energy of the trapping sites. The remained parameters $k_{untrap}(t, x)$ and $kb_{untrap}(t, x)$ in Eqs. (4.3.3) and (4.3.4), representing the rate that the trapping sites in the W sample still not capturing hydrogen atoms, are expressed as follows.

$$k_{untrap}(t, x) = \begin{cases} 1 - \frac{y_{trap}(t, x)}{y_{trap_0}}, & y_{trap}(t, x) \leq y_{trap_0} \\ 0, & y_{trap}(t, x) > y_{trap_0} \end{cases} \quad (4.3.11)$$

$$kb_{untrap}(t, x) = \begin{cases} 1 - \frac{y_{trapb}(t, x)}{y_{trapb_0}}, & y_{trapb}(t, x) \leq y_{trapb_0} \\ 0, & y_{trapb}(t, x) > y_{trapb_0} \end{cases} \quad (4.3.12)$$

Here, $y_{trap_0} = y_{trapb_0} [m^{-3}]$ represent the trapping sites density in the W sample. The required boundary and initial conditions for the calculation are shown in Eqs. (4.3.5) - (4.3.9).

On the sample surface $x = x_{sur}$, hydrogen is released as a molecule due to surface recombination effect as $K_r(T)y^2(t, x_{sur})$. As explained in the Chapter 2, determination of recombination coefficient $K_r(T)$ is important in this calculation. Additionally, quantifying the determination of hydrogen surface recombination coefficient in tungsten is significant, as shown in Fig. 2.1.2 and Fig. 2.2.3, so determining $K_r(T)$ is essential in the quantitative analysis through FESTA experiments.

The hydrogen desorption from the plasma-exposed sample using FESTA can be calculated by substituting the two-layer model with the sample temperature and plasma discharge conditions. In the calculation, Franzen's parameters (~ 600 K) [29][30], which are currently the most suitable for FESTA experiments, were used. The recombination coefficient of the plasma-exposed W sample at room temperature is evaluated as $K_r = 3.9 \times 10^{-33} m^4 s^{-1}$.

The results of the model calculations with the above parameters and experimental data are shown in Fig. 4.3.2. In the model calculations, only the initial conditions are changed, where the initial conditions in the first plasma exposure are shown as Eq. (4.3.9), and those in the second and third plasma exposure calculations were used the previous results, which are shown in Figs. 4.3.3-4.3.6.

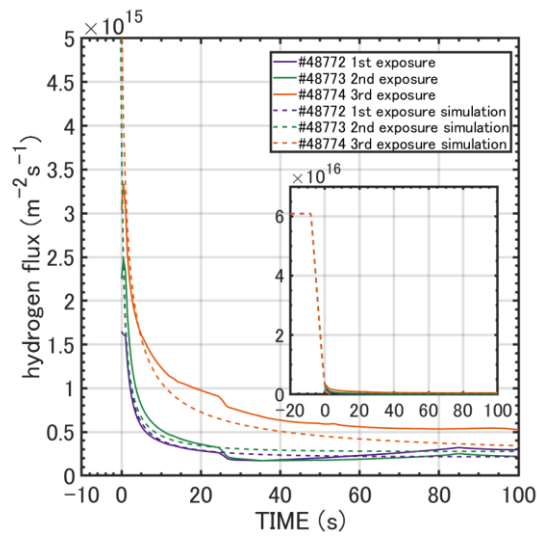


Fig. 4.3.2 Time evolution of hydrogen flux released from the plasma-exposed W specimen. The solid lines represent the experimental data, and the dashed lines show the simulations using the two-layer model from #48772 - #48774. The inset figure shows the hydrogen released fluxes before it is extracted into the FESTA test chamber.

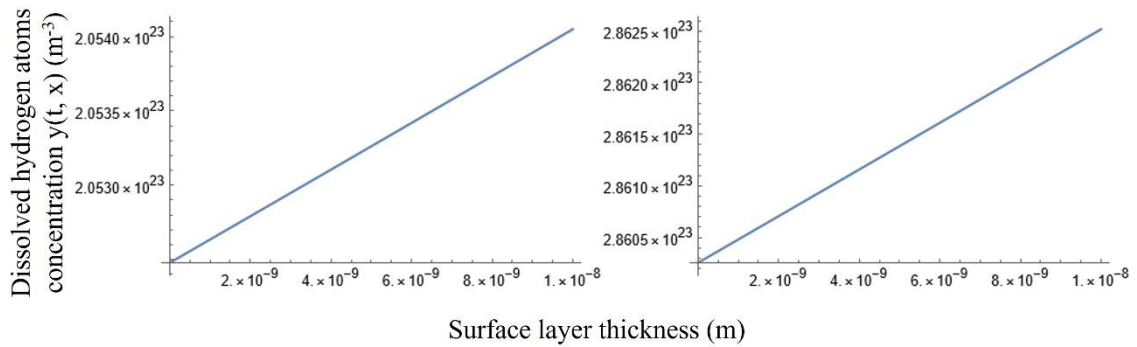


Fig. 4.3.3 Dissolved hydrogen atoms concentration profiles in the surface layer after the first (#48772 left) and second (#48773 right) measurement, which are viewed as the initial conditions in the next plasma exposure.

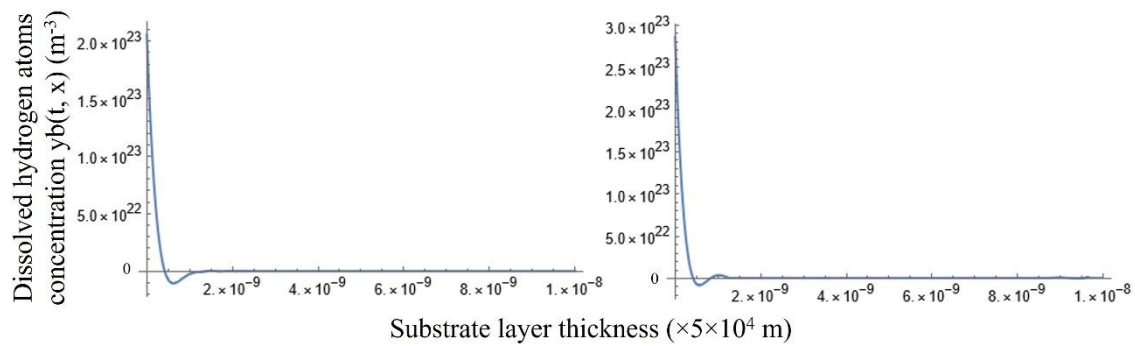


Fig. 4.3.4 Dissolved hydrogen atoms concentration profiles in the substrate layer after the first (#48772 left) and second (#48773 right) measurement, which are viewed as the initial conditions in the next plasma exposure. Due to the mesh in the model calculation for 0.5 mm substrate thickness in the calculation was still rough, a little calculation error happened, shown as the minus data. However, it could be predicted that hydrogen atoms could not be able to diffuse till ~25 μm depth in the sample.

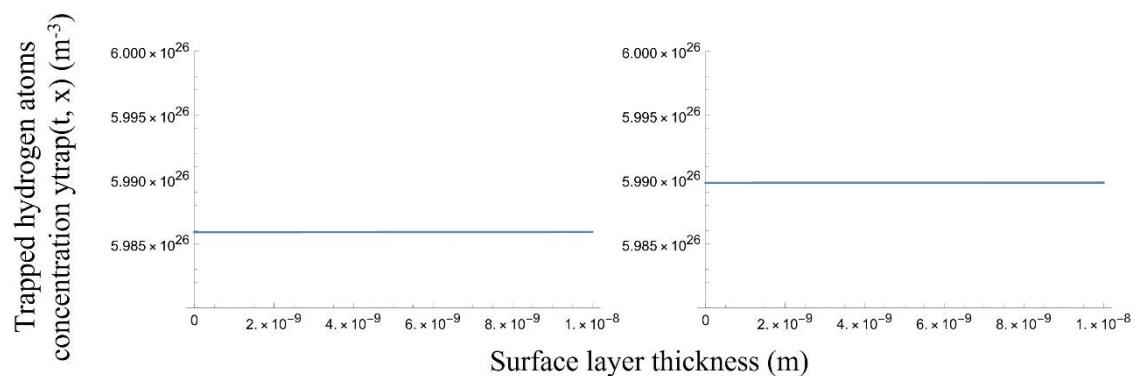


Fig. 4.3.5 Trapped hydrogen atoms concentration profiles in the surface layer after the first (#48772 left) and second (#48773 right) measurement, which are viewed as the initial conditions in the next plasma exposure. The trapped hydrogen atoms are hardly released until the next exposure experiment.

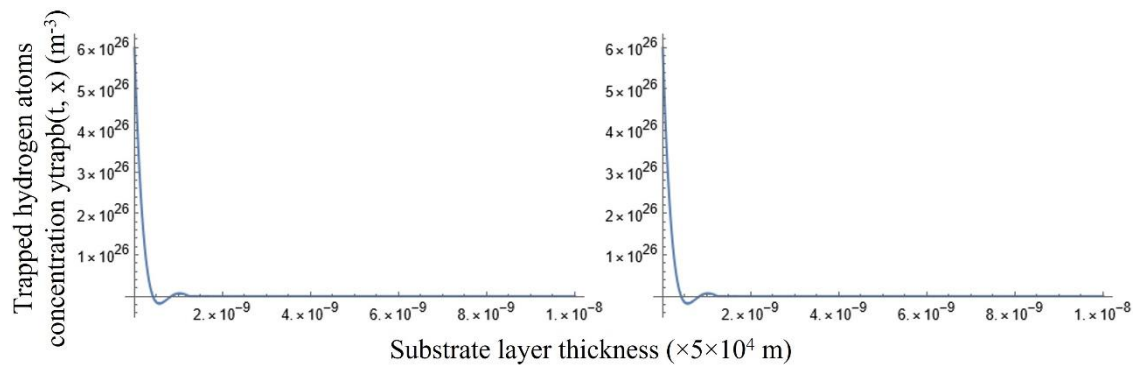


Fig. 4.3.6 Trapped hydrogen atoms concentration profiles in the substrate layer after the first (#48772 left) and second (#48773 right) measurement, which are viewed as the initial conditions in the next plasma exposure.

According to FESTA experiments and model analysis, it could be indicated that the surface state of materials facing high-temperature plasmas may change actively due to deposition, sputtering, collisions with impurities, etc. In Fig. 4.3.2, 0 s indicates the start of hydrogen desorption measurement using FESTA. As shown in Table 3.1.1, it takes 11 seconds to extract the plasma-exposed sample back into the test chamber. Therefore, the hydrogen desorption flux during this 11-second period cannot be measured. However, two-layer model could be used to predict hydrogen desorption over the entire time from the start of plasma exposure to the end of measurement, and the experimental data could be reproduced as well. It should be noted that during the 8 s before closing gate valve 2, the sample was still being exposed to the QUEST plasma, which was also taken into account. The model calculations were able to predict hydrogen adsorption and desorption throughout the entire plasma exposure and measurement period, and the increase in hydrogen desorption due to continuous plasma exposure was also reproduced. This increase is attributed to the increase in those dissolved hydrogen atoms

in the W sample as shown in Figs. 4.3.3 and 4.3.4 due to plasma exposure shot-by-shot, and those trapped ones as shown in Figs. 4.3.5 and 4.3.6 are hardly released from the sample at room temperature, according to the model analysis.

In this experiment, the incident hydrogen flux was obtained by particle balance [45]. During wall saturation state, the hydrogen influx to PFWs is the same of the outflux from PFWs [52][55]. Taking advantage of the fact, it has been found that the signal level of H_{α} intensity is able to be a good monitor of influx into the wall in QUEST. As shown in Fig. 4.3.7, the shot #48800 in the same campaign reached to wall saturation. The injected fuel hydrogen was not necessary to maintain the plasma around the end of plasma discharge. This indicated that the required hydrogen flux had been supplied by the desorption from PFWs.

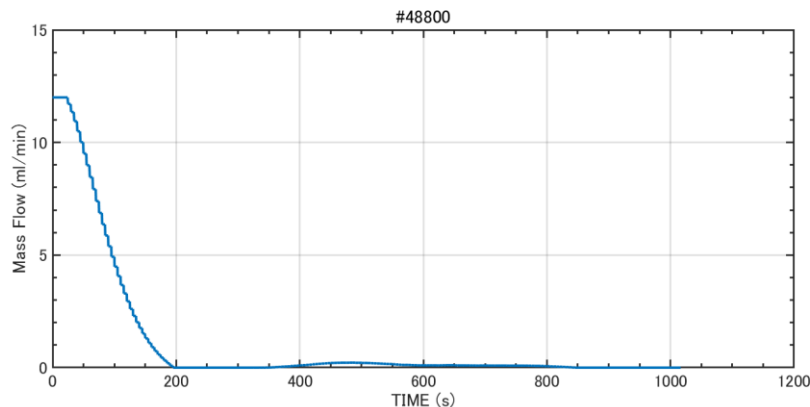


Fig. 4.3.7 Time evolution of provided hydrogen particles to keep H_{α} level during plasma in 2022S/S campaign. No fueling was executed after 200 s and 800 s. This means the fuel required to keep H_{α} level could be supplied from PFWs.

As described above, the relationship between hydrogen influx to the wall (= outflux) and the intensity of H_{α} was obtained as denoted in Fig. 4.3.8 during 2022S/S campaign.

The specimen was located at the same position of the wall during plasma exposure and the exposed flux for the specimen was decided by the H_{α} intensity signal as well.

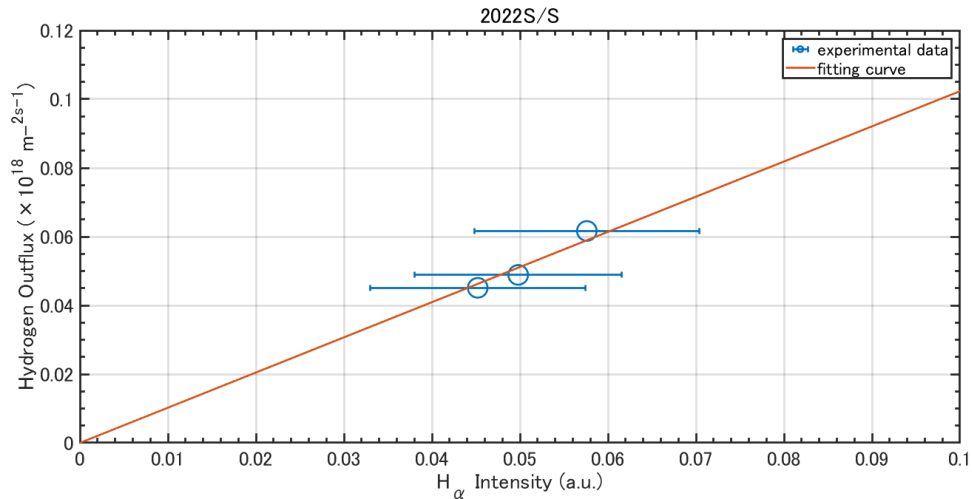


Fig. 4.3.8 Hydrogen outflux after plasma termination as a function of the H_{α} intensity, provided that the transmittance of the window does not change significantly, which is used to measure the H_{α} intensity. Typical error bars of the data are shown in the figure due to the calibration of the evacuating flux. The solid line denotes a fit of the data whose gradient is about $1.0 \times 10^{18} \text{ m}^{-2} \text{ s}^{-1} / (\text{a.u.})$.

Therefore, the hydrogen influx to the specimen could be determined and calculated as $6.3 \times 10^{16} \text{ m}^{-2} \text{ s}^{-1}$ in shot #48772 ~ #48774 during FESTA experiments whose typical plasma conditions have been already shown in Fig. 3.4.3. The hydrogen recycling rate is calculated as the ratio of the incident hydrogen flux to the released hydrogen flux. The hydrogen recycling desorption at the time of 0 s is $6.0 \times 10^{16} \text{ m}^{-2} \text{ s}^{-1}$ using the model calculation shown in the inset figure in Fig. 4.3.2, so the hydrogen recycling coefficient at the end of plasma exposure can be obtained as 0.9.

The surface recombination coefficient K_r of the W sample used in this experiment

without atmospheric exposure was determined to be $3.9 \times 10^{-33} \text{ m}^4 \text{ s}^{-1}$. Calculations were performed to assess the impact of trapping sites in the substrate layer by comparing results with and without them. However, as depicted in Fig. 4.3.9, the difference between the calculations is not apparent. This suggests that the desorption from the plasma-exposed W sample is not notably influenced by the uniform trapping sites throughout the whole sample in the model analysis, likely due to the strong adhesion at room temperature. Instead, it is primarily driven by the dissolved hydrogen in the W sample in FESTA experiments.

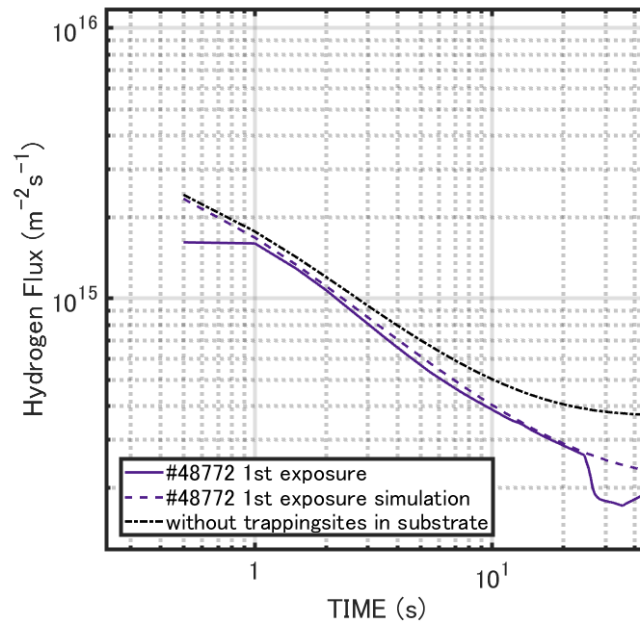


Fig. 4.3.9 Time evolution of hydrogen released flux (solid line) from the plasma-exposed tungsten sample using FESTA in the first plasma exposure. The dashed line denotes the simulation calculated by the two-layer model mentioned above. The pink chain line denotes the result through the two-layer model with trapping sites excluded in the substrate.

Chapter 5 Future Work

As mentioned in Chapter 2, the surface recombination coefficient K_r can be given in two different forms as Eq. (2.1.14) and Eq. (2.2.32), in which surface barrier potential E_C and subsurface barrier potential ΔE_{Surf} are pointed out to be significant, respectively. According to the K_r value determined in FESTA experiments, the E_C value in Eq. (2.1.14) can be evaluated as $E_C = 1.27 \text{ eV}$ and the ΔE_{Surf} value in Eq. (2.2.32) can be evaluated as $\Delta E_{Surf} = 0.24 \text{ eV}$, respectively, using FSETA parameters.

As shown in Fig. 5.1, in this study, the temperature of the tungsten sample exposed in FESTA experiments was only room temperature, so the K_r value dependent on temperature can only be plotted as one point. Moreover, only $\sim 0.1 \text{ eV}$ change also cause surface recombination coefficient K_r to change of several orders of magnitude.

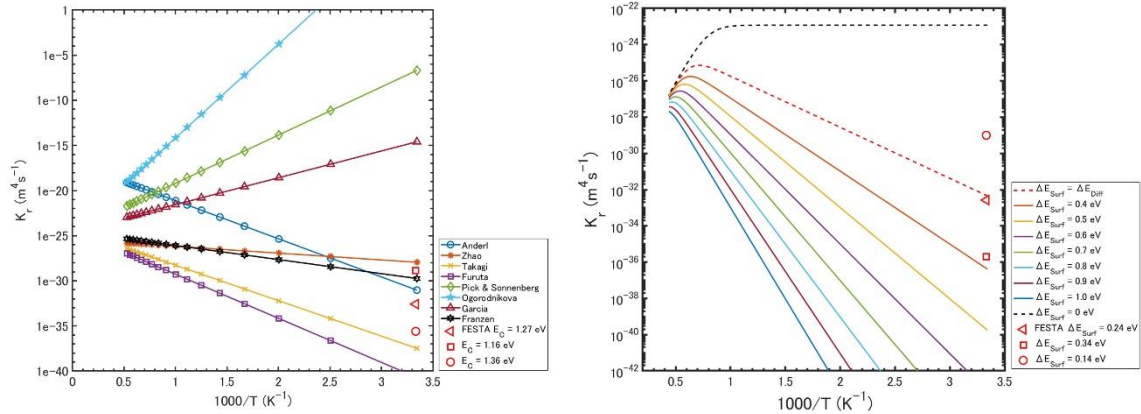


Fig. 5.1 The temperature dependence on K_r is obtained at room temperature by FESTA is shown as red \triangleleft , which is pointed out to be closely related to E_C (left) and ΔE_{Surf} (right) from Eq. (2.1.14) and Eq. (2.2.32), respectively. Red \square and \circ show that a $\sim 0.1 \text{ eV}$ change causes K_r to change of several orders of magnitude.

It is still hard to tell whether E_C or ΔE_{Surf} in a metal surface is more significant for

now. As a result, it is necessary to upgrade FESTA to control the plasma-exposed sample temperature. Within surface barrier potential E_C and subsurface barrier potential ΔE_{surf} evaluated by FESTA at different sample temperature with the same plasma conditions, it could be predicted the temperature dependence on the K_r value during long-duration plasma discharges in a plasma experimental device. This is a future work.

On the other hand, as denoted in Eq. (2.2.33), it is suggested that surface barrier potential E_C may also exist with ΔE_{surf} simultaneously, according to the calculation by K. Schmid. Distinguishing the effect from those two different barrier potentials in one monolayer will contribute to hydrogen behavior in a metal material, especially in W, which is another important future work.

Chapter 6 Discussion

Impact of QUEST plasma exposure

In fact, according to the model calculation, approximately 50% of the hydrogen desorption originates from the dissolved hydrogen rather than the trapped hydrogen. In contrast, it is observed that the majority of hydrogen desorption in the TDS case is attributed to the trapped hydrogen. The dissolved hydrogen, present during plasma exposure, has been released until TDS measurement. These findings strongly indicate that TDS and FESTA offer complementary methods for studying the recombination coefficient K_r .

In order to validate the impact of QUEST plasma exposure, the experimental results obtained by the thermal desorption spectroscopy (TDS) method were used in the calculation using two-layer model. The sample used in the TDS experiment was also W provided by Nilaco Co., the same characteristic as the sample used in FESTA experiments. Before TDS experiment, a 3 keV deuterium (D^{2+}) ion beam was used to irradiate the W sample at room temperature for 13453 s. The total fluence was $3 \times 10^{21} \text{ m}^{-2}$. After three hours waiting, the sample was placed in a TDS experimental vacuum chamber and the TDS experiment started. During TDS experiment, the sample was heated at a rate of 1 K/s for 949 seconds, and the hydrogen desorption from the sample was measured. In this study, the estimate of D desorption was obtained by summing the values for D_2 and DH. In the two-layer model calculation, it is assumed that the diffusion coefficient and surface recombination coefficient for D were the same as those for H, and other parameters were shown in Table 6.1 below.

Table 6.1 Parameters used in TDS model calculation

Parameter	Value	Remarks
Natural Trapping Sites		
Trap Energy	0.85 eV	P. Franzen
Concentration	$6.0 \times 10^{26} \text{ m}^{-3}$	
Ion-induced Trapping Sites 1		
Trap Energy	1.2 eV	Fit to TDS peak
Concentration	$6.4 \times 10^{27} \text{ m}^{-3}$	
Ion-induced Trapping Sites 2		
Trap Energy	1.5 eV	Fit to TDS peak
Concentration	$1.1 \times 10^{28} \text{ m}^{-3}$	
Ion-induced Trapping Sites 3		
Trap Energy	2.0 eV	Fit to TDS peak
Concentration	$2.2 \times 10^{28} \text{ m}^{-3}$	

Several hydrogen desorption peaks were observed without considering the trapping sites in the substrate layer upon heating, as shown in Fig. 6.1.

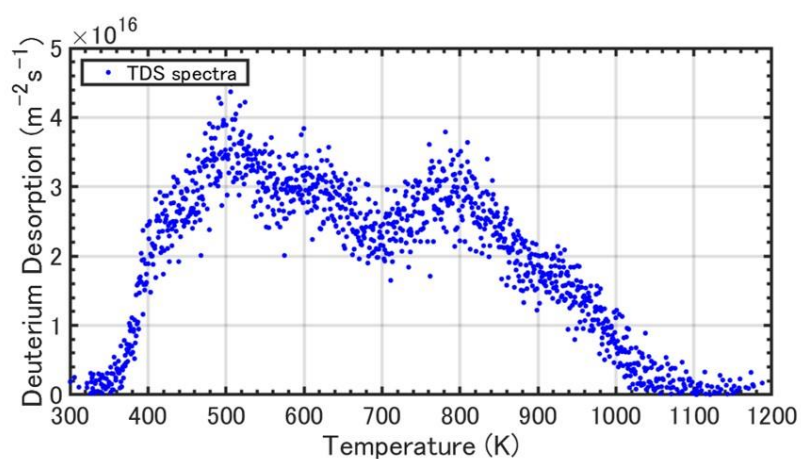


Fig. 6.1 Temperature dependence on deuterium desorption from the beam-irradiated W sample.

Taking Eq. (2.1.14) as an example, using the parameters in Table 5.1 and substituting the $K_r(T) = 3.9 \times 10^{-33} m^4 s^{-1}$ value determined in the FESTA experiments, TDS results were calculated by two-layer model as shown in Fig. 6.2, in which $E_C = 1.27 eV$ value evaluated in FESTA experiments was used.

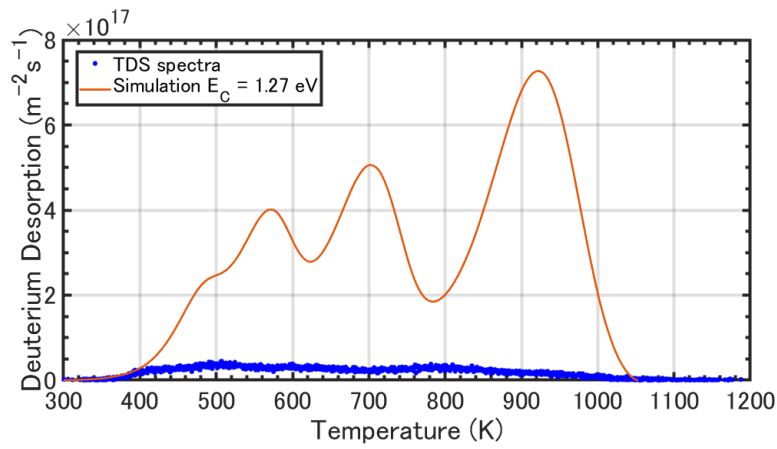


Fig. 6.2 Temperature dependence on deuterium desorption from the beam-irradiated W sample. The blue dots show the TDS spectra. The solid line indicates the desorption predicted using the above-described model calculation without considering trapping sites in the substrate layer, where the value of $E_C = 1.27 eV$ was used as the FESTA experiments using Eq. (2.1.14).

The difference between the calculation and experimental data indicates that the actual surface recombination coefficient value K_r of the sample used in TDS experiment should be much smaller than that evaluated in FESTA experiments, which is owing to the impact from the QUEST plasma exposure and air exposure during TDS experiments. On the other hand, the surface recombination coefficient $K_r = 1.3 \times 10^{-29} m^4 s^{-1}$ was

evaluated at room temperature, in which the surface barrier potential was evaluated as $E_C = 1.16 \text{ eV}$ in TDS experiments, as shown in Fig. 6.3, which is different from the K_r value determined in FESTA experiments using the same parameters above. It can also be inferred that such difference in the ΔE_{surf} value using Eq. (2.2.32) could be obtained as well, which shows the exact impact of QUEST plasma exposure in FESTA experiments.

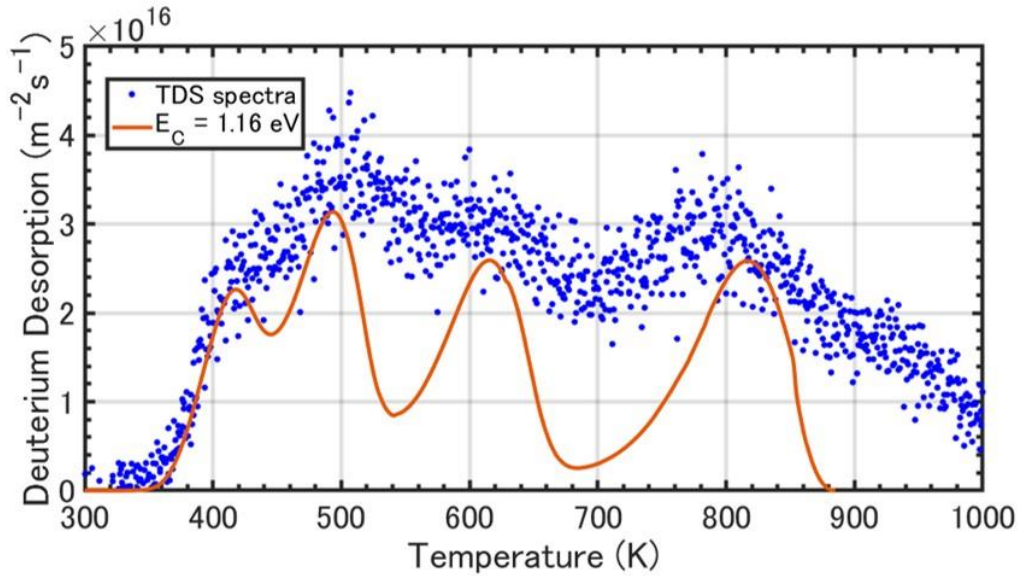


Fig. 6.3 Temperature dependence on deuterium desorption from the beam-irradiated W sample. The blue dots show the TDS spectra. The solid line indicates the desorption predicted using the above-described model calculation without considering trapping sites in the substrate layer, where the value of $E_C = 1.16 \text{ eV}$ was determined using Eq. (2.1.14).

The values of K_r at room temperature exhibit a significant difference of ~ 10 orders of magnitude as shown in Fig. 5.1. The variation in it observed between QUEST plasma exposure and TDS experiments is challenging to determine the exact phenomenon cause.

Furthermore, this difference may become more pronounced as plasma parameters, such as increased wall-injected hydrogen influx and energy. Therefore, conducting measurements of surface recombination coefficient K_r using FESTA during plasma discharges holds great potential for the study of other fusion-oriented experimental devices.

Chapter 7 Conclusion

A device named FESTA (Fast Ejecting System of Targeted sAmples) was developed to measure the hydrogen desorption and to evaluate hydrogen recycling and surface recombination coefficient during long-duration plasma discharges in QUEST. Its pre-programmed motion was proved successfully. A prepared tungsten sample at room temperature has been successfully exposed to QUEST long-duration plasma for three times using FESTA with a fixed interval of 70 minutes. An increase of hydrogen desorption from the plasma-exposed sample shot-by-shot was directly observed. To understand the physical processes, a hydrogen diffusion-desorption model called two-layer model including trapping/de-trapping effect was constructed. With the help of modelling, the experimental results were reproduced and the surface recombination coefficient K_r of the plasma-exposed sample was also evaluated. The reproduction of TDS results using a same tungsten sample without QUEST plasma exposure indicates the impact of QUEST plasma exposure. It could be implied that an in-situ measurement of hydrogen desorption is necessary, and FESTA has been designed as a valuable tool to evaluate fuel particle balance accurately.

There are two different calculations form for surface recombination coefficient K_r referred to previous research, in which surface barrier potential E_c and subsurface barrier potential ΔE_{surf} are pointed out to be significant. To confirm such effects from both barrier potential, hydrogen desorption from a W sample at different temperature is required using FESTA in the future.

Reference

- [1] J. Birman et al The International series of monographs on physics, 8
- [2] <https://optipedia.info/laser/handbook/laser-handbook-10th-section>
- [3] J.D. Lawson 1957 Proc. Phys. Soc. B70 6-10
- [4] M. Mori et al Achievement of high fusion triple product in the JT-60U high β_p H mode 1994 Nucl. Fusion 34 1045-1053
- [5] JT-60SA research plan - research objectives and strategy
- [6] P.M. Stubberfield et al 1991 Extrapolation of the high-performance JET plasmas to D-T operation Plasma Phys. and Controlled Fusion 33 1255-1287
- [7] C.H. Skinner et al 1997 Plasma wall interaction and tritium retention in TFTR J. Nucl. Mater. 241-243 214-226
- [8] X. Gong et al 2019 Integrated operation of steady-state long-pulse H-mode in Experimental Advanced Superconducting Tokamak Nucl. Fusion 59 086030
- [9] John Wesson 2011 Tokamaks Oxford Science Publications
- [10] Max Planck Institute for Plasma Physics, 2011 IPP Bilddatenbank, Graphic: Dr. Christian Brandt
- [11] G.M. Kalinin et al 1991 High-Z plasma-facing and related materials J. Nucl. Mater. 179-181 1193-1198
- [12] M. Sakamoto 2008 J. Plasma Fusion Res. Vol.84, No.12 918-923
- [13] R.B. Jensen et al 1977 Calculations of impurity radiation and its effects on tokamak experiments Nucl. Fusion 17 1187
- [14] J. László, W. Eckstein 1991 Sputtering and reflection from lithium, gallium and indium J. Nucl. Mater. 184 22-29
- [15] A. Miyahara and J.B. Whitley 1991 Thermal effects and other critical issues of

- plasma-facing components J. Nucl. Mater. 179-181 19-24
- [16]The JET Team et al 1990 A review of carbon blooms on JET and TFTR J. Nucl. Mater. 176-177 44-50
- [17]T. Maruyama and M. Haruyama 1992 Neutron irradiation effect on the thermal conductivity and dimensional change of graphite materials J. Nucl. Mater. 495 44
- [18]D.S. Gelles et al 1994 Radiation effects in beryllium used for plasma protection J. Nucl. Mater. 212-215 29-38
- [19]T. Loarer et al 2007 Gas balance and fuel retention in fusion devices Nucl. Fusion 47 1112
- [20]V. Philipps et al 2013 Dynamic fuel retention and release under ITER like wall conditions in JET J. Nucl. Mater. 438 S1067-1071
- [21]L. Frassinetti et al 2021 Role of the separatrix density in the pedestal performance in deuterium low triangularity JET-ILW plasmas and comparison with JET-C Nucl. Fusion 61 126054
- [22]M.A. Pick and K. Sonnenberg 1985 A model for atomic hydrogen–metal interactions—application to recycling, recombination and permeation J. Nucl. and Mater. 131 208-220
- [23]D. K. Brice and B.L. Doyle 1986 Simultaneous gas- and plasma-driven hydrogen transport in solids J. Vac. Sci. Technol. A 5 2311
- [24]T. Tanabe et al 1987 Hydrogen ion driven permeation through metals J. Nucl. Mater. 305 145–147
- [25]O.V. Ogorodnikova et al 2003 Deuterium retention in tungsten in dependence of the surface conditions J. Nucl. Mater. 469 313-316
- [26]A. Pisarev 2009 Hydrogen gas-driven permeation through the membrane with

asymmetric surface conditions J. Membr. Sci. 51-57 335

- [27]O.V. Ogorodnikova 2019 Recombination coefficient of hydrogen on tungsten surface J. Nucl. Mater. 522 74-79
- [28]O.V Ogorodnikova 2000 Comparison of hydrogen gas-, atom- and ion-metal interactions J. Nucl. Mater. 277 130-142
- [29]P. Franzen et al. 1997 Hydrogen trapping in and release from tungsten: Modeling and comparison with graphite with regard to its use as fusion reactor material J. Nucl. Mater. 241-243, 1082-1086
- [30]C. García-Rosales et al. Re-emission and thermal desorption of deuterium from plasma sprayed tungsten coatings for application in ASDEX-upgrade 1996 Nucl. Mater. 233-237, 803-808
- [31]R. A. Anderl et al. 1992 Deuterium Transport and Trapping in Polycrystalline Tungsten Fusion Tech. 21:2P2, 745-752
- [32]M. Zhao et al 2020 Deuterium recombination coefficient on tungsten surface determined by plasma driven permeation Fusion Eng. and Des. 160, 111853
- [33]I. Takagi et al 2011 Deuterium recombination coefficient on tungsten surface determined by plasma driven permeation J. Nucl. Mater. 417, 564-567
- [34]M.I. Baskes 1980 A calculation of the surface recombination rate constant for hydrogen isotopes on metals J. Nucl. Mater. 92 318-324
- [35]A.I. Livshitz 1979 Superpermeability of solid membranes and gas evacuation: Part I. Theory Vacuum 29 103
- [36]J.-S. Wang 1936 On the diffusion of gases through metals Math. Proc. Camb. Phil. Soc. 32 657
- [37]I. Ali-Kahn et al 1978 The rate of hydrogen release out of clean metallic surfaces J.

Nucl. Mater. 76–77 337-343

- [38] F.G. Waelbroeck et al Influence of bulk and surface phenomena on the hydrogen permeation through metals KFA Report JUL-1966 Forschungszentrum Julich Germany
- [39] A.A. Pisarev and O.V. Ogorodnikova 1997 Elementary processes near the interface between hydrogen gas and solid J. Nucl. Mater. 248 52
- [40] K. Schmid and M. Zibrov 2021 On the use of recombination rate coefficients in hydrogen transport calculations Nuclear and Fusion 61 086008
- [41] G. Holzner et al 2020 Solute diffusion of hydrogen isotopes in tungsten—a gas loading experiment Phys. Scr. T171 014034
- [42] R. Frauenfelder 1968 Solution and Diffusion of Hydrogen in Tungsten J. Vacuum Sci. & Tech. 6 388
- [43] A.P. Zakharov A P et al 1973 Hydrogen permeability of poly- and monocrystals of molybdenum and tungsten Fiz. Khim. Mekh. Mater. Vol.9 No.2 29-33
- [44] T. Otsuka et al 2009 Visualization of hydrogen depth profile by means of tritium imaging plate technique: determination of hydrogen diffusion coefficient in pure tungsten Phys. Scr. T138 014052
- [45] K. Hanada et al 2017 Investigation of hydrogen recycling in long-duration discharges and its modification with a hot wall in the spherical tokamak QUEST Nucl. Fusion 57 126061
- [46] T. J. Finlay et al 2013 Removal of deuterium from carbon-based codeposits by hydrogen isotope exchange, J. Nucl. Mater. 443 145-151
- [47] W. R. Wampler et al 2005 Measurements of carbon, deuterium and boron deposition in DIII-D J. Nucl. Mater. 339-339 134-138.

- [48]M. Yamagiwa et al 2011 In situ measurement of hydrogen isotope retention using a high heat flux plasma generator with ion beam analysis Phys. Scr. 014032
- [49]Y. Nakamura et al 2013 Study of hydrogen isotopes behavior in carbon based materials with in situ ion beam analysis under plasma exposure J. Nucl. Mater. Vol. 438 S1036-S1039
- [50]Q. Yue et al. 2020 Measurement of Dynamic Retention with Fast Ejecting System of Targeted Sample (FESTA) Plasma Fusion Res. 15 240201
- [51]Q. YUE 2021 Improving Fast Ejecting System of Targeted Sample (FESTA) and Gas Calibration Proceedings of International Exchange and Innovation Conference on Engineering & Science (IEICES) 7 71-76
- [52]K. Hanada et al 2019 Particle balance investigation with the combination of the hydrogen barrier model and rate equations of hydrogen state in long duration discharges on an all-metal plasma facing wall in QUEST Nucl. Fusion 59 076007
- [53]K. Hanada et al 2010 Steady-state operation scenario and the first experimental result on QUEST Plasma and Fusion Res. 5: S1007-S1007
- [54]Y. Ishihaha et al 2010 Adsorbed Moisture on Metal Surface and its Removal for Gas Supply System J. the Vacuum Society of Japan 53 9 527-532
- [55]S.K. Sharma et al 2012 Permeation measurements for investigation atomic hydrogen flux and wall pumping/fuelling dynamics in QUEST J. Nucl. Mater. 420, 83-93
- [56]J.F. Ziegler et al 1985 The Stopping and Range of Ions in Solids, Pergamon Press
- [57]A. Nayer et al 1997 The Metal Databook

Acknowledgement

In completing this thesis, I received so much assistance from many people, and I would like to express my gratitude here.

I would like to express my deep appreciation and gratitude to Professor Kazuaki Hanada, supervisor of Hanada Laboratory, Research Institute for Applied Mechanics, Kyushu University, who always warmly supported me throughout this whole research, provided me with appropriate advice, and guided me patiently. Professor Hanada has had a significant influence on both my research and personal life since I was a research student. I will never forget the kindness and knowledge he has given me.

I would like to express my deep appreciation and gratitude to Professor Naoki Yoshida, honorary professor, Research Institute for Applied Mechanics, Kyushu University; Dr. Makoto Oya, assistant professor, Faculty of Engineering Sciences, Kyushu University; and Shun Shimabukuro, technical staff, Research Institute for Applied Mechanics, Kyushu University, who gave me lots of support and advice about PWI throughout this research and experiments.

I would like to express my deep appreciation and gratitude to those who helped me throughout this research and the whole experiments from Research Institute for Applied Mechanics, Kyushu University: Professor Hiroshi Idei, Professor Ryuya Ikezoe, Professor Takeshi Ido, Professor Kengoh Kuroda, Assistant Professor Takumi Onchi and Assistant Professor Makoto Hasegawa, who afforded me lots of help the whole five years. I learnt a lot on QUEST, not only the knowledge of hardware, but also those of software which I was not so good at.

I would like to express my deep appreciation and gratitude to those technical staffs who helped me technically conduct experiments from Research Institute for Applied

Mechanics, Kyushu University: Aki Higashijima, Kaori Kono, Takahiro Nagata, Shoji Kawasaki, Masanori Yamashita, Dr. Zennifa Fadilla and Yoshio Ishimura. They taught me a lot of technical knowledge.

In my daily life, I would like to thank the students who always accompany with me and have fun: Toshiki Kinoshita, Junyao Zhou, Yunfei Wang, Pakkapawan Prapan, Ryosuke Hiraka, Hikona Sakai, Rikuya Miyata, Takahiro Yamaguchi, Toshimasa Koga, Tomohide Suetsugu, Yuji Koide, and Yuya Otsuka. I would also like to thank those who have graduated, Shinichiro Kojima, Canbin Huang, Yukai Liu, ELSerafy Hatem, Yifan Zhang, Masaharu Fukuyama, Miu Yunoki, Shogo Matsuo, Takumi Tsugiki, Daichi Ogata, Ryuichi Ashida, Takahiro Murakami, Yoshiki Hiranaka, Akihiro Kidani, Hitoshi Kudo, Ryoya Kato, Yang Wang and Seiya Sakai. Without their enthusiastic help and passion for this major, I could hardly progress and had such a nice research life.

I am deeply grateful to the administrative staff members, Yuki Urano, Yoko Minamizato, Kazumi Eijma, and Sayuri Yoshinaga for their assistance and support, which contributed to the smooth progress of my research activities and student life.

This research is also supported by Grants-in-Aid for Scientific Research <KAKENHI> JP21J21782 and let me thank my supervisor again for helping me modify my application and for the discussions and advice.

At last, I would like to give my deep and sincere appreciation to my family, who always stand for me and always give my support I want. Without them, there will be no me.

Appendix

```
#include <cvirte.h>
#include <userint.h>
#include <ansi_c.h> /*labwindows header we can use labwindows such as C*/
#include <formatio.h> /*labwindows formation for write file or readfile*/
#include <userint.h> /*labwindows for user Interface*/
#include <gpib.h> /*labwindows for GPIB*/
#include <visa.h>

#include <math.h> /*to use mathematical calculation*/
#include <stdlib.h> /*For ordinary utility and macro*/
#include <stdio.h> /*for input data and output data*/
#include <time.h> /*to use relating time*/
#include <string.h> /*to use relating character ex. to copy or to take length of
sentence*/
#include <errno.h> /* To understand what type of errno */
#include <limits.h> /*to dicide limit ex. int_max or schar_max */

int RS232Open(char *, int); /*Declare function of Open file on Actuator */
int RS232Write(char * ); /*Declare function of Wirte command to Actuator */
int RS232Read(char *); /*Declare function of Read position from Actuator
*/
int RS232Close(void); /*Declare function of Close file on Actuator */

/*VISA declaration*/
ViStatus status; /*For chacking errors*/
ViSession defaultRM, instr; /*Communication channels*/

#include "FESTA_20181211.h"
static int panelHandle;

char TERMCHAR[3]; /*データ列 配列 LF CR \n(NULL) が入る*/
float xset=0.0; /*setting position of x_y_z_axis*/
float xpos=0.0; /*reading position of x_y_z_axis*/
int ixflag=0; /*flag to stop Actuator. if flag number changed to*/
```

```

void sleep (long mswait) {          /*void 型 戻り値ない場合の関数定義
関数型 関数名 (引数名の型 引数名) */
    time_t EndWait = clock() + mswait * (CLOCKS_PER_SEC/1000); /*time_t
型 CLOCKS_PER_SEC は関数*/
    while (clock() < EndWait); /*Wait untill clock be EndWait*/
}

int intpow(int ix, int iy, int *ipow) //ix の iy 乗を作っている
{
    int i,ixy;

    ixy = 1;
    *ipow = ixy;
    if (iy==0) return 1;

    for(i=1;i<=iy;i++)
    ixy = ixy * ix;
    *ipow = ixy;
    return 0;
}

int SettingParameter8Hex(long lprm, char *U4Hex, char *L4Hex) /*ASCII コード
用*/
{
    int i, iHex, ipow;

    for(i=3;i>=0;i--)
    {
        U4Hex[i] = 48; //10 進法で ASCII を表す
        L4Hex[i] = 48;
    }
    for(i=7;i>=4;i--){
        intpow(16,i, &ipow);
        iHex = (int )(lprm/((long )ipow));
        if ( iHex >=1 )

```

```

        {
            if ( iHex <= 9 ) U4Hex[i-4] = (char)iHex+48;
            if ( iHex >=10 ) U4Hex[i-4] = (char)iHex+55;
/* 0x41 (65) => A i+55=A 以降の 16 進法*/
        }
        else U4Hex[i-4] = 48;
        lprm = lprm - ((long )(iHex))*((long )(ipow));
        if (lprm==0) return 0;
    }
    for(i=3;i>=0;i--){
        intpow(16,i, &ipow);
        iHex = (int )((lprm/((long )ipow)));
        if ( iHex >=1 ) {
            if ( iHex <= 9 ) L4Hex[i] = (char)iHex+48;
            if ( iHex >=10 ) L4Hex[i] = (char)iHex+55;
        }
        else L4Hex[i] = 48;
        lprm = lprm - ((long )(iHex))*((long )(ipow));
        if (lprm==0) return 0;
    }
    return 0;
}

```

```
int LRCCheck(char *sendbuffer)
```

```

{
    int i,j, ipow=0, LRCsum=0;
    char *e;
    char LRC[256] = {'\0'};
    char LRCbuffer[512];

    j=1;

    for(i=1;i<256;i++) {
        strncpy(LRCbuffer, sendbuffer+j, 2);
        j=j+2;
        ipow=strtol(LRCbuffer, &e, 16);
    }
}

```

```

        LRCsum=LRCsum + ipow;
        if (sendbuffer[i]==0) break;
    }

    LRCsum = -1 * LRCsum;

    sprintf(LRC, "%X", LRCsum);

    i = strlen(sendbuffer);
    sendbuffer[i] = LRC[6];
    sendbuffer[i+1] = LRC[7];
    sendbuffer[i+2] = 0;

    return 0;
}

int Xmove (float x) //直値移動 P220
{
    char U4Hex[4], L4Hex[4];
    int i, j;
    char sendbuffer[512], readbuffer[512], buff2[64] ;
    long lsetting;

    for(i=0;i<512;i++) sendbuffer[i] = readbuffer[i] = 0;

    sleep(1000);

    // strcpy(sendbuffer,":01050407FF00"); //ALRS
    // LRCCheck(sendbuffer); RS232Write(sendbuffer); RS232Read(readbuffer);
    // printf("ALRS FF: %s\n", readbuffer);
    // 1_axis
    // sleep(1000);
    // strcpy(sendbuffer,":010504070000"); //ALRS
    // LRCCheck(sendbuffer); RS232Write(sendbuffer); RS232Read(readbuffer);
    // printf("ALRS 00: %s\n", readbuffer);
    // 1_axis

```

```

//    sleep(1);
//    strcpy(sendbuffer,":01050408FF00"); //BLKOFF  ALM 点灯時はブレーキ
を強制解除する
//    LRCCheck(sendbuffer); RS232Write(sendbuffer); RS232Read(readbuffer);
//    printf("BLK 00: %s\n", readbuffer);
// 1_axis
    sleep(1000);
    strcpy(sendbuffer,":01050403FF00"); //ServoON
    LRCCheck(sendbuffer); RS232Write(sendbuffer); RS232Read(readbuffer);
    printf("SON FF: %s\n", readbuffer);
    sleep(1000);

    printf("Xmove xset: %f\n", x);

    for(i=0;i<512;i++) sendbuffer[i] = readbuffer[i] = 0;

    sleep(1000);

    lsetting = ((long )(x*100.+0.5));
    strcpy(sendbuffer,":01109900000912");
    SettingParameter8Hex(lsetting, U4Hex, L4Hex);
    i = strlen(sendbuffer);
    for(j=0;j<4;j++) {
        sendbuffer[i+j] = U4Hex[3-j];
    }
    for(j=4;j<8;j++) {
        sendbuffer[i+j] = L4Hex[7-j];
    }
    sendbuffer[i+8] = 0;

    /* 16進数で5桁になると動かないので要変更
    strcat(sendbuffer,"0000");
    sprintf(buff2,"%X",lsetting);
    strcat(sendbuffer,buff2);
    */

```

```

// strcat(sendbuffer,"0000000A00000318000100000000"); // 7.92mm/s
// strcat(sendbuffer,"0000000A000001F4000100000000"); // 5mm/s
// strcat(sendbuffer,"0000000A00000190000100000000"); // 4mm/s
// strcat(sendbuffer,"0000000A0000015E000100000000"); // 3.5mm/s
// strcat(sendbuffer,"0000000A0000012C000100000000"); // 3mm/s
// strcat(sendbuffer,"0000000A000007D0000100000000"); // 20mm/s
// strcat(sendbuffer,"0000000A00000BB8000100000000"); // 30mm/s
// strcat(sendbuffer,"0000000A00001388000100000000"); // 50mm/s
// strcat(sendbuffer,"0000000A00002710000100000000"); // 100mm/s
18690
// strcat(sendbuffer,"0000000A0000000F000100000000"); // max
speed ??mm/s
// strcat(sendbuffer,"0000000A0000FFFF000100000000"); // max
speed ??mm/s

if (x==0.00) {
    strcat(sendbuffer,"0000000A00002710007800000000"); // 原点
    に戻るときの速度=655.35mm/s
} else {
    if (x==280.00) {
        strcat(sendbuffer,"0000000A00002710007800000000");
    } else {
        strcat(sendbuffer,"0000000A00000BB8000100000000"); // それ
        以外の速度=300mm/s
    }
}
printf("%s\n",sendbuffer);
sleep(1000);

LRCCheck(sendbuffer);
// printf("LRCCheck OK");
// sleep(100);
RS232Write(sendbuffer);
// printf("RS232Write OK");
// sleep(100);

```

```

    RS232Read(readbuffer);
//    printf("RS232Read OK");
//    sleep(100);
    printf("XMove %s\n",readbuffer);

    return 0;
}

int PCONPositionMonitor ()
{
    long ldum;
    int i, ipow, idum[8];
    char cdum[9];

    char sendbuffer[512], readbuffer[512];

    for(i=0;i<512;i++) sendbuffer[i] = readbuffer[i] = 0;

    strcpy(sendbuffer,":010390000002");
    LRCCheck(sendbuffer); RS232Write(sendbuffer);

    sleep(1000);
    RS232Read(readbuffer);

//    printf("1_axis_Position: %s\n", readbuffer);

    for(i=7;i<15;i++) cdum[i-7] = readbuffer[i];
    cdum[8] = 0;
    ldum = 0;
    for(i=0;i<8;i++)
    {
        if ( (cdum[i]>=48) && (cdum[i]<=57) ) idum[i] = cdum[i]-48; /**/
        if ( (cdum[i]>=65) && (cdum[i]<=70) ) idum[i] = cdum[i]-55;

        intpow(16,(7-i), &ipow); /*16進法を10進法*/
        ldum = ldum + ipow*idum[i];
    }
}

```

```

    }
    xpos = ((float )ldum)/100.000000;

    printf(" xpos : %f\n", xpos);          //距離 10 進法で今の現在地を表示

// 1_axis

    //strncat(readbuf2, readbuffer+7,8);
    //ldum = strtol(readbuf2, &e, 16);      //16 進数→10 進数変換
    //fdum = ((double)ldum)/100.0000000000;

    //fdum = (float )n/100.0;
    //printf("変換数値=%f\n", ((double)ldum/100.0));
    //printf("fdum=%f\n", fdum);

    return 0;
}

int PCONPositionCheck ()
{
    for(;;){
        PCONPositionMonitor ();

        //          SetCtrlVal (panelHandle, PANEL_NUMERIC_X, xpos); //
        //          SetCtrlVal (panelHandle, PANEL_NUMERIC_Y, ypos); //
1_axis
        //          SetCtrlVal (panelHandle, PANEL_NUMERIC_Z, zpos); //
1_axis

        if (ixflag==1){
            if (fabs(xset-xpos)<=0.01) ixflag = 0;
        }
// 1_axis
/*          if (iyflag==1){
            if (fabs(yset-ypos)<=0.01) iyflag = 0;
        }

```

```

        if (izflag==1){
            if (fabs(zset-zpos)<=0.01) izflag = 0;
        }
    */
        if ((ixflag)==0) break;
    //    printf("%f, %f, %f\n",position[0],position[1],position[2]);
    }
    //    printf("%f, %f, %f\n",position[0],position[1],position[2]);
    return 0;
}

int Initialize(void)
{
    char IPAddress[32];
    int portnum;
    //    char TERMCHAR[3];
    char sendbuffer[512], readbuffer[512];
    //    ViSession defaultRM, instr;
    //    ViStatus status;
    int i;

    for(i=0;i<512;i++) sendbuffer[i] = readbuffer[i] = 0;

    strcpy(IPAddress, "192.55.52.91");
    portnum = 1;
    sprintf(TERMCHAR,"%c%c",0x0d,0x0a); /*0x0d=CR,0x0a=LF 打ち込み終了、行換え*/
    if (RS232Open(IPAddress, portnum)<0 ) return 0;
    //    printf("*****\n");
    sleep(1000);

    strcpy(sendbuffer,":01050427FF00"); //PMSL
    LRCCheck(sendbuffer); RS232Write(sendbuffer); RS232Read(readbuffer);
    printf("PMSL: %s\n", readbuffer);
    // 1_axis
    sleep(1000);

```

```

    strcpy(sendbuffer,":01050414FF00"); //Mod
    LRCCheck(sendbuffer); RS232Write(sendbuffer); RS232Read(readbuffer);
    printf("MOD: %s\n", readbuffer);
// 1_axis
    sleep(1000);
//    strcpy(sendbuffer,":01050408FF00"); //BLKOFF   RC パソコン対応ソフト
で ALM 点灯時は、//を外してブレーキを強制解除する
//    LRCCheck(sendbuffer); RS232Write(sendbuffer); RS232Read(readbuffer);
//    printf("BLK 00: %s\n", readbuffer);
// 1_axis
    sleep(1000);
    strcpy(sendbuffer,":01050407FF00"); //ALRS
    LRCCheck(sendbuffer); RS232Write(sendbuffer); RS232Read(readbuffer);
    printf("ALRS FF: %s\n", readbuffer);
// 1_axis
    sleep(1000);
    strcpy(sendbuffer,":010504070000"); //ALRS
    LRCCheck(sendbuffer); RS232Write(sendbuffer); RS232Read(readbuffer);
    printf("ALRS 00: %s\n", readbuffer);
// 1_axis
//    sleep(1);
//    strcpy(sendbuffer,":01050408FF00"); //BLKOFF   ALM 点灯時はブレーキ
を強制解除する
//    LRCCheck(sendbuffer); RS232Write(sendbuffer); RS232Read(readbuffer);
//    printf("BLK 00: %s\n", readbuffer);
// 1_axis
    sleep(1000);
    strcpy(sendbuffer,":01050403FF00"); //ServoON
    LRCCheck(sendbuffer); RS232Write(sendbuffer); RS232Read(readbuffer);
    printf("SON FF: %s\n", readbuffer);
    sleep(1000);

    return 0;
}

int main (int argc, char *argv[])

```

```

{
    if (InitCVIRTE (0, argv, 0) == 0)
        return -1;        /* out of memory */
    if ((panelHandle = LoadPanel (0, "FESTA_20181211.uir", PANEL)) < 0)
        return -1;
    DisplayPanel (panelHandle);

    SuspendTimerCallbacks();        /*Labwindows  funciton  timer  until
REsumeTimerCallbacks*/
    Initialize();
    PCONPositionMonitor(); //今の現在地を表示する

    xset = xpos;
    // SetCtrlVal (panelHandle, PANEL_XCNTPOSITION, xset); //コントロール
上の数値を xset に入れる

    RunUserInterface ();
    DiscardPanel (panelHandle);
    return 0;
}

int CVICALLBACK Quit (int panel, int control, int event,
                      void *callbackData, int eventData1, int
eventData2)
{
    char sendbuffer[512], readbuffer[512];
    int i;

    for (i=0;i<512;i++) sendbuffer[i] = readbuffer[i] = 0.0;

    switch (event)
    {
        case EVENT_COMMIT:
            strcpy(sendbuffer,":010504080000"); //BLKON
            LRCCheck(sendbuffer);                RS232Write(sendbuffer);
            RS232Read(readbuffer);

```

```

        sleep(1000);
        strcpy(sendbuffer,":010504030000"); //ServoOFF
        LRCCheck(sendbuffer);          RS232Write(sendbuffer);
RS232Read(readbuffer);
        sleep(1000);
        RS232Close();
        QuitUserInterface (0);
        break;
    }
    return 0;
}

```

```

int CVICALLBACK Zero (int panel, int control, int event,
                    void *callbackData, int eventData1, int
eventData2)

```

```

{
    char sendbuffer[512], readbuffer[512];
    int i;

    for (i=0;i<512;i++) sendbuffer[i] = readbuffer[i] = 0.0;

    switch (event)
    {
        case EVENT_COMMIT:
            //          xset=281.00;      // max 850.00
            //          ixflag = 1;
            //          if (ixflag==1) Xmove(xset);
            //          PCONPositionCheck();
            //          xset=181.00;      // max 850.00
            //          ixflag = 1;
            //          if (ixflag==1) Xmove(xset);
            //          PCONPositionCheck();
            //          xset=0.00;        // max 850.00
            //          ixflag = 1;
            //          if (ixflag==1) Xmove(xset);
            //          PCONPositionCheck();

```

```

        strcpy(sendbuffer,":010504030000"); //ServoOFF
        LRCCheck(sendbuffer);                RS232Write(sendbuffer);
RS232Read(readbuffer);
        sleep(1000);
        break;
    }
    return 0;
}

```

```

int CVICALLBACK Behind (int panel, int control, int event,
                        void *callbackData, int eventData1,
int eventData2)
{
    char sendbuffer[512], readbuffer[512];
    int i;

    for (i=0;i<512;i++) sendbuffer[i] = readbuffer[i] = 0.0;

    switch (event)
    {
        case EVENT_COMMIT:
            xset=185.00;    // max 850.00
            ixflag = 1;
            if (ixflag==1) Xmove(xset);
            PCONPositionCheck();
            strcpy(sendbuffer,":010504030000"); //ServoOFF
            LRCCheck(sendbuffer);                RS232Write(sendbuffer);
RS232Read(readbuffer);
            sleep(1000);
            break;
        }
    return 0;
}

```

```

int CVICALLBACK Ahead (int panel, int control, int event,
                        void *callbackData, int eventData1, int

```

```

eventData2)
{
    char sendbuffer[512], readbuffer[512];
    int i;

    for (i=0;i<512;i++) sendbuffer[i] = readbuffer[i] = 0.0;

    switch (event)
    {
        case EVENT_COMMIT:
            xset=280.00; // max 850.00
            ixflag = 1;
            if (ixflag==1) Xmove(xset);
            PCONPositionCheck();
            strcpy(sendbuffer,":010504030000"); //ServoOFF
            LRCCheck(sendbuffer);                RS232Write(sendbuffer);
RS232Read(readbuffer);
            sleep(1000);
            break;
    }
    return 0;
}

int CVICALLBACK Plasma (int panel, int control, int event,
                        void *callbackData, int eventData1,
int eventData2)
{
    char sendbuffer[512], readbuffer[512];
    int i;

    for (i=0;i<512;i++) sendbuffer[i] = readbuffer[i] = 0.0;

    switch (event)
    {
        case EVENT_COMMIT:
            xset=880.00; // max 850.00

```

```

        ixflag = 1;
        if (ixflag==1) Xmove(xset);
        PCONPositionCheck();
        strcpy(sendbuffer,":010504030000"); //ServoOFF
        LRCCheck(sendbuffer);                RS232Write(sendbuffer);
RS232Read(readbuffer);
        sleep(1000);
        break;
    }
    return 0;
}

```

```

int CVICALLBACK Finish (int panel, int control, int event,
                        void *callbackData, int eventData1,
int eventData2)

```

```

{
    char sendbuffer[512], readbuffer[512];
    int i;

    for (i=0;i<512;i++) sendbuffer[i] = readbuffer[i] = 0.0;

    switch (event)
    {
        case EVENT_COMMIT:
//            xset=281.00;    // max 850.00
//            ixflag = 1;
//            if (ixflag==1) Xmove(xset);
//            PCONPositionCheck();
//            xset=181.00;    // max 850.00
//            ixflag = 1;
//            if (ixflag==1) Xmove(xset);
//            PCONPositionCheck();
            xset=0.00;    // max 850.00
            ixflag = 1;
            if (ixflag==1) Xmove(xset);
            PCONPositionCheck();

```

```

        strcpy(sendbuffer,":010504030000"); //ServoOFF
        LRCCheck(sendbuffer);                RS232Write(sendbuffer);
RS232Read(readbuffer);
        sleep(1000);
            break;
    }
    return 0;
}

```

```

int CVICALLBACK Position (int panel, int control, int event,
                          void *callbackData, int
eventData1, int eventData2)

```

```

{
    switch (event)
    {
        case EVENT_COMMIT:
            ixflag = 1;
            printf("xset=%f, ixflag=%d\n",xset, ixflag);
            break;
    }
    return 0;
}

```

```

int RS232Open(char *IPAddress, int portnum)

```

```

{
    char instrDescriptor[VI_FIND_BUFLLEN];
    char buf[20];
    // ViSession defaultRM, instr;
    ViStatus status;

    /* First we will need to open the default resource manager. */
    status = viOpenDefaultRM (&defaultRM);
    if (status < VI_SUCCESS)
    {
        printf("Could not open a session to the VISA Resource Manager!\n");
        return -1;
    }
}

```

```

    }
//    *opendefaultRM = defaultRM;

/* Set descriptor to a serial port at port 2 of the serial device server
at IP address 130.164.41.41 */
/*strcpy(instrDescriptor, "ASRL::130.164.41.41::2::INSTR");*/
    strcpy(instrDescriptor, "ASRL");
/*    strcat(instrDescriptor, IPAddress); */
    sprintf(buf, "%d::INSTR", 3);
    strcat(instrDescriptor, buf);

/* Now we will open a session to the instrument we just found. */
    status = viOpen (defaultRM, instrDescriptor, VI_NULL, VI_NULL, &instr);
    if (status < VI_SUCCESS)
    {
        printf ("An error occurred opening a session to %s\n", instrDescriptor);
        viClose(defaultRM);
        return -1;
    }
//    *openinstr = (int)instr;

/* Set the baud rate to 115200. This takes effect immediately. */
/* Error checking has been removed from this point on for clarity. */
//    status = viSetAttribute(instr, VI_ATTR_ASRL_BAUD, 115200);
    status = viSetAttribute(instr, VI_ATTR_ASRL_BAUD, 38400);
    status = viSetAttribute(instr, VI_ATTR_ASRL_DATA_BITS, 8);
    status      =      viSetAttribute(instr,      VI_ATTR_ASRL_STOP_BITS,
VI_ASRL_STOP_ONE);
/*    status      =      viSetAttribute(instr,      VI_ATTR_ASRL_STOP_BITS,
VI_ASRL_STOP_TWO); */
    status      =      viSetAttribute(instr,      VI_ATTR_ASRL_PARITY,
VI_ASRL_PAR_NONE);

    status      =      viSetAttribute(instr,      VI_ATTR_TERMCHAR,
(int)(TERMCHAR[strlen(TERMCHAR)-1]) );
    status      =      viSetAttribute(instr,      VI_ATTR_WR_BUF_OPER_MODE,

```

```

VI_FLUSH_ON_ACCESS);
    status = viSetAttribute(instr, VI_ATTR_RD_BUF_OPER_MODE,
VI_FLUSH_DISABLE);
    // status = viSetAttribute(instr, VI_ATTR_ASRL_END_IN,
VI_ATTR_TERMCHAR);
    // status = viSetAttribute(instr, VI_ATTR_ASRL_END_OUT,
VI_ATTR_TERMCHAR);
    status = viSetAttribute(instr, VI_ATTR_ASRL_END_IN,
VI_ASRL_END_TERMCHAR);
    status = viSetAttribute(instr, VI_ATTR_ASRL_END_OUT,
VI_ASRL_END_TERMCHAR);

    return 0;
}

int RS232Write(char *buf)
{
    ViUInt32 retCount;
    ViStatus status;

    sleep(200);

    strcat(buf,TERMCHAR);
    status = viWrite(instr, buf, strlen(buf), &retCount);
    if ( status < 0 ){

        printf("Sending Error: %s [%d]\n", buf,retCount);
        return -1;
    }
    return 0;
}

int RS232Read(char *buf)
{
    long i=0, j= 0;
    char cdum[3], buf2[1024];

```

```

ViUInt32 retCount, numAvailBytes;
ViStatus status;

sleep(200);

for(;;) {
    status = viGetAttribute(instr, VI_ATTR_ASRL_AVAIL_NUM,
&numAvailBytes);
    if (numAvailBytes!=0) {
        status = viRead(instr, buf, numAvailBytes, &retCount);
        buf[retCount] = (char)0x00;
        for (j=0;j<=strlen(TERMCHAR);j++) cdum[j] =
buf[retCount-(strlen(TERMCHAR)-j)];
        if (!strcmp(cdum,TERMCHAR)) break;
    }
    i++;
    if (i>650000) {
        printf("Read Error: %s [%d]\n",buf, numAvailBytes);
        return -1;
    }
}
/*
printf("buf %s\n",buf);
status = viSetAttribute(instr, VI_ATTR_RD_BUF_OPER_MODE,
VI_FLUSH_ON_ACCESS);

status = viRead(instr, buf2, numAvailBytes, &retCount);
viSetAttribute(instr, VI_ATTR_RD_BUF_OPER_MODE,
VI_FLUSH_DISABLE);
if (status < 0) {
    printf("Reading Error: %s [%d]\n",buf2, retCount);
    return -1;
}
buf2[retCount] = (char)0x00;
if(strcmp(buf,buf2)!=0){
    printf("Reading Error: buf %s [buf2 %s]\n",buf, buf2);
}

```

```
        return -1;
    }
    */
    return 0;
}
int RS232Close()
{
    /* Close the session to the port. */
    viClose(instr);
    /* Close the resource manager session. */
    viClose(defaultRM);
    return 0;
}
```